University of Alberta

Semi-Analytical Proxy for Vapex Process Modeling

by

Jindong Shi

A thesis submitted to the Faculty of Graduate Studies and Research
in partial fulfillment of the requirements for the degree of

Master of Science
in
Petroleum Engineering

Department of Civil and Environmental Engineering

Spring 2014
Edmonton, Alberta

I dedicate this work to my parents and all my family members who always support and encourage me to pursue the best.

Abstract

Vapex (Vapor extraction) is a non-thermal process providing a more environmental-friendly and energy-efficient alternative to steam injection. The simulation process using numerical modeling techniques may become difficult when considering the uncertainty due to reservoir heterogeneity.

In this research, a physical-based semi-analytical proxy is developed to model solvent transport in Vapex process at isothermal conditions, detailed analytical formulations are derived and implemented in a calculation procedure to advance the solvent-oil interface and to estimate producing oil rate with time. The proposed approach is first validated against Hele-Shaw experimental data available in the literature, then modified to simulate homogeneous and heterogeneous reservoir cases, and further applied to rank a suit of geostatistical realizations and to assess reservoir uncertainty in subscale heterogeneity. Results from this model are compared against experimental data as well as detailed compositional simulation studies. Computational efficiency of the proxy in comparison to numerical simulations is also emphasized.

Acknowledgement

First and foremost, I express sincere appreciation to Dr. Juliana Leung for her support and insightful ideas throughout the research. This work would not have been possible without her continued guidance and unlimited patience during the whole parts of this study. I am also grateful to Dr. Hassan Dehghanpour and Dr. Vinay Prasad for coming to my final defense as examining committee members and giving me constructive comments and feedbacks.

I would like to thank all the professors for providing me solid knowledge and cutting-edge technologies of petroleum engineering. Learning from them gave me a good insight into this discipline, as well as motivated me to explore and discover more in oil and gas industry. I am also thankful to all the members of Dr. Leung's simulation group who helped and inspired me through different problems, and I would like to thank all the people who helped me during my two years MSc study.

My gratitude also goes to Petroleum Technology Research Centre (PTRC) for providing the Sustainable Technologies for Energy Production Systems (STEPS) program and the financial support. I would also like to thank the Computer Modeling Group (CMG) for providing the academic licenses for GEM and the University of Alberta for granting access to the Numerical and Statistical Server.

Finally, I am truly grateful to my family, for their love, understanding, and support throughout my life. They make me realize how great I can be, and enlighten my path towards the success.

Table of Content

List of tables

List of figures

Chapter 1: Introduction

Background

The world's total estimated reserves of heavy oil, tar sands and bitumen is approximately 6 trillion barrels of oil in place (Das 1998), which is about six times as big as the estimated conventional oil. A major part of these resources are in western Canada, reported as 1.8 trillion bbl of bitumen initially in-place in Alberta according to Energy Resources Conservation Board (2012). The size of estimated heavy oil and tar sand resources in the United States amounts to 100 billion bbl and 62 billion bbl of OIP, respectively (Stosur 1995).The province of Alberta and Saskatchewan contain significant heavy oil and oil sands deposits, such as Athabasca (McMurray Formation), Wabasca (Grand Rapids Formation), Cold Lake (Clearwater Formation), Peace River (Blue Sky/Gething Formation), Lloydminster (Mannville Formation) and Grosmont Formation deposits (Singhal et al. 1996).

The main challenge for recovery of heavy oil is the high viscosity of bitumen. For example, the oil viscosity of Athabasca bitumen is greater than 1×10^6 mPa.s at reservoir conditions and cannot be produced by conventional production. Also, due to the adverse mobility ratio between oil and displacing fluids, flooding techniques cannot enhance the recovery significantly. In-situ methods are often used in heavy oil/bitumen recovery involving the use of steam (heat source) and solvents. Five proven in-situ methods of bitumen extraction are SAGD, CSS,

VAPEX, THAI, and Cold Flow. Currently, SAGD and VAPEX have become popular techniques for the recovery of heavy oil and bitumen in oil industry.

Typically, recovery requires thermal process using Steam Assisted Gravity Drainage (SAGD). In this process, steam is injected continuously into reservoir through an upper horizontal well and heats the bitumen around the well. The viscosities of bitumen decrease drastically with increase in temperature by steam heating, so that the less viscous oil drains to another lower horizontal well by gravity. During the SAGD process, the injected steam first rises within the reservoir until it reaches the overburden. Then the steam starts to spread sideways to develop a steam chamber. At the steam-bitumen interface, the heated oil and condensed water will drain by gravity to the producer. Although SAGD process proved to be successful in many reservoirs in terms of high production rate, the energy efficiency and operation feasibility under certain reservoir conditions are still need to be considered. For SAGD, a large amount of heat loses to the underburden and overburden during production process, this situation typically exists in thin reservoirs. Besides, many reservoirs are underlain by aquifer layers, which may make SAGD process uneconomic due to the thermal energy release in aquifer rather than bitumen.

Introduction to Vapex

The idea of injecting solvent instead of steam can also reduce the viscosity of heavy oil and bitumen, which is known as the Vapor Extraction process (Vapex).

In this non-thermal process, vaporized solvent is injected through a horizontal injector dissolves into the oil and reduces oil viscosity, allowing the oil to flow to a horizontal production well via gravity forces.

The key recovery mechanisms are convection and molecular diffusion enhanced by various spreading mechanisms such as capillarity and velocity variations at the micro and macro scales, i.e., dispersion and mixing. As described by Das (1998), the solvent initially dissolves into the bitumen at the contact interface and rises slowly to form a vapor chamber above the injector. The diluted oil drains along the solvent-bitumen interface to the production well (producer) by gravity. When the chamber reaches the overburden, it spreads laterally until the reservoir boundary is reached.

In this process, production rate is related to the properties and quantity of injected solvent. Light alkenes, particularly ethane, propane and butane are the most suitable solvents for the Vapex process (Das and Butler 1994 a). Laboratory studies have indicated that the best performance of Vapex has been observed when propane, butane, or mixtures of propane-butane are used (Butler and Mokrys 1992, Das and Butler 1995). The use of CO_2 in the Vapex process is an economic and environmental friendly alternative that has also been studied by many researchers. Vapex experiments conducted with sand-pack, high-pressure stainless models shows that reduction of operation costs and environmental benefits justify the use of CO_2 at a lower operating pressure rather than methane (Talbi and Maini 2003).

Vapex is a solvent analogue of the SAGD process with similar production process physics. However, it is much more energy efficient than SAGD, which can serve as a potential alternative in certain situations such as thin reservoirs or reservoirs underlain by aquifers. There are several characteristics of the Vapex process that enhances its performance in comparison to SAGD, such as lower energy intensity, lower completion cost, more environmental friendly, production of superior quality oil, and lower volume of injected solvent.

Many research works related to Vapex were mainly based on experimental models and numerical simulations. Butler and Mokrys (1989) first proposed the Vapex process based on a small physical model, Hele-Shaw cell model. This simple laboratory model represented a direct experimental and theoretical analogy of SAGD process, but the predicted oil drainage rate was lower compared with those of SAGD. In numerous Hele-Shaw cell experiments, it was demonstrated that as solvent is injected into reservoir, it would dissolve in the bitumen at the solvent-bitumen interface. Then the diluted oil starts to drain to the production well by gravity. The solvent-bitumen interface would advance, diluting the bitumen along the chamber boundary. If the solvent concentration is high enough, the asphaltene may remain inside the model after the diluted and deasphalted oil drained out.

As for porous media, the basic mechanism of Vapex process is the same as in Hele-Shaw cell. The only difference appears at the solvent chamber boundary, at which the process takes place in a contact zone, instead of at a smooth interface observed in a Hele-Shaw cell. This provides a very high interfacial contact area

that yields a high mass transfer rate of solvent into bitumen (Das and Butler 1994 b). The mass transfer is enhanced by capillary imbibitions and the corresponding surface renewal. Although the diluted bitumen has a lower surface tension, due to its low viscosity it is quickly drawn away from the interface exposing a renewed interface of fresh bitumen to the solvent. The Hele-Shaw cell model assumes a pseudo steady concentration profile in the diffusion boundary layer. This assumption represents a lower mass transfer rate, which is reasonable for that small physical model with zero porosity. While in porous media, the early transient mass transfer is more prominent due to the periodic surface renewal, so that a very high diffusion coefficient is needed to match the actual mass transfer rate.

Other work involves using the commercial compositional reservoir simulator (GEM) to assess the Vapex process by using the Equation of State (EOS) (Nghiem et al.2001). They presented the important techniques for modeling the asphaltene precipitation, molecular diffusion, and convective dispersion with the use of an EOS for oil and gas phase behaviour. The diffusion coefficient can be used as parameters to history match the experimental data and field observations (Yazdani and Maini 2008, Nghiem et al. 2001).

Problem Statement

The key recovery mechanism in Vapex is molecular diffusion enhanced by dispersion that is a strong function of heterogeneities occurring at the micro and macro scales, such as those randomly distributed, discontinuous, thin shale lenses

commonly found in oil sands deposits. A primary difficulty in modeling lies in the inability to accurately assess and quantify the effects on dispersion caused by heterogeneities occurring at different scales.

While compositional simulators are available for assessing the Vapex performance, the simulation process may become challenging when taking into account the uncertainty due to reservoir heterogeneity. Given that heterogeneity modeling informed by incomplete data leads to uncertainty about rock properties, geologic uncertainty often exists at many scales. Most practical approaches require generation of large number of equi-probable realizations of rock properties at different scales.

Computational constraints preclude detailed numerical solution of the flow and transport differential equations, as often implemented in traditional flow simulators, to analyze recovery performance and optimize operating parameters, particularly in the presence of reservoir heterogeneities. Efficient alternatives, like proxy models, are used to mimic the transport physics without solving all the detailed equations. Therefore, a new proxy, similar to those in existing literature for modeling SAGD processes using Butler's formulation, will be developed to model solvent transport in Vapex at isothermal conditions, allowing us to assess the recovery performance of many geologic realizations efficiently.

Research Objectives

The objective of this research is to develop an approach that combines the analytical solutions, proxy models and geostatistical tools for Vapex process

modeling, to investigate the effects of both large-scale and sub-scale heterogeneities on effective dispersion, which entails:

(1) Numerical implementation of a proxy model for approximating solvent transport in a medium with spatially-varying properties.

(2) Calibration of results against detailed compositional flow simulations via tuning parameters.

(3) Application of the calibrated models over a suite of 2D cross-sectional reservoir realizations depicting both large-scale and sub- scale heterogeneities.

The physics-based proxy model developed in this research can be used as a complementary tool to expensive detailed flow simulations. Given that uncertainty in reservoir properties contributes to the overall uncertainty in recovery performance, this model can be used to evaluate or screen many geostatistical realizations representing heterogeneity at various scales quickly to identify a smaller, more manageable subset of models for further detailed flow simulations. The use of proxy model, as implemented in this research, also aims to minimize the computational cost which is a major shortcoming of traditional flow simulators. This type of proxy models can also be easily integrated in existing workflows and artificial intelligence algorithms (as implemented by many heavy oil operators) to optimize production scenarios in a quick and robust manner.

Main Methodology

Descriptions of key recovery mechanisms and governing equations in Vapex have been studied by various researchers over the past 30 years. Several proxies have been published in the literature for modeling of SAGD process, which focus on the spreading period; for example, some implemented Butler's formulation to approximate the heat penetration rate in a "S-shaped chamber", while others followed the method of slices using Reis' linear steam chamber model (Reis 1992). These methods are based on analytical solution of the momentum and mass balances between the chamber interface and the rest of the reservoir and have been applied successfully to 2D cross-sectional heterogeneous realizations. Due to the similarity of chamber formation in SAGD and VAPEX processes, Butler and other researchers have developed analytical solutions analogous to those of SAGD: heat transfer by conduction is replaced by mass transfer due to diffusion, where heated bitumen is replaced by diluted bitumen.

Numerous modifications must be made to those existing SAGD proxies to model the solvent analog process in several aspects: 1) thermal diffusivity is replaced by diffusion coefficient; 2) temperature gradient is replaced by solvent concentration gradient; 3) kinematic viscosity is a function of concentration instead of temperature. As indicated by other researchers, many assumptions and approximations are made in these proxies, it is important that we calibrate our proxy model against results from traditional flow simulations.

In this work, a physics-based proxy model is first developed to simulate the Vapex process on the analogy of SAGD process based on Butler's theory (Butler

1985). The proxy model allows the prediction of total drainage rate, drainage rate change with time, and the position change of solvent chamber boundary during the spreading chamber period. The model is based on the small physical model Hele-Shaw cell, but some assumptions are made to simplify the modeling process. A new parameter, mass penetration (analogous to heat penetration in SAGD) is introduced in our proposed formulation. Detailed formulations are derived and implemented in a calculation procedure to advance the solvent-bitumen interface and estimate the producing oil rate. The formulations are implemented in Matlab® program and have been applied to model for numerous 2-D solvent extraction experiments conducted in a Hele-Shaw cell.

Then, the original proxy model developed based on Hele-Shaw experiment is modified and popularized to porous media at a larger reservoir scale by introducing a calibration process. An empirical factor is introduced as "tuning parameter" to adjust the proxy performance to match more closely the numerical simulation results. The comparisons of oil rate, cumulative oil production, solvent chamber shape and computational time against flow simulator are carried out through homogeneous and heterogeneous reservoir cases to test the feasibility of the proxy model at field scale. Further applications are implemented to integrate proxy model with geostatistical techniques to generate a robust workflow in uncertainty assessment of heterogeneous reservoirs with various geological realizations.

Thesis Overview

This thesis is paper-based. Three papers which were submitted at different conferences and/or under revision for journal publications are presented through Chapter 2 to Chapter 4. Each chapter has its own introduction, case studies, conclusions and references. An overview for each of them is stated as follows:

In Chapter 2, a novel physical-based proxy is developed to model solvent transport in Vapex at isothermal conditions, in a way analogous to the SAGD model described by Butler (1985). Detailed analytical formulations are derived from Hele-Shaw cell experiment and implemented in a calculation procedure to advance the solvent-bitumen interface and to estimate producing oil rate with time. In our approach, solvent concentration and intrinsic diffusion coefficient are introduced in the model instead of temperature and thermal diffusivity in SAGD. A new mass penetration parameter is introduced and its change with time is modeled. Growth of solvent chamber and oil drainage rate predicted from the proxy model are in good agreement with Hele-Shaw experimental data available in the literature. Results predicted by proxy model also match well with scaled-up flow rates for a field case described by Das and Butler (1994 b).

In Chapter 3, analytical solutions and implementation details for the Vapex proxy is presented same as those in Chapter 2. The proposed approach is then applied to various reservoirs discretized with spatially varying rock porosity and permeability values; oil drainage rate and solvent penetration are calculated sequentially at grid blocks along the solvent-bitumen interface over incremental time steps. Results from this model are compared against experimental data

available in the literature as well as detailed compositional simulation studies. Computational requirement of the proxy in comparison to numerical simulations is also emphasized.

In Chapter 4, the modified proxy model described in Chapter 3 is further applied to a suite of geostatistical realizations to rank their recovery performance based on cumulative oil production, and the results demonstrate good agreement with those based on detailed compositional simulations but with significant savings in computational costs. Finally, this proxy is employed to assess impacts of uncertainty in subscale heterogeneity. An important contribution from this work is that the proposed proxy can be easily integrated in existing reservoir management workflows to optimize production scenarios in a quick and robust manner. It can be applied to rank numerous geostatistical realizations and quickly identify a smaller, more manageable subset of realizations for further simulation analysis.

References

Butler, R.M. 1985. A New Approach To the Modeling of Steam-Assisted Gravity Drainage. *Journal of Canadian Petroleum Technology* **24**(3): 42-51. Doi:10.2118/85-03-01

Butler, R.M. and Mokrys, I.J. 1989. Solvent Analog Model of Steam Assisted Gravity Drainage, *AOSTRA Journal of Research* **5**(1): 17-32.

Butler, R.M. and Mokrys, I.J. 1992. Recovery of Heavy Oils Using Vaporized Hydrocarbon Solvents: Further Development of the VAPEX Process. Technical

Meeting/Petroleum Conference Of The South Saskatchewan Section, Regina, Saskatchewan, 7 – 9 October. Doi:10.2118/SS-92-7

Das, S.K. 1998. Vapex: An Efficient Process for the Recovery of Heavy Oil and Bitumen. *SPE Journal* **3**(3): 232-237. Doi:10.2118/50941-PA

Das, S.K. and Butler, R.M. 1994 (a). Investigation of 'VAPEX' Process in a Packed Cell Using Butane As a Solvent. Canadian SPE/CIM/CANMET International Conference on Recent Advances in Horizontal Well Applications, Calgary, 20-24 March. Doi:10.2118/HWC-94-47

Das, S.K. and Butler, R.M. 1994 (b). Effect of Asphaltene Deposition on the Vapex Process: A preliminary Investigation Using a Hele-Shaw Cell. *Journal of Canadian Petroleum Technology* **33**(6): 39-45. Doi:10.2118/94-06-06

Das, S.K. and Butler, R.M. 1995. Extraction Of Heavy Oil And Bitumen Using Solvents At Reservoir Pressure. Technical Meeting/Petroleum Conference Of The South Saskatchewan Section, Regina, Saskatchewan, 16-18 October. Doi:10.2118/95-118

Energy Resources Conservation Board. 2012. *ST98-2012: Alberta's Energy Reserves 2011 and Supply/Demand Outlook 2012-2021*, June 2012. ISSN: 1910-4235

Nghiem, L.X., Kohse, B.F., and Sammon, P.H. 2001. Compositional Simulation of the VAPEX Process. *Journal of Canadian Petroleum Technology* **40**(8): 54-61.Doi:10.2118/01-08-05

Reis, J.C. 1992.A Steam-Assisted Gravity Drainage Model for Tar Sands: Linear Geometry. *Journal of Canadian Petroleum Technology* **31**(10): 14-20. Doi:10.2118/92-10-01

Singhal, A.K., Das, S.K., Leggitt, S.M., Kasraie, M., and Ito, Y. 1996. Screening of Reservoirs For Exploitation by Application of Steam Assisted Gravity Drainage/Vapex Process. International Conference on Horizontal Well Technology, Calgary, Alberta, 18-20 November. Doi:10.2118/37144-MS

Stosur, G.J. 1995. Heavy Oil Recovery in The Low Oil Price Regime. Sixth UNITAR Intl. Conference on Heavy Crude and Tar Sands, Houston, Texas, USA, 12-17 February.

Talbi, K. and Maini, B.B. 2003. Evaluation of CO2 Based Vapex Process for the Recovery of Bitumen from Tar Sand Reservoirs. SPE International Improved Oil Recovery Conference in Asia Pacific, Kuala Lumpur, Malaysia, 20-21 October. Doi: 10.2118/84868-MS

Yazdani, A. and Maini, B.B. 2008. Modeling of the VAPEX Process in a Very Large Physical Model. *Energy & Fuels* 2008 **22**(1): 535-544. Doi:10.1021/ef700429h

Chapter 2: Physics-Based Proxy Modeling of Solvent Transport in VAPEX Process[1]

Introduction

The world's total estimated reserves of heavy oil, tar sands, and bitumen is approximately 6 trillion barrels of oil in place, which is six times as much as the estimated conventional oil reserves (Das 1998). A major portion of these resources is deposited in western Canada; a recent report prepared by the Energy Resources Conservation Board (2012) suggested that there is 1.8 trillion bbl of bitumen initially in-place in Alberta. The size of estimated heavy oil and tar sand resources in the United States amounts to 100 billion bbl and 62 billion bbl of OIP, respectively (Stosur 1995).These energy resources have attracted much attention in recent years.

The main challenge for heavy oil recovery is the high viscosity of bitumen. For example, Athabasca bitumen has a viscosity of over 10^6 cp at reservoir conditions and cannot be produced by conventional technology. In-situ recovery methods often entail the use of steam (heat source) and solvents. Steam assisted gravity drainage (SAGD) is one of the most commonly adopted techniques for heavy oil recovery. Steam is injected continuously into the reservoir through a horizontal injection well. The injected steam rises within the reservoir until it reaches the overburden; it then advances horizontally away from the injection plane and a

[1] A version of this chapter was submitted and accepted by Canadian Journal of Chemical Engineering: Shi. J. and Leung, Y.J. 2013 (in press).Physics-Based Proxy Modeling ofSolvent Transport in VAPEX Process. Manuscript number:CJCE-13-0271.R1.

steam chamber is formed. At the steam-bitumen interface, the viscosity of the bitumen decreases drastically due to an increase in temperature by steam heating; the heated (less viscous) oil and condensed water would drain via gravitational force along the steam chamber edge to a horizontal production well located near the bottom of the reservoir. Although the SAGD process has been adopted successfully in many reservoirs with high production rate, energy efficiency and operation feasibility remains challenging under certain reservoir conditions. For example, significant heat loss to underburden and overburden during production process is a common concern, particularly in thin reservoirs. Thermal energy release to underlying aquifers can also render the SAGD process uneconomical.

VAPEX (vapor extraction) is a non-thermal process in which vaporized solvent mixture of low molecular-weight hydrocarbons, instead of steam, injected in-situ at a pressure close to its dew point through a horizontal injector dissolves into the oil and reduces its viscosity, allowing the oil to flow to a horizontal production well located near the bottom of the reservoir via gravitational forces. As described by Das (1998), the solvent dissolves into the bitumen at the contact interface and rises slowly to form a vapor chamber above the injector. The diluted oil drains along the solvent-bitumen interface to a horizontal production well by gravity. When the chamber reaches the overburden, it spreads laterally until the reservoir boundary is reached. The key recovery mechanisms are convection and molecular diffusion enhanced by various spreading mechanisms such as capillarity and velocity variations at the micro and macro scales, i.e., dispersion and mixing.

Beyond the similarities between VAPEX and SAGD, several fundamental differences between the two processes can be highlighted. In SAGD, recovery is enhanced due to the heat transfer from steam to the heavy oil, whereas in VAPEX, mass transfer of solvent from the injected vapor phase to the heavy oil controls the recovery performance: production rates are directly related to the bitumen viscosity reduction, which is the result of an increase of solvent concentration through diffusion. In addition, condensation of water from steam would create in a third immiscible phase and lead to reduction in oil relative permeability and gravity drainage potential. On the other hand, vaporized solvent would dissolve miscibly into the bitumen at the interface in VAPEX. When ignoring multiphase relative permeability effects, the mathematical formulations of governing equations for the two processes become comparable. Therefore, VAPEX is often considered as a solvent analogue of the SAGD process. If applied efficiently, VAPEX could offer several advantages over SAGD including lower energy and water consumption, reduced completion cost, and decreased CO_2 emission (Luhning et al. 2003).

Descriptions of key recovery mechanisms and governing equations in VAPEX have been studied by various researchers over the past 30 years. Many related studies in the literature were based on experimental models and numerical simulations. Butler and Mokrys (1989) first illustrated the fundamentals of VAPEX using a Hele-Shaw cell model. This simple laboratory set-up demonstrated a direct experimental and theoretical analogy between VAPEX and SAGD, but the predicted oil rate using a liquid solvent was lower compared to

those of SAGD. As molecular diffusivity of a solvent in bitumen is much lower than thermal diffusivity of bitumen, it was postulated that oil production rates could be enhanced considerably by vaporizing the solvents and deasphalting.

The mechanisms of VAPEX process in porous media are similar to those observed in a Hele-Shaw cell. The main difference appears at the solvent chamber boundary, at which the mass transfer takes place in a contact zone, instead of at a sharp interface detected in a Hele-Shaw cell. In a porous medium, increased surface area and tortuosity result in a large interfacial contact area; the overall mass transfer is further enhanced by capillary imbibitions and the corresponding surface renewal. Das and Butler (1994 a) explained that although the diluted bitumen has low surface tension, it can be quickly drawn away from the interface due to its low viscosity, exposing a renewed interface between fresh bitumen and solvent.

Yazdani and Maini (2008) conducted an experimental study using a large physical model that is 1m in height. The scale of the model was comparable to some very thin reservoirs in northern Canada. They concluded that dispersion coefficient, which was obtained in their study as a tuning parameter when matching production rates from the physical model with compositional simulation results, was much larger than molecular diffusion coefficient. The measured drainage rate tended to increase with drainage height at a much higher factor than the theoretical square root value. They argued that the higher production rate showed a more realistic performance of VAPEX in such thin reservoirs.

Other researchers have used various commercial compositional reservoir simulators to model the VAPEX process (Nghiem et al. 2001). In their works, mechanisms of asphaltene precipitation, molecular diffusion, and convective dispersion are incorporated. Complex phase behavior is modeled using an equation of state (EOS). While compositional simulators are available for assessing the VAPEX performance, computational constraints preclude detailed numerical solution of the flow and transport differential equations to analyze recovery performance and to optimize operating parameters, particularly in the presence of reservoir heterogeneities. Efficient alternatives, like proxy models, can be used to mimic the transport physics without solving all the detailed equations. Therefore, a new proxy, similar to those in existing literature for modeling SAGD processes using Butler's formulation, is presented in this paper to model solvent transport in VAPEX at isothermal conditions.

Several proxies have been published in the literature for modeling of SAGD process, which focus on the spreading period (Butler 1985); for example, some implemented the formulation in Butler's paper (Butler 1985) to approximate the heat penetration rate in a "S-shaped chamber" (Vanegas et al. 2008), while Azad and Chalaturnyk (2010) followed the method of slices using Reis' linear steam chamber model (Reis 1992). In these methods, analytical solutions of the momentum and mass balances performed at the solvent-oil interface are incorporated into a calculation sequence to advance the steam chamber interface and to compute oil recovery. These models have been applied successfully to 2D cross-sectional heterogeneous realizations (Vanegas et al. 2008). Due to the

similarity of chamber formation in SAGD and VAPEX processes, analytical solutions for oil drainage rate from a Hele-Shaw cell in a fashion analogous to those of SAGD formulations have also been derived by numerous researchers in the past: 1) heat transfer by conduction is replaced by mass transfer due to diffusion, where heated bitumen is replaced by diluted bitumen; 2) thermal diffusivity is replaced by diffusion coefficient; and 3) temperature gradient is replaced by solvent concentration gradient as the driving force for mass transfer (Butler and Mokrys 1989, Das and Butler 1994 b). However, analytical equations that describe solvent chamber advancement have not been published.

In this paper, analytical formulations presented by Butler and Mokrys (1989) are integrated into a physics-based proxy model to simulate solvent transport and recovery performance in a VAPEX process. The proxy is developed following its SAGD analog by Butler (1985) and Vanegas et al. (2008). A new parameter, mass penetration depth, is introduced in our proposed formulation. This parameter relates the advancement of solvent chamber interface to mass transfer and drainage velocity. Therefore, this proposed proxy model can be used to predict both total drainage rate with time and the advancement of solvent chamber boundary during the spreading chamber period. Since the analytical formulations originally presented by Butler and Mokrys (1989) are valid for conditions in a Hele-Shaw cell, certain modifications have been incorporated to model the process in porous media. Results obtained from this model are verified against published experimental data.

This paper is organized as follows: first, the governing equations and formulations for the proposed proxy are presented. Next, the calculation procedure and implementation details are discussed. Results of the proxy are compared to the published experimental data in two case studies to illustrate its applicability.

Theory and Mathematical Formulations

The original analytical model for VAPEX was developed by Butler and Mokrys (1989) following a series of Hele-Shaw cell experiments. The mass transfer mechanism occurring inside the mixing layer between the liquid solvent and heavy oil interface was modeled. In this section, the original model is presented followed by a discussion of modifications necessary for porous media. A new equation that describes mass penetration as a function of time is derived. The equations presented here are subsequently implemented in an explicit calculation sequence described in the next section.

Formulation for the original Hele-Shaw model

Consider a cross section of the solvent-bitumen interface as shown in **Figure 2-1**, where oil is flowing along the interface at a drainage rate of V. For a fully-developed solvent chamber, the solvent-bitumen interface is assumed to be advancing at a constant unspecified velocity U. Perform a one-dimensional mass balance at steady state over a thin segment inside the interface would give Eq.1:

$$U\frac{dC_s}{d\xi}+\frac{d}{d\xi}D_s\frac{dC_s}{d\xi}=0 \quad \text{..... (1)}$$

Where D_s is the intrinsic diffusion coefficient of solvent, C_s is the solvent concentration (volume fraction) at a distance ξ from the interface. Solvent flux due to diffusion is obtained from Fick's first law. Eq.1 can be approximated by Eq.2 if ξ is small:

$$U\Delta C_s + D_s \frac{dC_s}{d\xi} = 0 \quad \text{.....(2)}$$

Denoting C_{sr} as the initial solvent concentration in the reservoir at a distance far away from the interface (ξ=ξ_{max}), representing the minimum solvent concentration, a one-dimensional convection-diffusion equation can be obtained:

$$U\left(C_s - C_{sr}\right) + D_s \frac{dC_s}{d\xi} = 0 \quad \text{.....(3)}$$

$$d\xi = -\frac{D_s}{U}\frac{dC_s}{\left(C_s - C_{sr}\right)} \quad \text{.....(4)}$$

At steady state, the driving force created by gravity is identical to drag force induced by viscosity. Assuming the cell spacing between two plates is small enough so that the change in velocity gradient in the direction normal to the flow surface can be neglected (Butler and Mokrys 1989), the force balance within the diffusion layer is described by:

$$g\Delta\rho \sin\theta = \frac{V\mu_b}{k_o} \quad \text{.....(5)}$$

Where g is the gravitational constant, $\Delta\rho$ is the density difference between bitumen and solvent, θ is the angle between the interface and the horizontal axis, μ_b is the dynamic viscosity of bitumen in solution. At steady state, the solvent concentration is independent with time; hence the viscosity and density are

constant across the cell width. Effective permeability of the oil, k_o, in a Hele-Shaw cell with a spacing of b between the two glass plates is given by Lamb (1932):

$$k_o = \frac{b^2}{12} \quad \text{.....(6)}$$

The average drainage velocity in Eq.5can now be rearranged as follows:

$$V = \frac{k_o g \Delta\rho \sin\theta}{\mu_b} \quad \text{.....(7)}$$

At any given point along the interface, the bitumen drainage rate (q) per unit well length is given by the integral as shown in Eq.8:

$$q = \int_0^{\xi_{\max}} V(1 - C_s) d\xi \quad \text{.....(8)}$$

SubstitutingEq.4 and Eq.7into Eq.8and changing the limits of integration, q can be obtained usingEq.9:

$$q = \frac{k_o g \sin\theta}{U} N_s \quad \text{.....(9)}$$

The dimensionless number N_s is defined in Eq.10:

$$N_s = \int_{C_{sr}}^{C_{sc}} \frac{\Delta\rho D_s (1 - C_s) dC_s}{\mu_b (C_s - C_{sr})} \quad \text{.....(10)}$$

Where C_{sc} is the maximum value for C_s occurring at ξ=0. The term N_s consists of physical properties of the solvent-bitumen system which combines the effect of solvent concentration, solvent-bitumen density difference, diffusion coefficient of solvent, and viscosity. It has constant value for a fully developed solvent chamber (i.e., one that has reached the overburden) where temperature and pressure do not vary, although parameters $\Delta\rho$, D_s and μ_b are functions of C_s at $\xi > 0$. In a Hele-

Shaw cell, the intrinsic solvent diffusion coefficient D_s is also a function of overall diffusion coefficient D_o given by Eq.11:

$$D_s = \frac{D_o}{1 - aC_s} \quad \text{..... (11)}$$

The empirical constant "a" was proposed by Butler and Mokrys (1989); its value depends on the composition of bitumen samples (i.e., for Suncor bitumen, a = 0.947; for Athabasca bitumen, a = 0.969).

Considering mass transfer by diffusion of solvent into bitumen, the mass of solvent (m_r) accumulated in the reservoir ahead of the solvent-bitumen interface ($\xi > 0$) over an arbitrary area A is given by Eq.12:

$$\frac{\delta m_r}{\delta A} = \int_0^\infty \rho_s (C_s - C_{sr}) d\xi \quad \text{..... (12)}$$

We now introduce a new variable, γ_m, which is the mass penetration depth defined as the depth to which mass of solvent would have penetrated if C_s has achieved a uniform value of C_{sc} in the solvent-oil mixture. It can be also interpreted as the penetration capacity of solvent into the bitumen. This variable is analogous, in a way, to the heat penetration parameter in its SAGD analog (Butler 1985), and it is described by Eq.13 as follows:

$$\frac{\delta m_r}{\delta A} = \gamma_m \rho_s (C_{sc} - C_{sr}) \quad \text{..... (13)}$$

Assuming ρ_s is approximately constant and performing a change of variable using Eq.4, Eq.12 and Eq.13 can be equated to solve for γ_m as follows:

$$\gamma_m = \frac{1}{U(C_{sc} - C_{sr})} \int_{C_{sr}}^{C_{sc}} D_s dC_s \quad \text{..... (14)}$$

If D_s is independent constant of solvent concentration, Eq.14 can be further simplified as in Eq.15:

$$\gamma_m = \frac{D_s}{U} \quad \text{.....(15)}$$

Okazawa (2009) investigated the effects of concentration-dependent diffusion coefficient on VAPEX drainage rates and concluded that the base functionalities of bitumen rates to other key parameters remain unchanged with diffusion coefficient. Hence, the assumption of constant diffusion coefficient D_s is generally considered reasonable. Substituting Eq.15 into Eq.9, q can now be written as:

$$q = \frac{k_o g \sin\theta \gamma_m}{D_s} N_s \quad \text{.....(16)}$$

Following the derivations in Appendix A, mass penetration rate $d\gamma_m/dt$ can be obtained from Eq.17. This mass penetration rate is important to relate the interface advancement to mass transfer as discussed in Appendix A, so that the mass penetration can be updated and interface movement and oil production rate can be determined as a function of time.

$$\frac{d\gamma_m}{dt} = \frac{1}{\sqrt{\pi}}\left(\frac{D_s}{\gamma_m} - U\right) \quad \text{.....(17)}$$

The total amount of oil drained through the cross section per unit well length at a particular location (x, y) over the time t is represented by the shaded area in **Figure 2-2**. It can also be calculated using Eq.18:

$$\int_0^t q dt = \int_y^h x dy \quad \text{.....(18)}$$

Differentiating Eq.18 with respect to y and then t gives the horizontal displacement velocity of the interface at any point:

$$\left(\frac{\partial q}{\partial y}\right)_t = -\left(\frac{\partial x}{\partial t}\right)_y \quad \text{.....(19)}$$

A similar expression for the vertical displacement can be derived and shown in Eq.20:

$$\left(\frac{\partial q}{\partial x}\right)_t = \left(\frac{\partial y}{\partial t}\right)_x \quad \text{.....(20)}$$

The total production rate for one-half of the solvent chamber is given by Eq.21 (see Appendix B for details):

$$Q = \sqrt{2k_o ghN_s} \quad \text{.....(21)}$$

Where h is the total vertical height for drainage process, and Q is the drainage rate per unit length for the half-side drainage. As opposed to a line source in a Hele-Shaw experiment where oil drains on one side, the solvent chamber in typical reservoir settings would develop around the well pair, allowing oil to drain to the producer on both sides.

Formulation for a porous medium

In the Hele-Shaw model, a sharp solvent-oil interface is typically assumed (Figure 2-1), where the oil saturation changes from its residual value (i.e., zero in a Hele-Shaw cell) to its initial value (i.e., unity in a Hele-Shaw cell) across the interface. While in the porous media, the mass transfer process takes place in a contact zone or the diffusion boundary layer as described by Das (2005). To obtain meaningful predictions for VAPEX process in porous media, Das and Butler (1998) derived the expressions for oil drainage rate that account for the effects of capillary pressure and surface tension on the overall mass transfer. Formulations for the

original Hele-Shaw model can be modified to account for the effects of porosity ϕ, oil saturation S_o, and tortuosity (Das and Butler 1998, Boustani 2001). Analogous expressions for Eqs.3, 16 and 10 for a porous medium can be derived as follow:

$$U(C_s - C_{sr}) + \phi S_o D_s \frac{dC_s}{d\xi} = 0 \quad \text{.....(22)}$$

$$q = \frac{k_o g \sin\theta \gamma_m}{\phi S_o D_s} N_s \quad \text{.....(23)}$$

Where:

$$N_s = \int_{Csr}^{Csc} \frac{\Delta\rho \phi S_o D_s (1 - C_s) dC_s}{\mu_b (C_s - C_{sr})} \quad \text{.....(24)}$$

For the sake of simplicity in the formulation of Eq.22, it is assumed the tortuosity effect has already been incorporated into the definition of D_s. Das and Butler (1998) has noted that in porous media, the value of D_s should be corrected using a cementation factor Ω, which is a measure of consolidation and tortuosity in a porous medium. In this work, we have adopted a value of 2 for Ω (Boustani 2001).

In addition, the mass penetration parameter γ_m introduced in Eqs.12-15 can be modified as:

$$\frac{\delta m_r}{\delta A} = \int_0^\infty \rho_s \phi S_o (C_s - C_{sr}) d\xi \quad \text{.....(25)}$$

$$\frac{\delta m_r}{\delta A} = \gamma_m \rho_s \phi S_o (C_{sc} - C_{sr}) \quad \text{.....(26)}$$

$$\gamma_m = \frac{\phi S_o}{U(C_{sc} - C_{sr})} \int_{C_{sr}}^{C_{sc}} D_s dC_s \quad \text{.....(27)}$$

$$\gamma_m = \frac{\phi S_o D_s}{U} \quad \text{.....(28)}$$

Similarly, the mass penetration rate expression in Eq.17 can be modified as (see Appendix A for details):

$$\frac{d\gamma_m}{dt} = \frac{1}{\phi S_o \sqrt{\pi}} \left(\frac{\phi S_o D_s}{\gamma_m} - U \right) \quad \text{..... (29)}$$

Finally, accounting for ϕ and ΔS_o (the difference between initial oil and residual oil saturation) in Eqs.18-21 would result in the following set of equations (see Appendix B for details):

$$\int_0^t q dt = \phi \Delta S_o \int_y^h x dy \quad \text{.....(30)}$$

$$\left(\frac{\partial q}{\partial y} \right)_t = -\phi \Delta S_o \left(\frac{\partial x}{\partial t} \right)_y \quad \text{.....(31)}$$

$$\left(\frac{\partial q}{\partial x} \right)_t = \phi \Delta S_o \left(\frac{\partial y}{\partial t} \right)_x \quad \text{.....(32)}$$

$$Q = \sqrt{2 k_o g \phi \Delta S_o h N_s} \quad \text{.....(33)}$$

Calculation Procedure and Implementation Details

The above equations can be used in sequence to determine the growth of a fully developed solvent chamber in the spreading period, as well as to calculate the oil drainage rate with time. Following a similar SAGD proxy formulation described by Butler (1985) and later by Vanegas et al. (2008), the previously derived analytical equations are implemented in an explicit calculation sequence using MATLAB®.

1. Discretize the solvent-bitumen interface into a number of evenly distributed nodes as shown in **Figure 2-3**, which move laterally along the reservoir width (or plate width for Hele-Shaw cell) as the solvent chamber grows.

2. Initialize values of mass penetration γ_m for all nodes defined in step 1. The criterion for assigning the initial values seems arbitrary when referring to Butler (1985) in describing the initialization the analogous heat penetration parameter for SAGD. He stated that the values of γ_m should increase from top to bottom (i.e., largest near the well pair and smallest near the chamber top). Different types of distribution of γ_m along interface are used in this study to assess its sensitivity and will be discussed later.

3. Calculate the oil flow rate q for each node using Eqs.23-24. It is convenient to assume interface angle θ is 90° at t=0. The oil rate right below the overburden is set to zero, as γ_m at the first grid node next to the upper boundary is assumed to be zero.

4. Calculate the interface change in the horizontal or vertical direction at the next time step using Eq.31 or Eq.32. If the interface is nearly vertical (θ>45°), the horizontal movement of interface can be determined using Eq.31, whereas if it is generally horizontal (θ<45°), advance of the interface vertically can be calculated using Eq.32. Consider a small time step Δt, employing central difference approximation in space and forward difference approximation in time, Eq.31 and Eq.32 can be discretized as follows:

$$\frac{q_{i+1}^n - q_{i-1}^n}{y_{i+1}^n - y_{i-1}^n} = -\phi \Delta S_o \frac{x_i^{n+1} - x_i^n}{\Delta t} \quad \text{.....(34)}$$

$$\frac{q_{i+1}^n - q_{i-1}^n}{x_{i+1}^n - x_{i-1}^n} = \phi \Delta S_o \frac{y_i^{n+1} - y_i^n}{\Delta t} \quad \text{.....(35)}$$

Where superscript n and n+1 stands for the present time level t and the next time level $t+\Delta t$, respectively. The subscripts i indicate the i^{th} interface node being investigated and its neighboring interface nodes are denoted by the subscripts i-1 and i+1, as shown in Figure 2-3. The notation x and y presents the coordinates of each interface node at different time levels. Eq.34 and Eq.35 are used to advance the horizontal and vertical movement for each node explicitly with time.

5. Calculate the length (approximated by L_i in Figure 2-3) between two neighboring nodes around i:

$$L_i = \sqrt{(x_{i-1} - x_{i+1})^2 + (y_{i-1} - y_{i+1})^2} \quad \text{.....(36)}$$

Similarly, the interface angle θ for grid node i can be evaluated using the trigonometric relation in Eq.37:

$$\theta_i = arcsin(\frac{y_{i-1} - y_{i+1}}{L_i}) \quad \text{.....(37)}$$

6. Calculate the advancing velocity of interface using mass balance equation as shown in Eq.38:

$$U = -\frac{1}{\phi \Delta S_o} \frac{\partial q}{\partial L} \quad \text{.....(38)}$$

The above equation can be discretized as follows:

$$U_i^n = -\frac{1}{\phi \Delta S_o} \frac{q_{i+1}^n - q_{i-1}^n}{L_i^n} \quad \text{.....(39)}$$

7. Update the value of γ_m for the next time step. The value of D_s is replaced by a constant average D_{savg}. Eq.29 can now be discretized as in Eq.40:

$$\frac{\gamma_{m,i}^{n+1}-\gamma_{m,i}^{n}}{\Delta t}=\frac{1}{\sqrt{\pi}(\phi S_o)_i^n}\left(\frac{\phi S_o D_{savg}}{\gamma_{m,i}^{n}}-U_i^n\right) \quad \text{.....(40)}$$

8. Use new mass penetration calculated in step 7 and steps 2 to 7 until the final time.

Results and Discussion

In this section, two case studies are presented in which results obtained from the proxy model are compared to published experimental observations.

Case study 1: Comparison with experimental data for Athabasca and Suncor bitumen sample

Butler and Mokrys (1989) performed a series of Hele-Shaw cell experiments using toluene as the solvent, in which the glass cell was constructed using two closely assembled plates that were separated by a spacing *b*. The equivalent permeability for this equipment was determined using Eq.6. The Hele-Shaw cell was filled with Athabasca or Suncor bitumen and exposed on one side to toluene solvent injected from a linear source at 20°C and atmospheric pressure. Other experimental conditions and parameters are given in **Table 2-1**.

The overall diffusion coefficient D_o for Hele-Shaw experiment was obtained by the static-free diffusion method for both Athabasca and Suncor bitumen samples at 20°C. The integral value of N_s was calculated in their work (Butler and Mokrys 1989) as 9.44×10^{-7} for Athabasca oil and 2.50×10^{-6} for Suncor oil. These values are used in this case study.

This experiment is simulated using the proxy model described in the previous section using a grid of 12×9×1 blocks with Δx and Δy equal to 1cm.The total simulation time was 67 hours with a time step of 1 minute, and the execution time was about 2 seconds using the University of Alberta's Numerical and Statistical Server with two 3GHz quad core Xeon processors and 64 GB RAM.

Oil drainage rate and the chamber shape obtained with our proxy are compared to the experimental observations. **Figure 2-4** presents a comparison of solvent-bitumen interface position between the laboratory photographs and the proxy model. The solid lines represent the chamber boundary identified from photographs of a typical cross section taken when an Athabasca bitumen sample was drained by toluene. At the early time, the boundary of solvent chamber is almost vertical and the interface tends to advance horizontally, hence Eq.34 is used to determine the interface position at the next time step. Due to a stronger gravitational force being exerted along a vertical interface, the flow rate is higher at this time. During the spreading period, the assumption of steady-state flow is reasonable and thus the forecasted interface matches quite well with experimental observation. Once the interface has reached the no-flow boundary at the other end of the Hele-Shaw cell, solvent chamber starts to progress towards the bottom. The steady-state assumption may be invalid during this boundary-dominated flow period; therefore, the predicted interface position shows a larger discrepancy with experimental measurement. Nevertheless, interface positions obtained from the proxy model demonstrate reasonable agreement with those observed from the experiment.

A plot of predicted solvent chamber growth for the whole drainage process over 67.5 hours with a time interval of 6000s (100min) is shown in **Figure 2-5**. It is interesting to note that the solvent chamber shape for VAPEX is similar to the steam chamber shape in SAGD (Butler 1985), illustrating the analogy between two processes. As time increases, the near vertical portion shortens and the "S-curve" portion flattens out. Drainage starts at the top of the Hele-Shaw cell and the solvent chamber expands along the top and progresses downward.

The producing oil flow rate can also be predicted from the proxy model. As the diluted oil starts to drain by gravity, the flow is directed downward along the interface, and the flow rate at each node calculated by Eq.16will cumulate downward to the bottom node. As a result, the flow rate q determined using Eq.16 at the bottom interface node can be treated as the total drainage rate. It is comparable to the constant total flow rate Q predicted by Eq.21. The comparison of average bottom node flow rate q, predicted total flow rate Q and experimental observed flow rate is listed in **Table 2-2**. Predictions from the proposed proxy corroborate with the lab data and validate the predictability of the proxy model for a homogeneous case.

Figure 2-6 illustrates the change in q of bottom interface node. It indicates that the rate of oil drainage increases slightly at the beginning as mass migrates horizontally. Higher velocities near the injection point increases both convection and mixing between solvent and bitumen, accelerating the drainage of the mobile bitumen solution from interface to the producer. After a time of about 200 minutes, the flow rate reaches a maximum value; after reaching this peak value,

the flow rate declines slowly as the solvent-bitumen interface extends horizontally and convection becomes less important. **Figure 2-7** gives an intuitive illustration of element flow rate change with time. At a given time, the oil cumulates along the interface toward to producer located at the bottom, resulting in an increasing trend of flow rate from top to the bottom.

In **Figure 2-8** and **Figure 2-9**, total drainage or production between experimental data and proxy-predicted values are compared at different permeability for the Hele-Shaw model. Provided that all other parameters are kept constant, and a linear relationship between Q and $k_o^{0.5}$ is attained, in accordance with Eq.21. The results also indicate good agreement between proxy model predictions with the experimental data. It should be noted that the permeability values used in Figures 2-8 and Figure 2-9 are within the range of observed values for typical oil sands reservoirs; those high-permeability Hele-Shaw experiments presented by Butler and Mokrys (1989) are excluded.

In Figure 2-8, a little deviation is observed for the Athabasca bitumen sample – a higher value is predicted from the proxy than the experimental data. This discrepancy is also mentioned by Butler and Mokrys (1989) in their earlier work. A modification based on the "Tandrain" assumption introduced by Butler and Stephens (1981) stated that the factor "2" within square root sign in Eq.21 should be replaced by "1.5" for SAGD process; same modification can be used here for the VAPEX case. Readers should refer to the references for additional theoretical discussions and details.

Sensitivity Analysis of Initial Mass Penetration

The calculation method described in the previous section has introduced a new parameter – mass penetration, denoted as γ_m. As discussed in the previous section, the criterion for its initialization at time zero often seem arbitrary as we refer to discussion regarding the analogous heat penetration parameter found in SAGD literature. In this study, different initialization schemes of γ_m as shown in **Figure 2-10** are tested to assess its sensitivity.

In the previous section, an initial mass penetration profile labeled as "Base case" was used. Since the producer and injector are located at the bottom of the reservoir, it is reasonable to expect that the solvent would penetrate further near the injector (Butler 1985). It has been demonstrated that a good match between predicted results with experimental values is obtained.

A sensitivity analysis using four other initial mass penetration distributions is conducted for the Athabasca bitumen sample. All other parameters remain the same. **Figure 2-11** shows the comparison of solvent-bitumen interface change for different cases. For a 67.5 hours drainage process, the interface predictions for these five different configurations are similar, suggesting that the initial mass penetration would have little influence on the interface position. **Figure 2-12** compares the predicted flow rate change for the four different initial mass penetration distributions. They all show a similar trend as observed in Figure 2-6.

Finally, **Table 2-3** summarizes the predicted flow rates for the four cases and the base case. Only a very small difference can be observed. It is noted that when using an initial profile with larger gradient, the predicted oil rate will increase

slightly. Again, these observations indicate that predictions of chamber growth and resulting flow rate are not overly sensitive to the initial mass penetration distribution. Our suggestion is that a distribution similar to the base case would suffice.

Sensitivity Analysis of Grid Size

A sensitivity analysis of grid size (resolution) is conducted. In addition to a base case with the original grid size of 1 cm, two new cases with grid sizes equal 1.5 cm and 0.5 cm are introduced. A comparison of the predicted solvent chamber growth for the 67.5 hours drainage process for the different grid sizes is shown in **Figure 2-13**. **Figure 2-14** compares the solvent-bitumen interface position among the three cases at a number of snapshots of time (with an interval of 13.5 hours). The predicted flow rates for the three cases are presented in **Figure 2-15**. This sensitivity analysis suggests that results obtained with the proxy do not seem to be overly sensitive to grid sizes. Only minor differences are observable by comparing the three cases. It is expected that a finer grid resolution would produce a smoother solvent-bitumen interface. The total execution time for each case is approximately two seconds.

Case study 2: Application to field-scale model for Peace River bitumen sample

In this case study, the proxy is applied to a field-scale model described by Das and Butler (1994 b), who proposed a procedure to scale-up production rates from

laboratory measurements to field-scale values for typical heavy oil and bitumen reservoirs. A new parameter called VAPEX parameter denoted by α was introduced in their work:

$$\alpha = \sqrt{2k_o g\phi\Delta S_o N_s} \quad \text{.....(41)}$$

It can be readily defined based on Eq.33 by incorporating all reservoirs, solvent and bitumen properties together at a certain temperature and pressure condition. The VAPEX parameters for lab condition and field condition are related by Eq.42:

$$\alpha_{(f)} = \alpha_{(l)}\sqrt{\frac{k_{o(f)}\phi_{(f)}\Delta S_{o(f)}}{k_{o(l)}\phi_{(l)}\Delta S_{o(l)}}} \quad \text{.....(42)}$$

Where the subscript *l* and *f* represents lab and field conditions, respectively.

In a reservoir, oil will drain to the producer from both sides and total oil rate given by Eq.33 should be doubled. Also, Hele-Shaw cell height *h* is replaced by total reservoir height *H* in Eq.33. Thus, the flow rate from the horizontal production well of length L_w can be given by Eq.43:

$$Q_{(f)} = 2L_w\alpha_{(f)}\sqrt{H} \quad \text{.....(43)}$$

Das and Butler (1994 b) conducted a similar experiment in Hele-Shaw cell by using vaporized propane to extract oil from a Peace River bitumen sample. Eq.42 and Eq.43were then applied to scale-up the flow rate obtained at lab conditions to practical field conditions. Relevant input parameters for this case study are shown in **Table 2-4**, while predicted flow rates at both lab and field conditions using the proxy are shown in **Table 2-5**.

$\alpha_{(l)}$ was measured as 1.95×10^{-3} $m^{1.5}$/hr (or $0.0468 m^{1.5}$/d) at 21°C and a cell pressure of 0.8739 MPa for Peace River bitumen using propane as solvent (Das and Butler 1994 b). The scaled-up VAPEX parameter $\alpha_{(f)}$ was estimated from Eq.42 to be $7\times10^{-4} m^{1.5}$/d, giving a field production rate of 9.25 m^3/d. Predictions from the proxy model for both experimental and field production rates are in good agreement with those reported by Das and Butler (1994 b). This indicates a good potential of further application in the reservoir case.

Conclusions

1. A proxy model has been proposed to model solvent transport and oil recovery for the VAPEX process. The model is based on Butler's analytical solution that was developed for the conditions applicable for typical Hele-Shaw cell experiments. An explicit calculation sequence of the analytical equations is presented to predict the solvent-oil interface position and producing oil rate as a function of time. The original formulations have been extended to account for porous medium properties. In addition, a new parameter of mass penetration is introduced. The derivations of the proxy formulations follow closely of those developed for its SAGD analog.

2. The results obtained from the proposed proxy shows good agreement with published experimental observations in terms of solvent-bitumen interface position and oil production rate. The proxy model also shows a significant reduction in terms of computational efforts.

3. It also shows a good match to results obtained with scale-up relationships, implying promising future application to field cases.

4. A thorough sensitivity analysis on the mass penetration distribution has been performed and it is concluded that a linear relationship as employed in the base case would suffice.

5. An important contribution from this work is that process physics are built directly into this proxy, giving it an advantage over other data-driven modeling approaches (i.e., regression). It can be used as an efficient alternative to expensive detailed flow simulations. This type of proxy models can also be easily integrated in existing workflows to optimize production scenarios. It presents an important potential for assessing the uncertainty in reservoir properties on effective mass transfer and the ensuing recovery performance, as well as assisting decisions-making for future pilot and field development planning.

Acknowledgements

This research was supported by the Sustainable Technologies for Energy Production Systems (STEPS) program managed by the Petroleum Technology Research Centre (PTRC). The authors would also like to thank the Computer Modeling Group (CMG) for providing the academic licenses for GEM and the University of Alberta for granting access to the Numerical and Statistical Servers.

Nomenclature

a = experimental constant coefficient proposed by Butler and Mokrys (1989)

b = Hele-Shaw cell spacing, μm

g = gravity acceleration, m/d^2 (g=7.3×10^{10}m/d^2)

h = vertical drainage height for Hele-Shaw cell, m

k_o = effective oil permeability of reservoir, m^2

m_r = mass of solvent accumulated in reservoir, kg

q = cell flow rate for a certain grid block, m^2/d

t = time, days

A = cross-section area of the steam chamber at time t, m^2

C_s^* = solvent concentration distribution in the diffusion layer

C_s = solvent concentration (volume fraction) at a distance ξ from interface

C_{sc} = solvent concentration in the edge of solvent chamber

C_{sr} = solvent concentration in the reservoir

D_o = overall diffusion coefficient of solvent, m^2/d

D_s = intrinsic diffusion coefficient of solvent, m^2/d

D_{savg} = average diffusion coefficient of solvent, m^2/d

H = total reservoir thickness, m

L_i = length along interface between two neighboring nodes around i, m

L_w = length of horizontal production well, m

N_s = dimensionless integral

q = flow rate at a particular location per unit length, m^3/d·m

Q = total oil drainage rate per unit length of well, m^3/d·m

S_o = oil saturation, %

S_{oi} = initial oil saturation, %

S_{or} = residual oil saturation, %

ΔS_o= initial oil saturation minus residual oil saturation, %

U = frontal advancing velocity of interface, m/d

V = average drainage velocity due to gravity, m/d

Greek symbols:

α =VAPEX parameter

ϕ = porosity, %

γ_m = mass penetration, m

μ_b = dynamic viscosity of bitumen in solution, kg/m d

θ = the angle of interface from horizontal, °

$\Delta\rho$ = density difference between solvent and bitumen, kg/m^3

Ω = cementation factor

ξ = distance from interface, m

Subscripts:

f = at field condition

i = grid block index

l = at lab condition

max = maximum

Superscripts:

n = time level

References

Azad, A. and Chalaturnyk, R.J. 2010. A Mathematical Improvement to SAGD using Geomechanical Modeling. *Journal of Canadian Petroleum Technology* **49**(10): 53-64. Doi: 10.2118/141303-PA

Boustani, A. 2001. Investigation of Interfacial Mass Transfer in Vapor Extraction Process. Master'sThesis. University of Calgary, AB, Canada.

Butler, R.M. and Stephens, D.J. 1981. The Gravity Drainage of Steam-heated Heavy Oil to Parallel Horizontal Wells. *Journal of Canadian Petroleum Technology* **20**(2): 90-96. Doi: 10.2118/81-02-07

Butler, R.M. 1985. A New Approach to the Modeling of Steam-Assisted Gravity Drainage. *Journal of Canadian Petroleum Technology* **24**(3): 42-51. Doi: 10.2118/85-03-01

Butler, R.M. and Mokrys, I.J. 1989. Solvent Analog Model of Steam Assisted Gravity Drainage. *AOSTRA Journal of Research* **5**(1): 17-32.

Das, S.K. and Butler, R.M. 1994 (a). Investigation of 'VAPEX' Process in a Packed Cell Using Butane As a Solvent. Canadian SPE/CIM/CANMET International Conference on Recent Advances in Horizontal Well Applications, Calgary, Alberta, Canada, 20-24 March. Doi: 10.2118/HWC-94-47

Das, S.K. and Butler, R.M. 1994 (b). Effect of Asphaltene Deposition on the Vapex Process: A Preliminary Investigation Using a Hele-Shaw Cell. *Journal of Canadian Petroleum Technology* **33**(6): 39-45. Doi: 10.2118/94-06-06

Das, S.K. and Butler, R.M. 1998. Mechanism of the Vapor Extraction Process for Heavy Oil and Bitumen. *Journal of Petroleum Science and Engineering* **21**(1-2): 43-59. Doi: 10.1016/S0920-4105(98)00002-3

Das, S.K. 1998. Vapex: An Efficient Process for the Recovery of Heavy Oil and Bitumen. *SPE Journal* **3**(3): 232-237. Doi: 10.2118/50941-PA

Das, S.K. 2005. Diffusion and Dispersion in the Simulation of Vapex Process.SPE/PS-CIM/CHOA International Thermal Operations and Heavy Oil Symposium, Calgary, Alberta, Canada, 1-3 November. Doi: 10.2118/97924-MS

Energy Resources Conservation Board. 2012. *ST98-2012: Alberta's Energy Reserves 2011 and Supply/Demand Outlook 2012-2021*, June 2012.

Genuchten, M.T.V. and Alves, W.J. 1982. Analytical Solutions of the One-Dimensional Convective-Dispersive Solute Transport Equation. *U.S. Department of Agriculture Technical Bulletin* **1661**: 9-10.

Lamb, H. 1932. *Hydrodynamics,* 6th edition. Dover Publications, New York.

Luhning, R.W., Das, S.K., Fisher, L.J., Bakker, J., Grabowski, J., Engleman, J.R., Wong, S., Sullivan, L.A., and Boyle, H.A. 2003. Full Scale Vapex Process – Climate Change Advantage and Economic Consequences. *Journal of Canadian Petroleum Technology* **42**(2): 29-34. Doi: 10.2118/03-02-02

Nghiem, L.X., Kohse, B.F., and Sammon, P.H. 2001. Compositional Simulation of the VAPEX Process.*Journal of Canadian Petroleum Technology* **40**(8): 54-61. Doi: 10.2118/01-08-05

Ogata, A. and Banks, R.B. 1961. A Solution of the Differential Equation of Longitudinal Dispersion in Porous Media. *U.S.Geological Survey Professional Paper* **411-A**, A1-A9.

Okazawa, T. 2009. Impact of Concentration-Dependence of Diffusion Coefficient on VAPEX Drainage Rates. *Journal of Canadian Petroleum Technology* **48**(2): 47-53. Doi: 10.2118/09-02-47

Reis, J.C. 1992. A Steam-Assisted Gravity Drainage Model for Tar Sands: Linear Geometry. *Journal of Canadian Petroleum Technology* **31**(10): 14-20. Doi: 10.2118/92-10-01

Jaiswal, D.K., Kumar, A. and Yadav, R.R. 2011. Analytical Solution to the One-Dimensional Advection-Diffusion Equation with Temporally Dependent Coefficients. *Journal of Water Resource and Protection* **3**: 76-84. Doi: 10.4236/jwarp.2011.31009

Stosur, G.J.1995. Heavy Oil Recovery in The Low Oil Price Regime. Sixth UNITAR Intl. Conference on Heavy Crude and Tar Sands, Houston, Texas, USA, 12-17 February.

Vanegas, J.W.P., Deutsch, C.V. and Cunha, L.B. 2008. Uncertainty Assessment of SAGD Performance Using a Proxy Model Based on Butler's Theory.SPE Annual Technical Conference and Exhibition, Denver, Colorado, USA, 21-24 September. Doi: 10.2118/115662-MS

Yazdani, A. and Maini, B.B. 2008. Modeling of the VAPEX Process in a Very Large Physical Model. *Energy & Fuels* **22**(1): 535-544. Doi: 10.1021/ef700429h

Tables

Table 2-1. Summary of Hele-Shaw cell experimental set-up in Butler and Mokrys' work (1989)

Hele-Shaw cell geometry		
Height (h)	Width	Cell spacing (b)
cm	cm	μm
12	9	114.3
Bitumen and Solvent Densities at 20 ℃		
Athabasca bitumen	Suncor bitumen	Toluene solvent
g/cm^3	g/cm^3	g/cm^3
1.0283	1.003	0.866
Other Properties		
Porosity(ϕ)	Initial oil saturation(S_{oi})	Residual oil saturation (S_{or})
1	1	0

Table 2-2. Comparison of flow rate between proxy prediction and Hele-Shaw cell experimental observation for the Athabasca bitumen sample in Case Study 1

Permeability (k_o)		Height (h)		Temperature	
Darcy		cm		℃	
1103		12		20	
Predicted flow rate of the bottom interface node (Eq.16)		Predicted total flow rate (Eq.21)		Experimental flow rate	
cm^2/h	cm^2/s	cm^2/h	cm^2/s	cm^2/h	cm^2/s
1.52	4.21×10^{-4}	1.77	4.92×10^{-4}	1.54	4.28×10^{-4}

Table 2-3. Sensitivity analysis of predicted oil flow rate to γ_m initialization for the Athabasca oil sample in Case Study 1

Initial mass penetration distribution(γ_m)	Average flow rate at the bottom grid node calculated using Eq.16
	cm^2/s
Base case	4.2088×10^{-4}
Case1: Linear distribution (large gradient)	4.2050×10^{-4}
Case2: Linear distribution (small gradient)	4.2002×10^{-4}
Case3:Non-linear distribution (small gradient)	4.2062×10^{-4}
Case4:Non-linear distribution (large gradient)	4.2109×10^{-4}

Table 2-4. Input data for the Peace River bitumen under experimental and field conditions for Case Study 2

Input parameter	Experimental case	Field case
Height(m)	0.08	45
Porosity	1	0.35
Permeability (Darcy)	1344	1
ΔS_o	1	0.86

Table 2-5. Oil rates estimated using different methods for the Peace River bitumen sample in Case Study 2

	Experimental flow rate	Field production rate
	m^2/s	m^3/d
Das and Butler (1994 b)	1.53×10^{-7}	9.25
Proxy model (Eq.43)	1.60×10^{-7}	9.40

Figures

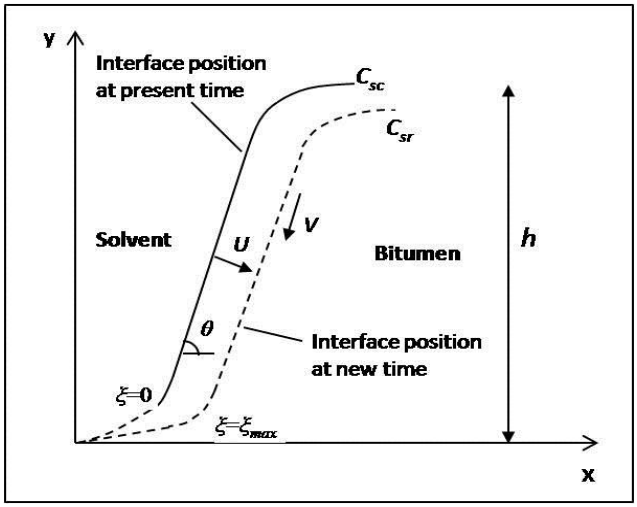

Figure 2-1. Schematic of solvent-bitumen interface (adapted from Butler and Mokrys 1989).

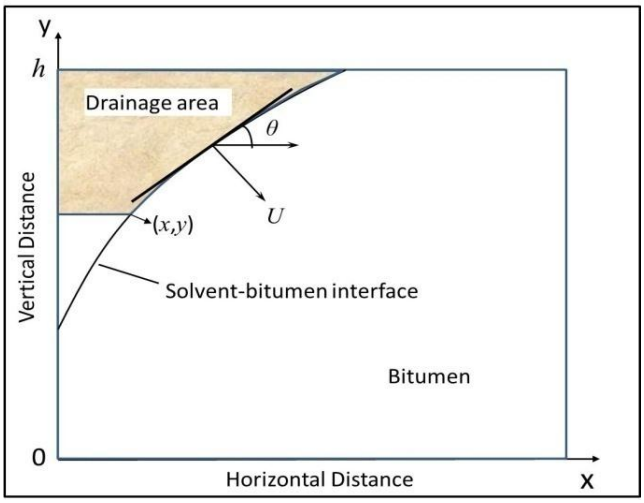

Figure 2-2. Illustration of the drainage area observed in a Hele-Shaw cell VAPEX experiment (adapted from Butler and Mokrys 1989).

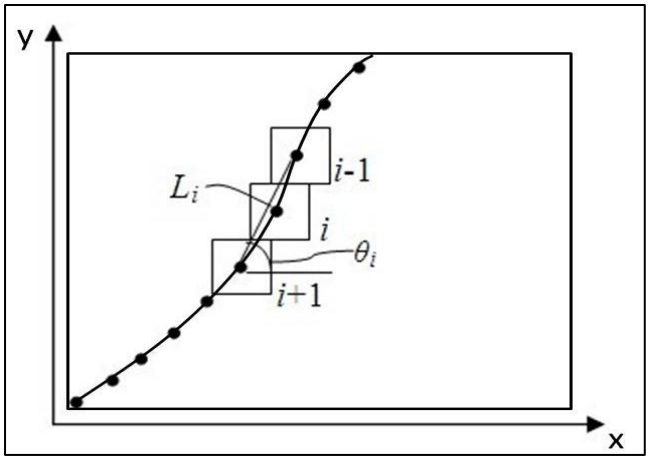

Figure 2-3. Schematic of the discretizing procedure along the solvent-bitumen interface. Solid circles represent the centers of each grid block where the interface nodes are located.

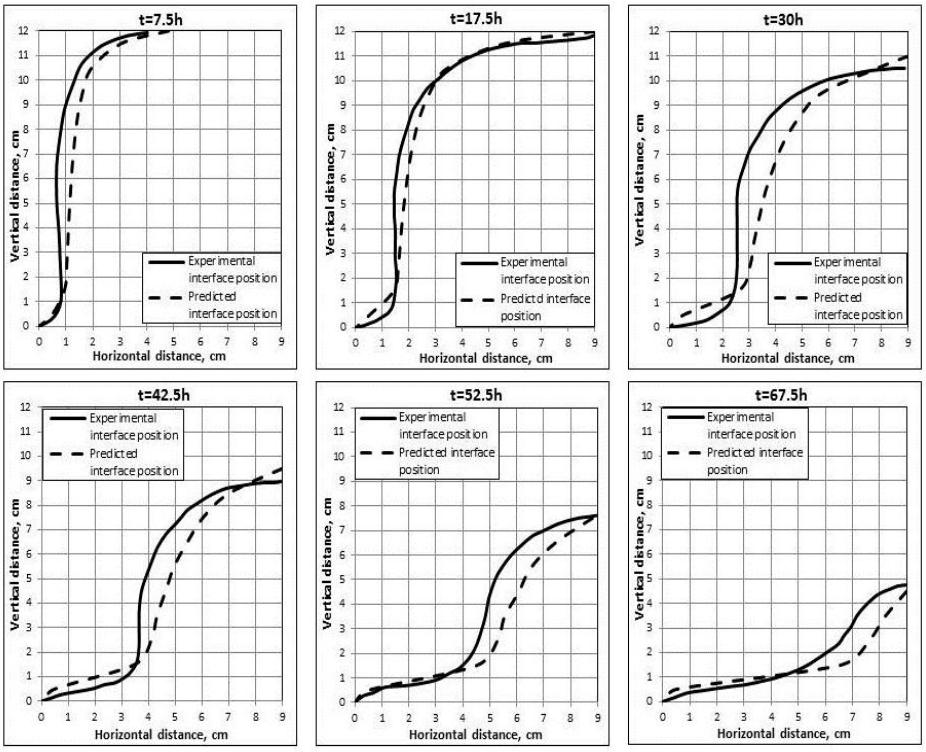

Figure 2-4. Comparison of solvent-bitumen interface position between the Hele-Shaw experimental results (Butler and Mokrys 1989) and proxy model predictions for the Athabasca bitumen sample.

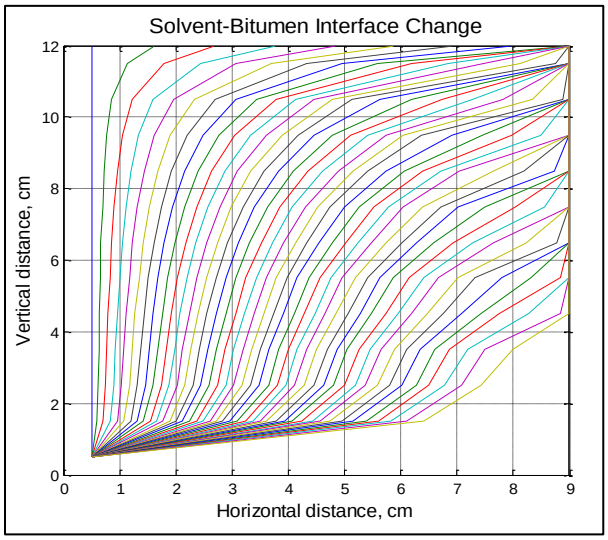

Figure 2-5. Predicted solvent chamber growth for Athabasca sample over a production time of 67.5 hours.

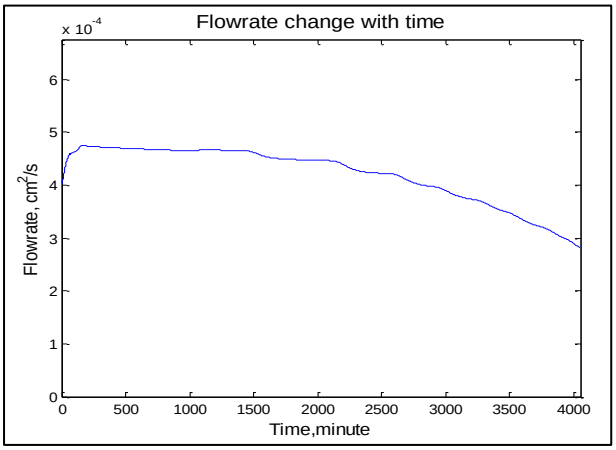

Figure 2-6. Flow rate as a function of time for the Athabasca bitumen sample over a production time of 67.5 hours.

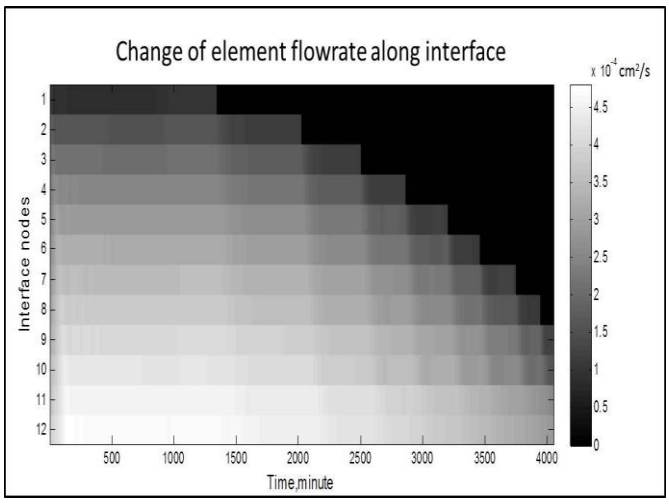

Figure 2-7. Element flowrate at each interface node as a function of time for the Athabasca bitumen sample over a production time of 67.5 hours.

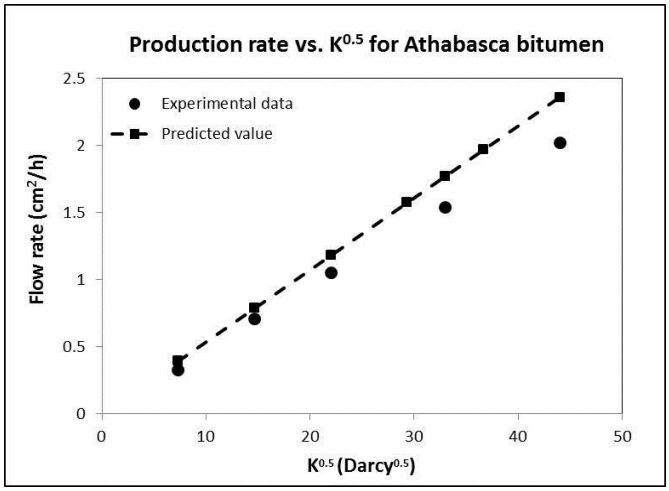

Figure 2-8. Comparison of production rates between experimental data and proxy-predicted values for the Athabasca bitumen sample using different permeability values.

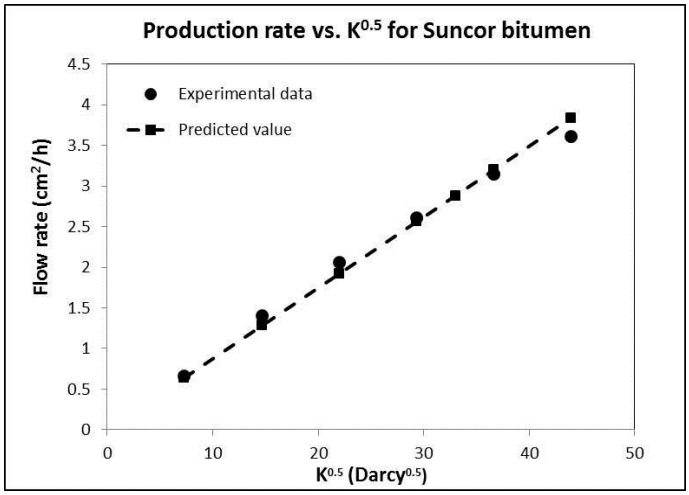

Figure 2-9. Comparison of production rates between experimental data and proxy-predicted values for the Suncor bitumen sample using different permeability values.

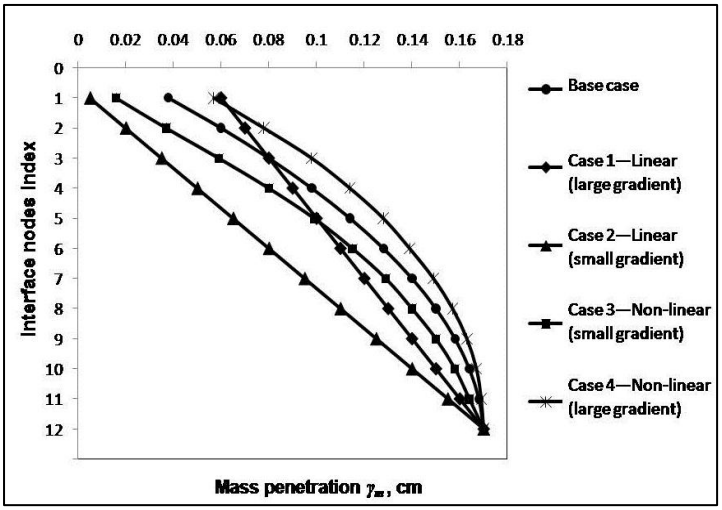

Figure 2-10. Different initial mass penetration distributions for modeling the Hele-Shaw cell experiment with Athabasca bitumen sample in Case Study 1.

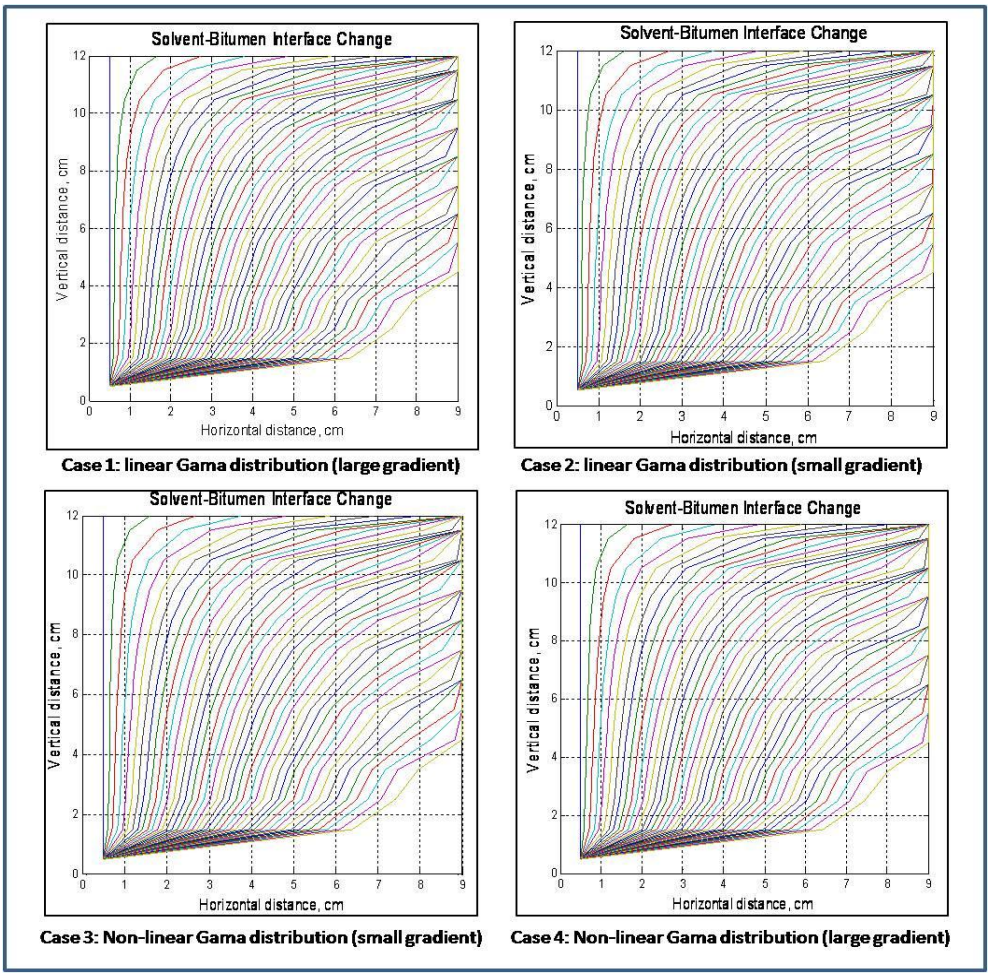

Figure 2-11. Comparison of the resultant interface change for the different initial mass penetration distributions shown in Figure 2-10.

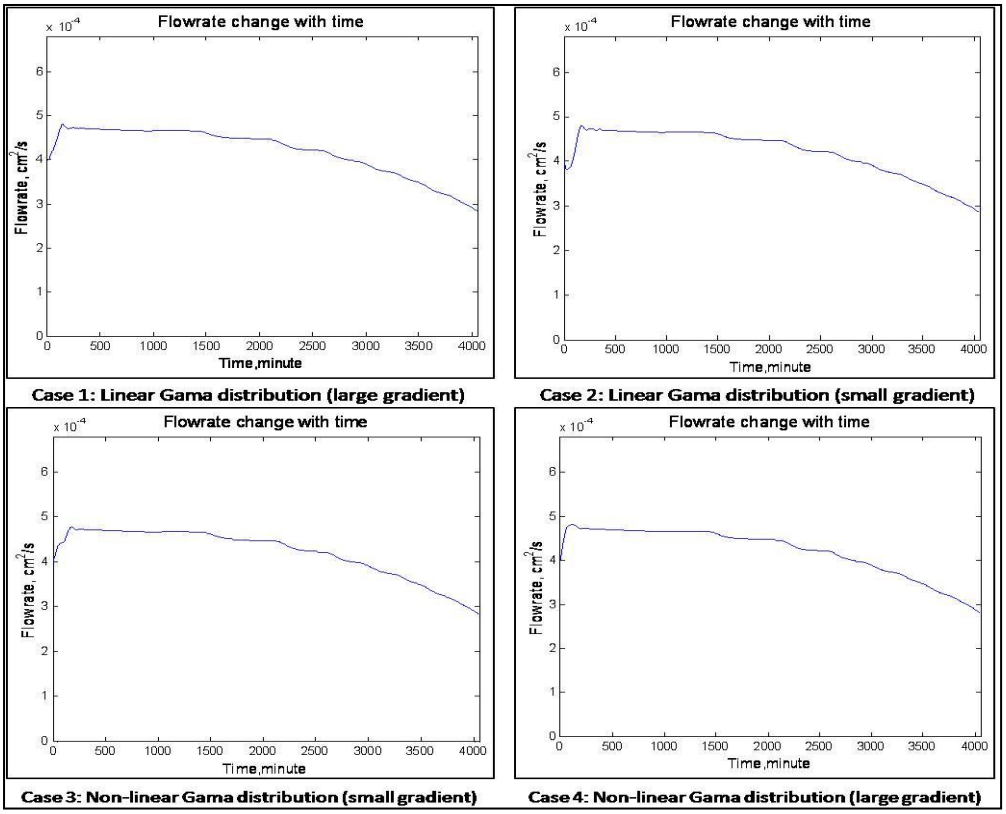

Figure 2-12. Comparison of the resultant flow rate change over a production time of 67.5 hours for the different initial mass penetration distributions shown in Figure 2-10.

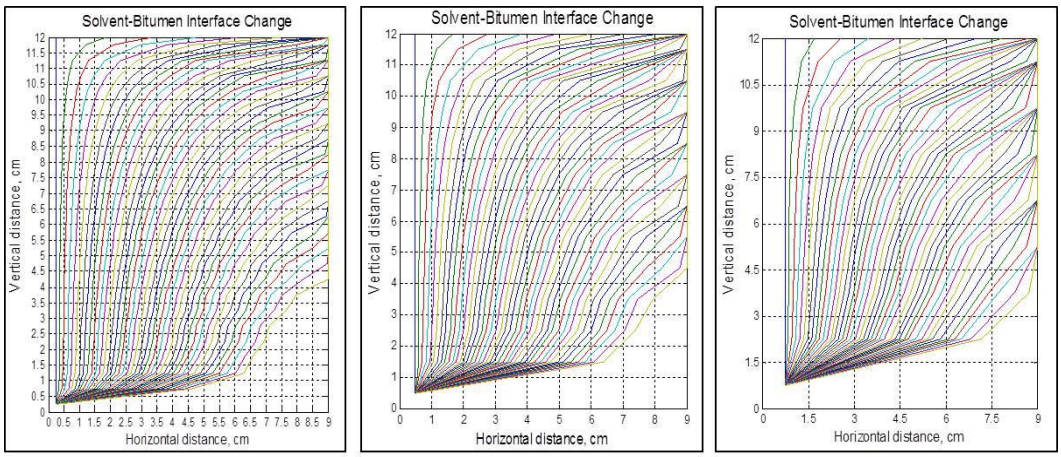

Decrease grid size: 0.5cm Original grid size: 1cm Increase grid size: 1.5cm

Figure 2-13. Solvent chamber growth for Athabasca sample as predicted by the proxy model over a production time of 67.5 hours using three different grid sizes.

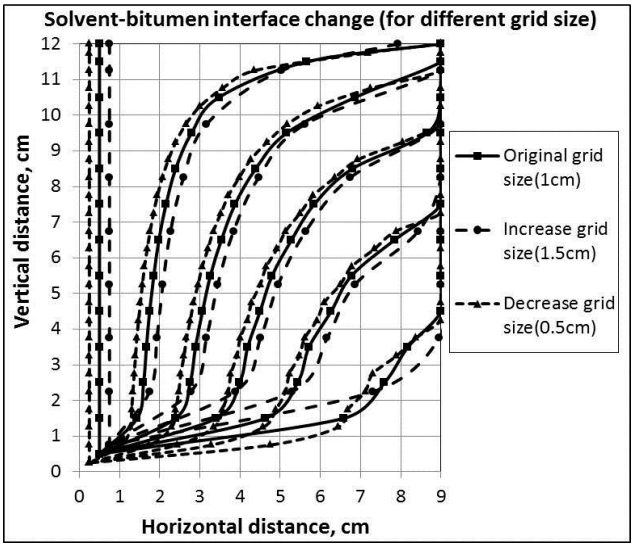

Figure 2-14. Comparison of solvent-bitumen interface advancement at five snapshots of times for different grid sizes.

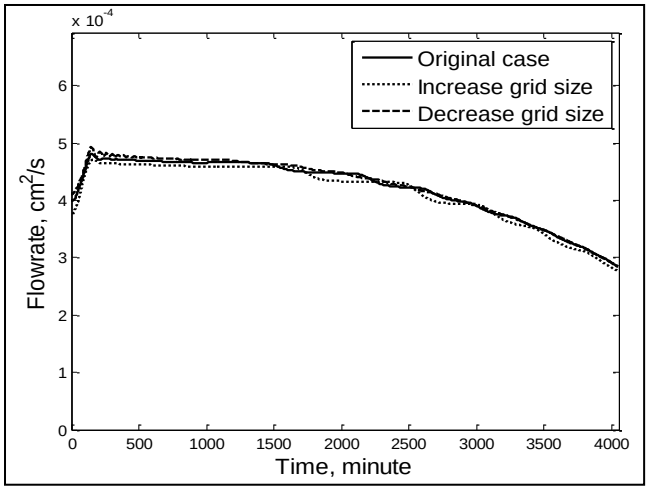

Figure 2-15. Comparison of the resultant flow rate change over a production time of 67.5 hours for the different grid sizes shown in Figure 2-14.

Appendix

Section A. Derivation of mass penetration rate with time

We begin by performing a mass balance over the cell element in Figure 2-1. Mass of solvent is transported into the bitumen with a forward flux:

$$Mass(\ forward) = -\phi S_o D_s\big|_{C_s=C_{sc}} \rho_s \left(\frac{\partial C_s}{\partial \xi}\right)_{\xi=0} \quad \text{.....(A1)}$$

Mass of solvent being left behind in the reservoir because of the forward motion of the front:

$$Mass(left) = U\rho_s\left(C_{sc} - C_{sr}\right) \quad \text{.....(A2)}$$

Thus net result of these two fluxes is the rate of mass accumulated ahead of the front, as shown in Eq.A3:

$$\frac{1}{A}\frac{dm_r}{dt} = -\phi S_o D_s\big|_{C_s=C_{sc}} \rho_s \left(\frac{\partial C_s}{\partial \xi}\right)_{\xi=0} - U\rho_s\left(C_{sc} - C_{sr}\right) \quad \text{.....(A3)}$$

Eq.A3 can be written in terms of the mass penetration variable γ_m as in Eq.A4:

$$\frac{d(\frac{\partial m_r}{\partial A})}{dt} = \frac{d(\gamma_m \phi S_o \rho_s (C_{sc} - C_{sr}))}{dt} = -\phi S_o D_s\big|_{C_s = C_{sc}} \rho_s \left(\frac{\partial C_s}{\partial \xi}\right)_{\xi=0} - U\rho_s (C_{sc} - C_{sr}) \,. \quad \text{(A4)}$$

Considering the term $\phi S_o \rho_s (C_{sc}\text{-}C_{sr})$ being constant with time and factoring it out of the derivative. Eq.A4 can be rearranged to obtain the mass penetration rate in Eq.A5:

$$\frac{d\gamma_m}{dt} = \frac{-D_s\big|_{C_s = C_{sc}} \left(\frac{\partial C_s}{\partial \xi}\right)_{\xi=0}}{(C_{sc} - C_{sr})} - \frac{U}{\phi S_o} \quad \text{(A5)}$$

Define the dimensionless solvent concentration distribution C_s* as:

$$C_s^{\,*} = \frac{C_s - C_{sr}}{C_{sc} - C_{sr}} \quad \text{(A6)}$$

Then the solvent concentration gradient $\frac{\partial C_s^{\,*}}{\partial \xi}$ can be expressed as:

$$\frac{\partial C_s^{\,*}}{\partial \xi} = \frac{1}{C_{sc} - C_{sr}} \frac{\partial C_s}{\partial \xi} \quad \text{(A7)}$$

At solvent-bitumen interface where ξ= 0, Eq.A7 can be expressed as:

$$\left(\frac{\partial C_s^{\,*}}{\partial \xi}\right)_{\xi=0} = \frac{1}{C_{sc} - C_{sr}} \left(\frac{\partial C_s}{\partial \xi}\right)_{\xi=0} \quad \text{(A8)}$$

Substituting Eq.A8 in Eq.A5 gives:

$$\frac{d\gamma_m}{dt} = -D_s\big|_{C_s = C_{sc}} \left(\frac{\partial C_s^{\,*}}{\partial \xi}\right)_{\xi=0} - \frac{U}{\phi S_o} \quad \text{(A9)}$$

The above equation can be solved by following the approximation in Butler (1985) and assessing the solvent concentration gradient $\left(\frac{\partial C_s^*}{\partial \xi}\right)_{\xi=0}$ at two extreme cases:

1) Steady state case: $\frac{d\gamma_m}{dt} = 0$, and the solvent concentration gradient is given:

$$\left(\frac{\partial C_s^*}{\partial \xi}\right)_{\xi=0} = -\frac{U}{\phi S_o D_s|_{C_s=C_{sc}}} \quad \text{.....(A10)}$$

With diffusion coefficient D_s being constant, substitute Eq.28 into Eq.A10 to obtain Eq.A11:

$$\left(\frac{\partial C_s^*}{\partial \xi}\right)_{\xi=0} = -\frac{1}{\gamma_m} \quad \text{.....(A11)}$$

2) Stationary interface case: C_s=C_{sc} at ξ=0 at $t \geq 0$. The solvent concentration distribution is given by analytical solution to the one-dimensional advection-dispersion solute transport equation for the stated boundary and initial conditions (Ogata and Banks 1961, Genuchten and Alves 1982, Jaiswal et al. 2011):

$$C_s^* = erfc\left(\frac{\xi}{2\sqrt{\phi S_o D_s t}}\right) \quad \text{.....(A12)}$$

The derivative of C_s* with respect to ξ evaluated at the interface is then given by Eq.A13:

$$\left(\frac{\partial C_s^*}{\partial \xi}\right)_{\xi=0} = -\frac{2e^{-\left(\frac{\xi}{2\sqrt{\phi S_o D_s t}}\right)^2}}{\sqrt{\pi}}\left[\frac{1}{2\sqrt{\gamma_m{}^2}}\right] = -\frac{1}{\sqrt{\pi}\gamma_m} \quad \text{.....(A13)}$$

In reality, it is expected that the actual interface advancing velocity would be bounded between the two limiting cases. Therefore, Butler (1985) suggested that

in the case of SAGD, the temperature gradient at the interface can be approximated by assuming that it varies linearly between the two limits. We propose here that a similar assumption can be made to estimate the actual concentration gradient at the interface ($\xi = 0$) for VAPEX as in Eq.A14 (similar to Eq.19 in Butler 1985):

$$\left(\frac{\partial C_s^*}{\partial \xi}\right)_{\xi=0} = -\frac{1}{\sqrt{\pi}\gamma_m} - \left(1 - \frac{1}{\sqrt{\pi}}\right)\frac{U}{\phi S_o D_s} \quad \text{..... (A14)}$$

Eq.A14 is still valid for the two extreme cases. If U = 0, the limiting case of stationary interface applies, and Eq.A14 would yield the same result as Eq.A13; if U is constant, the limiting case of steady-state applies, and Eq.A14 would be equivalent to Eq.A11. Finally, we substitute Eq.A14 into Eq.A9. The mass penetration rate can be obtained:

$$\frac{d\gamma_m}{dt} = \frac{D_s\big|_{C_s=C_{sc}}}{\sqrt{\pi}\gamma_m} + \frac{UD_s\big|_{C_s=C_{sc}}}{\phi S_o D_s}\left(1 - \frac{1}{\sqrt{\pi}}\right) - \frac{U}{\phi S_o} \quad \text{..... (A15)}$$

Eq.A15 can be rearranged and simplified to obtain the expression for dγ_m/dt as shown in Eq.29 for a porous medium:

$$\frac{d\gamma_m}{dt} = \frac{D_s}{\sqrt{\pi}\gamma_m} - \frac{1}{\sqrt{\pi}}\frac{U}{\phi S_o} = \frac{1}{\phi S_o\sqrt{\pi}}\left(\frac{\phi S_o D_s}{\gamma_m} - U\right) \quad \text{..... (29)}$$

If ϕ and S_o are set to unity as in the case for a Hele-Shaw cell, the above equation becomes Eq.17 as presented in the formulation for the original Hele-Shaw model:

$$\frac{d\gamma_m}{dt} = \frac{1}{\sqrt{\pi}}\left(\frac{D_s}{\gamma_m} - U\right) \quad \text{..... (17)}$$

Section B. Derivation of the total production rate for half-side drainage

The vertical and horizontal displacement of the interface at any point is given by Eq.31 and Eq.32, respectively:

$$\left(\frac{\partial q}{\partial y}\right)_t = -\phi \Delta S_o \left(\frac{\partial x}{\partial t}\right)_y \quad \text{.....(31)}$$

$$\left(\frac{\partial q}{\partial x}\right)_t = \phi \Delta S_o \left(\frac{\partial y}{\partial t}\right)_x \quad \text{..... (32)}$$

Interface geometry gives:

$$U = -\cos\theta \left(\frac{\partial y}{\partial t}\right)_x \quad \text{..... (B1)}$$

Substituting Eq.B1 into Eq.31gives:

$$\left(\frac{\partial q}{\partial x}\right)_t = \frac{\phi \Delta S_o U}{-\cos\theta} \quad \text{..... (B2)}$$

Eq.B2 can be rearranged to obtain the expression for U as:

$$U = -\frac{\cos\theta}{\phi \Delta S_o}\left(\frac{\partial q}{\partial x}\right)_t \quad \text{..... (B3)}$$

Substitute Eq.B3 into Eq.9 to obtain:

$$q = \frac{k_o g \sin\theta}{U} N_s = -\frac{k_o g \sin\theta}{\frac{\cos\theta}{\phi \Delta S_o}\left(\frac{\partial q}{\partial x}\right)_t} N_s \quad \text{..... (B4)}$$

Also, from the interface geometry,

$$\frac{\sin\theta}{\cos\theta} = \frac{\partial y}{\partial x} \quad \text{..... (B5)}$$

Eq.B4 can be written as:

$$q = -\frac{k_o g \phi \Delta S_o}{\left(\frac{\partial q}{\partial y}\right)_t} N_s \quad \text{..... (B6)}$$

Integrating Eq.B6 by separation of variables would provide the total production rate for half-side drainage as presented in Eq.33 previously:

$$Q = \sqrt{2k_o g \phi \Delta S_o h N_s} \quad \text{.....(33)}$$

If ϕ and S_o are set to unity as in the case for a Hele-Shaw cell, the above equation becomes Eq.21 as shown previously:

$$Q = \sqrt{2k_o g h N_s} \quad \text{.....(21)}$$

Chapter 3: Semi-Analytical Proxy for Vapex Process Modeling in Heterogeneous Reservoirs[2]

Introduction

The high viscosity of Canadian heavy oil and bitumen poses a serious challenge for efficient recovery of this resource by conventional methods. Since the early 1990's, Vapex has emerged as a new method that attracted a great deal of attention in the oil industry (Das and Butler 1994). This method provides an environmental-friendly alternative to steam injection, especially for reservoirs with low thermal conductivity, overlying gas cap, underlying aquifer, high water saturation, low porosity, and thin pay zone, where heat loss to overburden/underburden or in-situ water is excessive.

Vapex process is a non-thermal bitumen recovery technique that is analogous to the commonly adopted SAGD (steam assisted gravity drainage) for heavy oil recovery. Vaporized solvent, instead of steam, is injected below the vapor pressure continuously into reservoir through a horizontal injection well. The viscosity of the bitumen around the injector decreases as the solvent dissolves into the oil, allowing the less viscous oil to drain to a horizontal production well near the bottom of the reservoir via gravitational force. Since mass transfer (diffusion/dispersion) of solvent into the in-situ is the primary recovery

[2]A version of this chapter was presented as the SPE HOCC conference and is currently under review by a referred journal: Shi. J. and Leung, Y.J. 2013. Physics-Based Proxy for Vapex Process Modeling in Heterogeneous Reservoirs. Paper 165558-MS presented at 2013 SPE Heavy Oil Conference, Calgary, Alberta, Canada, 11-13 June.

mechanism in Vapex, as opposed to heat transfer in SAGD (Forster 2008), it provides a more energy-efficient production strategy for bitumen compared to steam injection.

Descriptions of key recovery mechanisms and governing equations in Vapex have been studied by various researchers over the past 30 years (Das and Butler 1998). Butler and Mokrys (1989) presented and evaluated the initial physical model of the Vapex process in a series of Hele-Shaw cell experiments. Subsequent improvements to the process based on Hele-Shaw cell experiments have been proposed by many researchers over the years (Das and Butler 1994, Yazdani and Maini 2008). There have been many experimental works focusing on the effects of different system and operating parameters (i.e., model dimensions, permeability, solvent type and injection rate etc.) on oil production in laboratory-scale models (Das and Butler 1994, Yazdani and Maini 2005). Many researchers have attempted to describe and quantify the mass transfer mechanisms via detailed measurements of solvent's diffusivity in heavy oil conducted in a Hele-Shaw cell (Boustani and Maini 2001, Das 2005).

The key recovery mechanism is molecular diffusion enhanced by various spreading mechanisms such as velocity variations due to dispersion, which is a strong function of heterogeneities occurring at various scales, including those randomly distributed, discontinuous, thin shale lenses commonly found in oil sands deposits (Das 1998, Cheng et al. 2008). Molecular diffusion observed in a Hele-Shaw cell at the laboratory scale is not sufficient to quantify the amount of mass transfer occurring at the reservoir scale. A primary difficulty in modeling

lies in the inability to assess and quantify the effects on dispersion caused by heterogeneities occurring at different scales. The complexities of its recovery mechanisms render numerical modeling of such process in heterogeneous reservoirs highly cumbersome and expensive, limiting the use of conventional flow simulations in optimization and decision making. Efficient alternatives, like proxy models, can overcome such computational challenges by providing an approximate solution without solving all the detailed equations.

Several proxies that are based on analytical formulations have been published in the literature for modeling of SAGD process, which focus on the spreading period; for example, Vanegas et al. (2008) implemented the formulation in Butler (1985) to approximate the heat penetration rate in a "S-shaped chamber", while Azad and Chalaturnyk (2010) followed the method of slices using linear steam chamber model in Reis (1992). These methods are based on analytical solution of the momentum and mass balances between the chamber interface and the rest of the reservoir and have been applied successfully to 2-D cross-sectional heterogeneous realizations. Due to the similarity of chamber formation in SAGD and Vapex processes, Butler and other researchers have developed analytical solutions for oil drainage rate from a Hele-Shaw cell in a fashion analogous to those of SAGD: heat transfer by conduction is replaced by mass transfer due to diffusion, where heated bitumen is replaced by diluted bitumen (Butler and Mokrys 1989, Das and Butler 1994).

In this paper, a semi-analytical proxy is proposed to model the process, in a way analogous to the SAGD model described by Butler (1985). The proxy model

allows the prediction of total drainage rate with time and the position change of solvent chamber boundary during the spreading chamber period. Certain modifications are incorporated to model the Vapex process in porous media. A new parameter, mass penetration, which is analogous to the heat penetration in SAGD described in Butler (1985), is derived in our proposed formulation. Reservoirs with spatially varying rock porosity and permeability values are discretized; bitumen drainage rate and solvent penetration are calculated sequentially at grid blocks along the solvent-bitumen interface over incremental time steps. Results from this model are compared against experimental data available in the literature as well as detailed compositional simulation studies for both homogeneous and heterogeneous cases. As indicated by other researchers such as Vanegas et al. (2008), many assumptions and approximations are made in these proxies, it is important that we calibrate our model against results from traditional flow simulations. An empirical factor is introduced as a "tuning parameter" to adjust the proxy predicted flow rate to match more closely the numerical simulation results.

This paper is organized as follows: first, analytical solutions for the Vapex model in porous media are derived in detail and their analogy to the SAGD formulations is highlighted; next, implementation details of the proposed proxy are presented. In order to illustrate the applicability of the proposed method, three case studies are presented where results from the proxy model are compared against experimental data available in the literature as well as detailed

compositional simulation studies for both homogeneous and heterogeneous reservoirs.

Theory and Mathematical Formulations

The original analytical model for Vapex was developed by Butler and Mokrys (1989) following a series of Hele-Shaw cell experiments, in which the mass transfer mechanism occurring inside the mixing layer between the liquid solvent and heavy oil interface was modeled.

Formulation for the original Hele-Shaw model

Consider a cross section of the solvent-bitumen interface as shown in **Figure 3-1**, where oil is flowing along the interface at a drainage rate of *V*. Assuming a fully-developed solvent chamber, the solvent-bitumen interface is advancing at a constant unspecified velocity *U*. After performing a steady-state mass balance over a thin segment inside the interface, we obtain a one-dimensional convection-diffusion equation:

$$U\left(C_s - C_{sr}\right) + D_s \frac{dC_s}{d\xi} = 0 \quad \text{..... (1)}$$

Where D_s is the intrinsic diffusion coefficient of solvent, C_s is the solvent concentration (volume fraction) at a distance ξ from the interface. C_{sr} denotes the solvent concentration in the reservoir at a distance far away from the interface (ξ=ξ_{max}), representing the minimum solvent concentration. At steady state, the average drainage velocity due to gravity is given by Darcy's law in Eq.2:

$$V = \frac{k_o g \Delta\rho \sin\theta}{\mu_b} \quad \text{..... (2)}$$

Where k_o is the effective permeability of oil, g is the gravitational constant, θ is the angle between the interface and the horizontal axis, μ_b is the dynamic viscosity of bitumen in solution, and $\Delta\rho$ is the density difference between bitumen and solvent. The effective permeability in a Hele-Shaw cell with a spacing of b is given by Lamb (1932):

$$k_o = \frac{b^2}{12} \quad \text{..... (3)}$$

At any given point along the interface, the bitumen drainage rate (q) in terms of vertical area drained is given by the integral of an element of width $d\xi$, as shown in Eq.4:

$$q = \int_0^{\xi_{\max}} V(1 - C_s) d\xi \quad \text{..... (4)}$$

Substituting Eq.2 into Eq.4 and changing the limits of integration, q at a point along interface is given by Eq.5:

$$q = \frac{k_o g \sin\theta}{U} N_s \quad \text{..... (5)}$$

The dimensionless number N_s is given by Eq.6:

$$N_s = \int_{C_{sr}}^{C_{sc}} \frac{\Delta\rho D_s (1 - C_s) dC_s}{\mu_b (C_s - C_{sr})} \quad \text{..... (6)}$$

Where C_{sc} is the maximum value for C_s occurring at ξ=0. N_s consists of physical properties of the solvent-bitumen system, and it is a constant for a fully-

developed interface (i.e. solvent chamber has reached the overburden) where temperature and pressure do not vary. It should be noted that the parameters $\Delta\rho$, D_s and μ_b are functions of C_s at ξ>0. In a Hele-Shaw cell, the intrinsic solvent diffusion coefficient D_s is a function of overall diffusion coefficient D_o given by Eq.7:

$$D_s = \frac{D_o}{1 - aC_s} \quad \text{..... (7)}$$

The empirical constant "*a*" was proposed by Butler and Mokrys (1989) in their Hele-Shaw cell experiments as 0.969 for Athabasca bitumen sample. Considering the mass transfer by diffusion of solvent into bitumen, the mass of solvent stored behind a section of interface (m_r) with an area *A* is given by Eq.8:

$$\frac{\delta m_r}{\delta A} = \int_0^\infty \rho_s (C_s - C_{sr}) d\xi \quad \text{..... (8)}$$

We introduce a new variable, γ_m, which is the mass penetration depth to which mass of solvent would have penetrated if C_s has achieved a uniform value of C_{sc} in the solvent-oil mixture. It can be also interpreted as the penetration capacity of solvent into the bitumen. This variable is analogous to the heat penetration parameter in its SAGD analog (Butler 1985), and it is related to mass transfer in Eq.9 as follows:

$$\frac{\delta m_r}{\delta A} = \gamma_m \rho_s (C_{sc} - C_{sr}) \quad \text{..... (9)}$$

Assuming ρ_s is constant, Eq.9 can be re-written as:

$$\gamma_m = \frac{1}{U(C_{sc} - C_{sr})} \int_{C_{sr}}^{C_{sc}} D_s \, dC_s \quad \text{..... (10)}$$

For constant D_s, Eq.10 can be further simplified as in Eq.11:

$$\gamma_m = \frac{D_s}{U} \quad \text{..... (11)}$$

The assumption of constant diffusion coefficient D_s is generally considered reasonable. Okazawa (2009) investigated the effects of concentration-dependence of diffusion coefficient on Vapex drainage rates and concluded that the base functionalities of bitumen rates to other key parameters remain unchanged with a concentration-dependent D_s. Substituting Eq.11 into Eq.5, the flow rate at a point along the interface can be written as:

$$q = \frac{k_o g \sin\theta \gamma_m}{D_s} N_s \quad \text{..... (12)}$$

Following the derivations in Appendix A, mass penetration rate can be expressed by Eq.13. This mass penetration rate is important to relate the interface advancement to mass transfer as discussed in Appendix A, so that the mass penetration can be updated and interface movement and oil production rate can be determined as a function of time.

$$\frac{d\gamma_m}{dt} = \frac{1}{\sqrt{\pi}} \left(\frac{D_s}{\gamma_m} - U \right) \quad \text{..... (13)}$$

The total amount of oil drained through the cross section at that particular coordinate (x, y) over the time t is represented by the shaded area in **Figure 3-2**. It can also be calculated using Eq.14:

$$\int_0^t q\,dt = \int_y^h x\,dy \quad \text{..... (14)}$$

Differentiating Eq.14 with respect to *y* and then *t* gives the horizontal displacement velocity of the interface at any point:

$$\left(\frac{\partial q}{\partial y}\right)_t = -\left(\frac{\partial x}{\partial t}\right)_y \quad \text{.....(15)}$$

A similar expression for the vertical displacement can be derived and shown in Eq.16:

$$\left(\frac{\partial q}{\partial x}\right)_t = \left(\frac{\partial y}{\partial t}\right)_x \quad \text{..... (16)}$$

The total production rate for one-half of the solvent chamber is given by Eq.17 (see Appendix B for details):

$$Q = \sqrt{2k_o g h N_s} \quad \text{..... (17)}$$

Where *h* is the total vertical height for drainage process, and *Q* is the drainage rate per unit length for the half-side drainage. As opposed to a line source in a Hele-Shaw experiment where oil drains on one side, the solvent chamber in typical reservoir settings would develop around the well pair, allowing oil to drain to the producer on both sides.

Formulation for a porous medium

In the Hele-Shaw model, a sharp solvent-oil interface is typically assumed (Figure 3-1), where the oil saturation changes from its residual value (i.e., zero in a Hele-

Shaw cell) to its initial value (i.e., unity in a Hele-Shaw cell) across the interface. While in the porous media, the mass transfer process takes place in a contact zone that is called the diffusion boundary layer (Das 2005). **Figure 3-3** illustrates the oil saturation profile obtained from a flow simulation example using CO_2 as a solvent. Oil saturation changes gradually from 1-S_{wi} to S_{or}, where S_{wi} is the irreducible water saturation and S_{or} is the residual oil saturation. To obtain meaningful predictions for Vapex process in porous media, Das and Butler (1998) derived the expressions for oil drainage rate that accounts for the effects of capillary pressure and surface tension on the overall mass transfer. Incorporating the influences of porosity, tortuosity (Das and Butler 1998, Boustani 2001), and oil saturation, formulations for the original Hele-Shaw model can be modified as follow to derive analogous expressions for Eqs.1, 5 or 12, and 6 for a porous medium with porosity ϕ and oil saturation S_o:

$$U\left(C_s - C_{sr}\right) + \phi S_o D_s \frac{dC_s}{d\xi} = 0 \quad \text{.....(18)}$$

$$q = \frac{k_o g \sin\theta \gamma_m}{\phi S_o D_s} N_s \quad \text{..... (19)}$$

Where:

$$N_s = \int_{Csr}^{Csc} \frac{\Delta\rho \phi S_o D_s \left(1 - C_s\right) dC_s}{\mu_b \left(C_s - C_{sr}\right)} \quad \text{..... (20)}$$

For the sake of simplicity in the formulation of Eq.18, it is assumed the tortuosity effect has already been incorporated into the definition of D_s. Das and Butler (1998) has noted that in porous media, the value of D_s should be corrected

using a cementation factor Ω, which is a measure of consolidation and tortuosity in a porous medium. In this work, we have adopted a value of 2 for Ω (Boustani 2001). In addition, the mass penetration parameter γ_m introduced in Eqs.8-11 can be modified as:

$$\frac{\delta m_r}{\delta A} = \int_0^{\infty} \rho_s \phi S_o (C_s - C_{sr}) d\xi \quad \text{.....(21)}$$

$$\frac{\delta m_r}{\delta A} = \gamma_m \rho_s \phi S_o (C_{sc} - C_{sr}) \quad \text{.....(22)}$$

$$\gamma_m = \frac{\phi S_o}{U(C_{sc} - C_{sr})} \int_{C_{sr}}^{C_{sc}} D_s dC_s \quad \text{.....(23)}$$

$$\gamma_m = \frac{\phi S_o D_s}{U} \quad \text{.....(24)}$$

Similarly, the mass penetration rate expression in Eq.13 can be modified as (see Appendix A for details):

$$\frac{d\gamma_m}{dt} = \frac{1}{\phi S_o \sqrt{\pi}} \left(\frac{\phi S_o D_s}{\gamma_m} - U \right) \quad \text{.....(25)}$$

Finally, accounting for ϕ and ΔS_o (the difference between initial oil and residual oil saturation) in Eqs.14-17 would result in the following set of equations (see Appendix B for details):

$$\int_0^t q dt = \phi \Delta S_o \int_y^h x dy \quad \text{.....} \quad (26)$$

$$\left(\frac{\partial q}{\partial y} \right)_t = -\phi \Delta S_o \left(\frac{\partial x}{\partial t} \right)_y \quad \text{.....} \quad (27)$$

$$\left(\frac{\partial q}{\partial x}\right)_t = \phi \Delta S_o \left(\frac{\partial y}{\partial t}\right)_x \quad \text{..... (28)}$$

$$Q = \sqrt{2k_o g \phi \Delta S_o h N_s} \quad \text{..... (29)}$$

The modified formulations described above are valid for modeling Vapex in both Hele-Shaw cells and porous media. In a Hele-Shaw cell, both porosity and initial oil saturation are unity; thus the term ϕS_o is equal to one. In addition, the residual oil saturation in a Hele-Shaw cell is zero; hence the term $\phi \Delta S_o$ should be equal to one as well.

Recall that effective permeability of oil k_o is a function of fluid saturation in a porous medium. The oil-phase relative permeability (k_{ro}) can be obtained by laboratory measurements or using correlations (Burdine 1953, Kjosavik and Ringen 2000). The effective oil permeability is obtained by multiplying the absolute permeability (k) with k_{ro} in Eq.30:

$$k_o = k_{ro} \times k \quad \text{..... (30)}$$

Given that the oil saturation varies gradually across the diffusion boundary layer, a constant value for the average oil saturation S_{oavg} (See Figure 3-3) can be used to replace S_o in Eqs.19-30. We also ignored the effects of mobile water. It should be emphasized that our model assumes that an interface can be defined and exists at $\xi = 0$, and its movement with time along with the size of the diffusion boundary layer (i.e., γ_m), where C_s decreases along $\xi > 0$, are tracked. The spatial concentration profile across the diffusion zone, however, is not explicitly

calculated; hence, detailed discretization across the diffusion boundary layer is not necessary.

Methodology

Calculation procedure and implementation details

The analytical formulations can be applied in a proxy model to determine the growth of a fully developed solvent chamber in the spreading period and to calculate the oil drainage rate. Following a similar SAGD proxy formulation described by Butler (1985) and later by Vanegas et al. (2008), the previously derived analytical equations are implemented in an explicit calculation sequence as follows:

1. Discretize the solvent-bitumen interface into some evenly distributed nodes as shown in **Figure 3-4**, which move laterally along the reservoir width (or plate width for Hele-Shaw cell) as the solvent chamber grows.
2. Initialize values of mass penetration γ_m for all nodes defined in step 1. The criterion for assigning the initial values seems arbitrary when referring to Butler (1985) as he described the initialization of the analogous heat penetration parameter for SAGD. He stated that the value of heat penetration should decrease from bottom to top (i.e., largest near the well pair and smallest near the chamber top).
3. Calculate the oil flow rate q for each node using Eqs.19-20. It is convenient to assume an interface angle θ of $90\,°$ at the beginning of the spreading period. The oil rate right below the overburden is set to zero by assuming the mass

penetration value at the first grid node next to the upper boundary to be zero. To calculate N_s, it is necessary to determine the correlation of $\Delta\rho$ and μ_b as functions of solvent concentration C_s. This can be achieved using an equation of state such as the Peng-Robinson (PR-EOS) model (Sandler 1999). For a heterogeneous medium, arithmetic averages of permeability and porosity evaluated along the interface at time level *n* are used in Eqs.19-20. The average values are calculated using k_o and ϕ values of the grid blocks that are intersecting with the interface.

4. Calculate the interface change in x or y direction at next time step using Eq.27 or Eq.28. If the interface is nearly vertical (θ>45°), the horizontal movement of interface can be determined by Eq.27, whereas if it is generally horizontal (θ>45°), vertical advance of the interface can be calculated by Eq.28. Consider a small time step Δt, using central difference approximation in space and forward difference approximation in time, Eq.27 and Eq.28 can be discretized as follows:

$$\frac{q_{i+1}^n - q_{i-1}^n}{y_{i+1}^n - y_{i-1}^n} = -\phi\Delta S_o \frac{x_i^{n+1} - x_i^n}{\Delta t} \quad \text{..... (31)}$$

$$\frac{q_{i+1}^n - q_{i-1}^n}{x_{i+1}^n - x_{i-1}^n} = \phi\Delta S_o \frac{y_i^{n+1} - y_i^n}{\Delta t} \quad \text{..... (32)}$$

The superscripts *n* and *n*+1 refer to quantities evaluated at the present and next time levels. The subscripts *i* indicate the i^{th} interface node and its neighboring interface nodes are denoted by the subscripts *i*-1 and *i*+1, as shown in Figure 3-4. The variables *x* and *y* represents the coordinates of each interface node at

different time levels. By using Eq.31 and Eq.32, the horizontal and vertical locations for each node can be advanced explicitly with time.

5. Calculate length (approximated by L_i in Figure 3-4) between two neighboring nodes around *i*:

$$L_i = \sqrt{(x_{i-1} - x_{i+1})^2 + (y_{i-1} - y_{i+1})^2} \quad \text{..... (33)}$$

Similarly, the interface angle θ for grid node *i* can be evaluated using the trigonometric relation in Eq.34:

$$\theta_i = \arcsin\left(\frac{y_{i-1} - y_{i+1}}{L_i}\right) \quad \text{..... (34)}$$

6. Calculate the advancing velocity of interface using Eq.35 (derived by combining Eqs.27-28 with trigonometric relationship between U and θ in Figure 3-1; see Appendix B for details):

$$U = -\frac{1}{\phi \Delta S_o}\frac{\partial q}{\partial L} \quad \text{..... (35)}$$

Rewrite Eq.35 in its discretized form as follows:

$$U_i^n = -\frac{1}{\phi \Delta S_o}\frac{q_{i+1}^n - q_{i-1}^n}{L_i^n} \quad \text{..... (36)}$$

7. Calculate a new value of mass penetration at the next time level. Replacing D_s with D_{savg} in Eq.25, the discretized form of Eq.25 can be written as Eq.37:

$$\frac{\gamma_{m,i}^{n+1} - \gamma_{m,i}^n}{\Delta t} = \frac{1}{\sqrt{\pi}(\phi S_o)_i^n}\left(\frac{\phi S_o D_{savg}}{\gamma_{m,i}^n} - U_i^n\right) \quad \text{..... (37)}$$

8. Repeat steps 2 to 7 until the final time is reached.

Calibration and tuning parameters

Numerous assumptions and approximations are invoked in the analytical formulations employed in our proxy. Therefore, it is important that we calibrate our proxy model against results from traditional flow simulations. Vanegas et al. (2008) proposed some empirical factors, which they referred to as "tuning parameters" in their SAGD proxy formulations to adjust the proxy-predicted values to match more closely with the flow simulation results. They emphasized that the empirical factors must be calibrated a priori for each application.

In our work, a slightly different observation is noted. The case studies presented in the next section will show that the solvent-oil interface position predicted by our proxy is always in good agreement with numerical simulation results. The producing oil rate calculated using either Eq.29 (the square-root expression of Q as a function of constant average fluid and reservoir properties) or Eq.19 (flow rate q estimated at the bottom or last interface node) has shown good agreement with the published Hele-Shaw cell data. The value predicted using Eq.19 changes with each time level, in a fashion similar to that obtained from detailed flow simulations. However, as we compare our predictions to flow simulation results for a set of porous media in this study (both homogeneous or heterogeneous), it is observed that the value of Q (Eq.29) matches well with flow simulation results, while the value of q from the bottom interface node (Eq.19) is approximately 4 times larger than the flow simulated values. The approximations of average oil saturation S_{oavg} (see Figure 3-3), average relative permeability at that saturation and average diffusion coefficient D_{savg} in the diffusion boundary

layer may have caused the deviations from detailed transport calculations. Another possible explanation is that analytical formulation does not permit the bottom of the chamber to advance away from the producer, while in reality, the chamber grows slowly away from the well pair; hence the direct comparison of flow rate value obtained at the bottom interface node using the proxy model to actual producing rate from flow simulation might reveal some discrepancy. Additional details about the proposed tuning parameter are presented in the case studies.

Results and Discussions

Three case studies are presented in this section. Results obtained from the proxy are compared to the published experimental data in Hele-Shaw cell (case study 1) and detailed compositional flow simulation predictions for reservoirs with homogeneous (case study 2) and heterogeneous (case study 3) properties.

Case Study 1: Comparison with Hele-Shaw cell experimental data

Butler and Mokrys (1989) performed a series of Hele-Shaw cell experiments using toluene as the solvent, in which the glass cell was constructed using two closely assembled plates. The Hele-Shaw cell was filled with Athabasca bitumen and exposed on one side to toluene solvent injected from a linear source at 20 ℃ and atmospheric pressure. Other experimental conditions and parameters are summarized in **Table 3-1**. The overall diffusion coefficient D_o for Hele-Shaw experiment was obtained by the static-free diffusion method for Athabasca

bitumen sample at 20 ℃. They calculated the integral value of N_s as 9.44×10^{-7} for Athabasca oil.

This experiment is simulated using our proposed proxy model using a grid of 12×9×1 blocks with Δx and Δy equal to 1cm. The total simulation time is 67 hours with a time step of 1 minute, and the computational time is about 2 seconds using the University of Alberta's Numerical and Statistical Server with two 3 GHz quad core Xeon processors and 64 GB RAM.

Oil drainage rate and the chamber shape obtained with our proxy are compared to the experimental observations. **Figure 3-5** presents a comparison of solvent-bitumen interface position between the laboratory photographs and the proxy model. The solid lines represent the chamber boundary obtained from photo shots of a typical cross section taken when an Athabasca bitumen sample was drained by toluene. The dash lines indicate the solvent-bitumen interface position predicted from our proxy model. It is interesting to note that the solvent chamber shape for Vapex is similar to the steam chamber shape in SAGD (Butler 185), illustrating the analogy between two processes. As time increases, the near vertical portion shortens and the S-curve portion flattens out. Drainage starts at the top of the Hele-Shaw cell and the solvent chamber expands along the top and progresses downward. The interface positions show a good match with those observed from the experiment.

Table 3-2 compares flow rates computed using the proxy model with those measured from the experiment at the same temperature, permeability, and pressure. As the diluted oil starts to drain by gravity, the flow is directed

downward along the interface, and the flow rate at each node calculated by Eq.19 will cumulate toward the bottom node. As a result, the flow rate q determined at the bottom interface node can be treated as the total drainage rate. It is comparable to the constant total flow rate Q predicted by Eq.29. The comparison of average value for q, predicted total Q, and experimental observed flow rate are listed in Table 3-2. Our proxy predictions corroborate with the published lab data and validate the predictability of the proxy model for a lab-scale homogeneous case.

Case Study 2: Comparison with detailed compositional flow simulations for a homogeneous reservoir

A synthetic 2-D cross-sectional reservoir is constructed using the base case presented by Forster (2008). A grid of $120 \times 30 \times 1$ with a block size of $\Delta x = \Delta y = \Delta z = 1$ft (0.3048 m) is prepared, given the size of the diffusion boundary layer is approximately 5 m as shown in Figure 3-3. Two horizontal wells of unit length oriented along the j direction are used. The production well is located at the bottom of the reservoir and the injection well is located 5 ft (1.52 m) above the producer. Only half of the solvent vapor chamber is modeled.

Fluid properties of a heavy oil sample provided by Sharma (1994) for the Schrader Bluff oil pool is used. A detailed description of the fluid model and all the corresponding PVT properties are given in Forster (2008). The oil sample has a viscosity of 41 cp at reservoir conditions, with an API gravity of 18 and bubble-point pressure of 1300 psia.

Initial reservoir conditions and other operating constrains are summarized in **Table 3-3**. Homogeneous and isotropic permeability and porosity values are

assumed. The water saturation remains at residual saturation. Vaporized CO_2 is injected as a solvent. The injection and producing pressures are fixed at just below the CO_2 vapor pressure at reservoir temperature (82 F°) to ensure that CO_2 is injected as a gas phase. The integral value of N_s is evaluated using the trapezoidal rule, and the value is calculated as 2.474×10^{-4}.

Compositional simulation is performed using GEM® (2011) over a production period of 10 years. The computation time is 32474 seconds (approximately 9 hours) using a 3.4 GHz, 16GB of RAM, Intel® Core™ i7-2600 CPU. The proxy model takes only 3 seconds, representing a huge improvement in terms of calculation efficiency.

Figure 3-6 compares the solvent chamber position between proxy model prediction and flow simulation results at three different times. In this figure, the oil saturation profile obtained from flow simulation is used for comparison. Some literature prefers to delineate the solvent chamber based on solvent mole fraction (Nghiem et al. 2001, Das 2005); however, in the analytical formulation (or Figure 3-1), the solvent-oil interface is defined at which the oil saturation decreases from its initial value; therefore, oil saturation profile from flow simulation is used in this work for comparison of interface position. Nevertheless, the predicted solvent-bitumen interface given by proxy model matches well with the oil saturation profile obtained from simulation. The typical 'S' shape interface is also similar to what is observed in Hele-Shaw cell from case study 1.

The predicted average bottom-node flow rate q and total flow rate Q are compared to the producing oil rate from flow simulation. It is observed that

although the value for Q matches well with the simulation results, the value of q is approximately four times larger. For reasons discussed in the previous section, this discrepancy is adjusted using a tuning factor. Dividing the average bottom node flow rate by a factor of 4, the producing oil flow rates obtained from the proxy model are in good agreement with simulation results (See **Table 3-4**). Oil production rate as a function of time is plotted in **Figure 3-7**. A similar trend is observed: production rate peaks at a maximum value after some time and then declines slowly to a stabilized constant value according to Figure 3-7 (a). A closer look of the production profile after 600 days is also given in Figure 3-7 (b). As the solvent-bitumen interface has approached the no-flow boundary at the other edge of the reservoir, it begins to advance downwards; the steady-state assumption of the proxy model may be invalid during this boundary-dominated flow period. Therefore, the oil production rate predicted with the proxy shows a larger discrepancy in comparison with the simulation result at the later time. Nevertheless, the stabilized rate obtained from the proxy model demonstrates reasonable agreement with those predicted with simulation.

Figure 3-8 also shows a comparison of the cumulative oil production with time. The discrepancy between proxy and simulator results at the early and late time is consistent with oil rate comparison in Figure 3-7. Flow simulation predicts that at the early time, the solvent chamber continues to rise as it is not developed fully; a small amount of oil is produced as evidenced by the slow increase in cumulative oil production at $t < 400$ days predicted by the flow simulation in Figure 3-8 (a). However, the proxy model assumes a fully-developed solvent

chamber at t > 0. In order to compare only the oil production volume from a fully-developed chamber, incremental production obtained from flow simulation: $Q = Q_t - Q_{400}$, where Q_t = cumulative production at actual time t and Q_{400} = cumulative production at 400 days, as a function of incremental time $t = t - 400$, is plotted against values of Q_t and t obtained from the proxy in Figure 3-8 (b). In other words, If we ignore the solvent chamber rising period in flow simulation and display incremental production after the solvent chamber is fully developed, it is apparent that predictions given by the proxy model and flow simulator are very close as show in Figure 3-8 (b), the only minor difference observed near the end can be attributed to boundary effects as discussed previously.

Case Study 3: Comparison with detailed compositional flow simulations for a heterogeneous reservoir

Based on the homogeneous case discussed above, a heterogeneous case is investigated in this section. The model set-up is entirely identical to case study 2, with the absolute permeability and porosity (**Figure 3-9**) distribution being adopted from Leung (2012). Permeability is assumed to be isotropic locally (i.e., $k_x = k_y = k_z$).

Compositional simulation is performed over a production period of 5 years. The computation time is 18125 seconds (approximately 5 hours). The proxy model takes only 4 seconds, indicating the modifications due to heterogeneous reservoir properties do not incur significant computational burden.

A plot of predicted solvent chamber growth for 2.5 years, 3.5 years and 4.5 years production is shown in **Figure 3-10**. The results from proxy model on the left side gives a smooth interface position because at each time step, an average permeability and porosity along the interface is used to advance the solvent growth. This approximation is equivalent to advancing the interface over a series of different homogeneous reservoirs at different time steps, resulting in the smooth interface shapes as observed for the homogeneous case. Although the exact jagged interface predicted from detailed flow simulations cannot be captured by the proxy model, the proxy model has provided a reasonable representation of the interface advancement with time.

Comparison of producing oil rate and cumulative production with time between proxy predictions and simulator results are shown in **Figure 3-11** and **Figure 3-12**. The deviation between two results is increased compared to the homogeneous model in case study 2, and it can be attributed to the up-scaling schemes introduced to average heterogeneous rock properties along the interface. Nevertheless, the proxy results give a reasonable match of the stabilized oil rate and the incremental oil production in the later part of the production period, where the chamber is fully developed, as shown in Figure 3-11 (b) and Figure 3-12 (b).

Finally, **Table 3-5** summarizes the flow rates predicted from the proxy model and their comparison with flow simulation. After applying the same tuning parameter as in case study 2 (a factor of 4), all three values are in good agreement.

Conclusions

1. A new proxy model, similar to those in existing literature for modeling SAGD processes, is developed to model solvent transport in Vapex at isothermal conditions. The model is based on Butler's analytical solution developed for conditions applicable for typical Hele-Shaw cell experiments. The original formulations have been extended in details in this paper to account for properties representative of a porous medium. A new parameter of mass penetration is derived.

2. An explicit calculation sequence of the analytical equations is presented to predict the solvent-oil interface position and producing oil rate as a function of time.

3. Modifications via a set of averaging schemes are implemented for heterogeneous reservoirs. One empirical tuning parameter is introduced to obtain a more reliable estimate of producing oil rate from the proxy model.

4. The results obtained from the proposed proxy show good agreement with published experimental observations and results from flow simulation in terms of solvent-bitumen interface position and oil production rate, implying promising future application to field cases.

5. The proxy model also shows a significant reduction in terms of computational efforts.

6. Given that heterogeneity modeling informed by incomplete data leads to uncertainty about rock properties, most practical approaches require generation of large number of equi-probable realizations of rock properties at reservoir scales.

Computational constraints preclude detailed numerical solution of the flow and transport differential equations, as often implemented in traditional flow simulators, using the entire suite of plausible realizations. The proposed proxy can be used to mimic the transport physics without solving all the detailed equations, allowing us to assess the recovery performance of many geologic realizations efficiently.

7. This type of proxy models can also be easily integrated in existing workflows to optimize production scenarios. This model can be used to evaluate or screen many geostatistical realizations representing heterogeneity at various scales quickly to identify a smaller, more manageable subset of models (i.e. P10, P90) for further detailed flow simulations.

Acknowledgement

This research was supported by the Sustainable Technologies for Energy Production Systems (STEPS) program managed by the Petroleum Technology Research Centre (PTRC). The authors would also like to thank the Computer Modeling Group (CMG) for providing the academic licenses for GEM and the University of Alberta for granting access to the Numerical and Statistical Server.

Nomenclature

a = experimental constant coefficient proposed by Butler and Mokrys (1989)

b = Hele-Shaw cell spacing, μm

g = gravitational constant, m/d^2

h = vertical drainage height, m

k = absolute permeability of reservoir, m^2

k_o = effective oil permeability, m^2

k_{ro} = relative permeability of oil

k_x = absolute permeability in x direction, m^2

k_y = absolute permeability in y direction, m^2

k_z = absolute permeability in z direction, m^2

m_r = mass of solvent accumulated in reservoir, kg

q = cell flow rate for a certain grid block, m^2/d

t = time, days

A = cross-section area of the solvent chamber at time t, m^2

C_s^* = dimensionless solvent concentration distribution

C_s = solvent concentration (volume fraction) at a distance ξ from interface

C_{sc} = solvent concentration in the edge of solvent chamber

C_{sr} = the solvent concentration in the reservoir

D_o = overall diffusion coefficient, m^2/d

D_s = intrinsic diffusion coefficient of solvent, m^2/d

D_{savg} = average diffusion coefficient of solvent, m^2/d

L_i = length along interface between two neighboring nodes around i, m

N_s = dimensionless integral

Q = total oil drainage rate per unit length of well, $m^3/d \cdot m$

S_o = oil saturation, %

S_{oavg} = average oil saturation in diffusion boundary layer, %

S_{oi} = initial oil saturation, %

S_{or} = residual oil saturation, %

S_{wi} = irreducible water saturation, %

ΔS_o = oil saturation difference between initial and residual, %

U = frontal advancing velocity of interface, m/d

V = average drainage velocity due to gravity, m/d

Greek symbols:

ξ = distance from interface, m

ρ_s = solvent density, kg/m^3

μ_b = dynamic viscosity of bitumen in solution, kg/m d

θ = the angle of interface from horizontal, °

ϕ = porosity, %

γ_m = mass penetration, m

$\Delta\rho$ = density difference between solvent and bitumen, kg/m^3

Ω = cementation factor

Subscripts

i = grid block index

max = maximum

Superscripts

n = time level

References

Azad, A. and Chalaturnyk, R.J. 2010. A Mathematical Improvement to SAGD using Geomechanical Modeling. *Journal of Canadian Petroleum Technology* **49**(10): 53-64. Doi: 10.2118/141303-PA

Boustani. A. 2001. Investigation of Interfacial Mass Transfer in Vapor Extraction Process. MSc thesis dissertation. University of Calgary, AB, Canada.

Boustani, A. and Maini, B.B. 2001. The Role of Diffusion and Convective Dispersion in Vapour Extraction Process. *Journal of Canadian Petroleum Technology* **40** (4): 68-77. Doi: 10.2118/01-04-05

Burdine, N.T. 1953. Relative Permeability Calculations From Pore Size Distribution Data. *Journal of Petroleum Technology* **5**(3): 71-78. Doi: 10.2118/225-G

Butler, R.M. 1985. A New Approach to the Modeling of Steam-Assisted Gravity Drainage. *Journal of Canadian Petroleum Technology* **24**(3): 42-51. Doi: 10.2118/85-03-01

Butler, R.M. and Mokrys, I.J. 1989. Solvent Analog Model of Steam Assisted Gravity Drainage. *AOSTRA Journal of Research* **5**(1):17-32.

Chen, Q., Gerritsen, M.G. and Kovscek, A.R. 2008. Effects of Reservoir Heterogeneities on the Steam-Assisted Gravity Drainage Process. *SPE Reservoir Evaluation & Engineering* **11**(5): 921-932. Doi: 10.2118/109873-PA

Computer Modeling Group. 2011. GEM: Advanced Compositional Reservoir Simulator User's Guide (Version 2011). Computer Modeling Group Limited, Calgary, Alberta, Canada.

Das, S.K. and Butler, R.M. 1994. Investigation of 'VAPEX' Process in a Packed Cell Using Butane As a Solvent. Canadian SPE/CIM/CANMET International Conference on Recent Advances in Horizontal Well Applications, Calgary, Alberta, Canada, 20-24 March. Doi: 10.2118/HWC-94-47

Das, S.K. 1998. Vapex: An Efficient Process for the Recovery of Heavy Oil and Bitumen. *SPE Journal* **3**(3): 232-237. Doi: 10.2118/50941-PA.

Das, S.K. and Butler, R.M. 1998. Mechanism of the Vapor Extraction Process for Heavy Oil and Bitumen. *Journal of Petroleum Science and Engineering* **21**(1-2): 43-59. Doi: 10.1016/S0920-4105(98)00002-3

Das, S.K. 2005. Diffusion and Dispersion in the Simulation of Vapex Process.SPE/PS-CIM/CHOA International Thermal Operations and Heavy Oil Symposium, Calgary, Alberta, Canada, 1-3 November. Doi:10.2118/97924-MS

Forster, L.J. 2008. Numerical Modeling of the VAPEX Process in Heterogeneous Media. MSc thesis dissertation. University of Texas at Austin, Austin, Texas,

Kjosavik, A. and Ringen, J.K. 2000. Relative Permeability Correlation for Mixed-Wet Reservoirs. SPE/DOE Improved Oil Recovery Symposium, Tulsa, Oklahoma, 3-5 April. Doi: 10.2118/59314-MS

Lamb, H. 1932. *Hydrodynamics*, 6th edn. Dover Publications, New York.

Leung, J.Y. 2012. Scale-up of Effective Mass Transfer in Vapor Extraction Process for Heterogeneous Reservoirs. SPE Improved Oil Recovery Symposium, Tulsa, Oklahoma, USA, 14-18 April. Doi: 10.2118/153862-MS

Nghiem, L.X., Kohse, B.F., and Sammon, P.H. 2001. Compositional Simulation of the Vapex Process. *Journal of Canadian Petroleum Technology* **40**(8):54-61.Doi:10.2118/01-08-05

Okazawa, T. 2009. Impact of Concentration-Dependence of Diffusion Coefficient on VAPEX Drainage Rates. *Journal of Canadian Petroleum Technology* **48**(2): 47-53. Doi: 10.2118/09-02-47.

Reis, J.C. 1992. A Steam-Assisted Gravity Drainage Model for Tar Sands: Linear Geometry. *Journal of Canadian Petroleum Technology* **31**(10): 14-20. Doi: 10.2118/92-10-01

Sandler, S.I. 1999. *Chemical, Biochemical and Engineering Thermodynamics*,4th *Edition*, John Wiley & Sons, Inc. New York.

Sharma, G.D. 1994. Study of Hydrocarbon Miscible Solvent Slug Injection Process for Improved Recovery of Heavy Oil from Schrader Bluff Pool, Milne Point Unit, Alaska. U.S. Department of Energy, Annual Report, January 1, 1994-December 31, 1994

Vanegas, J.W.P., Deutsch, C.V. and Cunha, L.B. 2008. Uncertainty Assessment of SAGD Performance Using a Proxy Model Based on Butler's Theory.SPE Annual Technical Conference and Exhibition, Denver, Colorado, USA, 21-24 September. Doi: 10.2118/115662-MS

Yazdani, A. and Maini, B.B. 2008. Modeling of the VAPEX Process in a Very Large Physical Model. *Energy & Fuels* **22**(1): 535-544. Doi: 10.1021/ef700429h

Yazdani, A. and Maini, B.B. 2005. Effect of Drainage Height and Grain Size on Production Rates in the Vapex Process: Experimental Study. *SPE Reservoir Evaluating & Engineering* **8**(3): 205-213. Doi: 10.2118/89409-PA

Tables

Table 3-1. Summary of Hele-Shaw cell experimental set-up in Butler and Mokrys (1989)

Hele-Shaw cell geometry		
Height (h)	Width	Cell spacing (b)
cm	cm	μm
12	9	114.3
Bitumen and Solvent Densities at 20 ℃		
Athabasca bitumen		Toluene solvent
g/cm^3		g/cm^3
1.0283		0.866
Other Properties		
Porosity(ϕ)	Initial oil saturation(S_{oi})	Residual oil saturation (S_{or})
1	1	0

Table 3-2. Comparison of flow rate between proxy prediction and experimental observation for the Athabasca bitumen sample in case study 1

Permeability (k_o)		Height (h)		Temperature	
Darcy		cm		℃	
1103		12		20	
Predicted average flow rate of the bottom interface node (Eq.19)		Predicted total flow rate (Eq.29)		Experimental flow rate	
cm^2/h	cm^2/s	cm^2/h	cm^2/s	cm^2/h	cm^2/s
1.52	4.21×10^{-4}	1.77	4.92×10^{-4}	1.54	4.28×10^{-4}

Table 3-3. Initial reservoir and operating conditions for case study 2

Initial reservoir conditions					
Temperature	Pressure	Porosity (ϕ)	Permeability (k_x=k_y=k_z)	Irreducible water saturation(S_{wi})	Diffusion coefficient(D_o)
F °	psi	%	md	%	cm^2/s
82	1300	28	267	20	5×10^{-5}

Operating conditions			
Solvent injected	Producing pressure	Injection pressure	Flow rate constrains
	psi	psi	
CO_2	967.5	968	None

Table 3-4. Flow rate comparison for homogeneous case study 2

Predicted average flow rate of the bottom interface node (Eq.19) divided by tuning parameter	Predicted total flow rate from square root equation (Eq.29)	Average producing oil rate from detailed flow simulation
m^3/day	m^3/day	m^3/day
0.0537	0.0523	0.0519

Table 3-5. Flow rate comparison for heterogeneous case study 3

Predicted average flow rate of the bottom interface node (Eq.19) divided by tuning parameter	Predicted total flow rate from square root equation (Eq.29)	Average producing oil rate from detailed flow simulation
m^3/day	m^3/day	m^3/day
0.0243	0.0237	0.0245

Figures

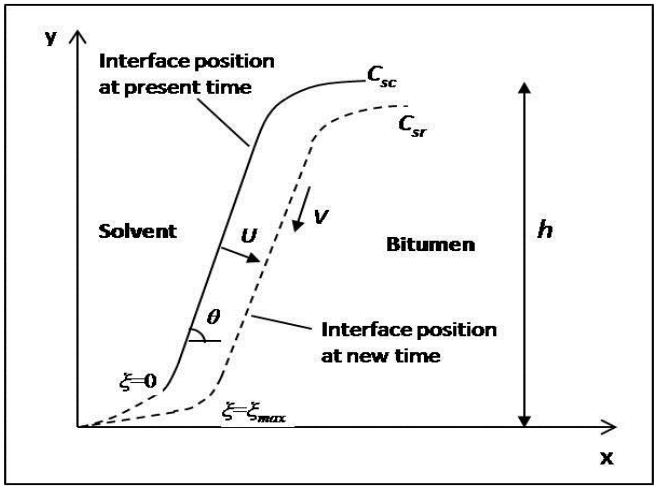

Figure 3-1. Schematic of the solvent-bitumen interface in Vapex (adapted from Butler and Mokrys 1989).

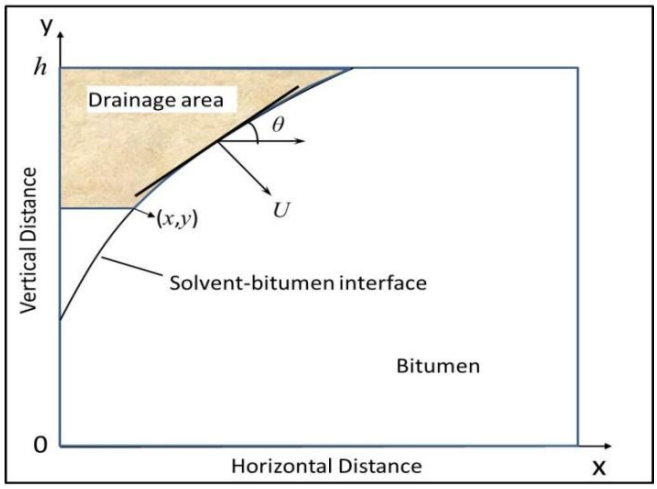

Figure 3-2. Illustration of the drainage area of observed in a Hele-Shaw cell Vapex experiment (adapted from Butler and Mokrys 1989).

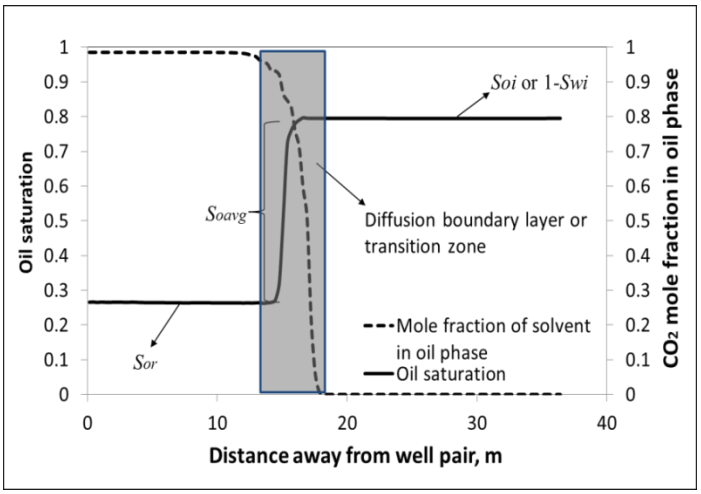

Figure 3-3. Oil saturation and solvent (CO_2) mole fraction profile at a distance away from the injector-producer well pair. The oil saturation gradually changes from 1-$S_{wi}$to S_{or}. The shaded area indicates the diffusion zone in a porous medium.

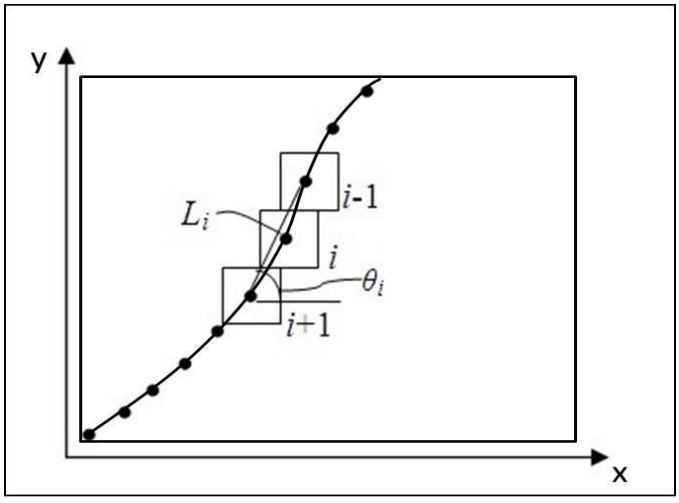

Figure 3-4. Discretization of the solvent-bitumen interface: dots denote centers of grid blocks where the interface nodes are located.

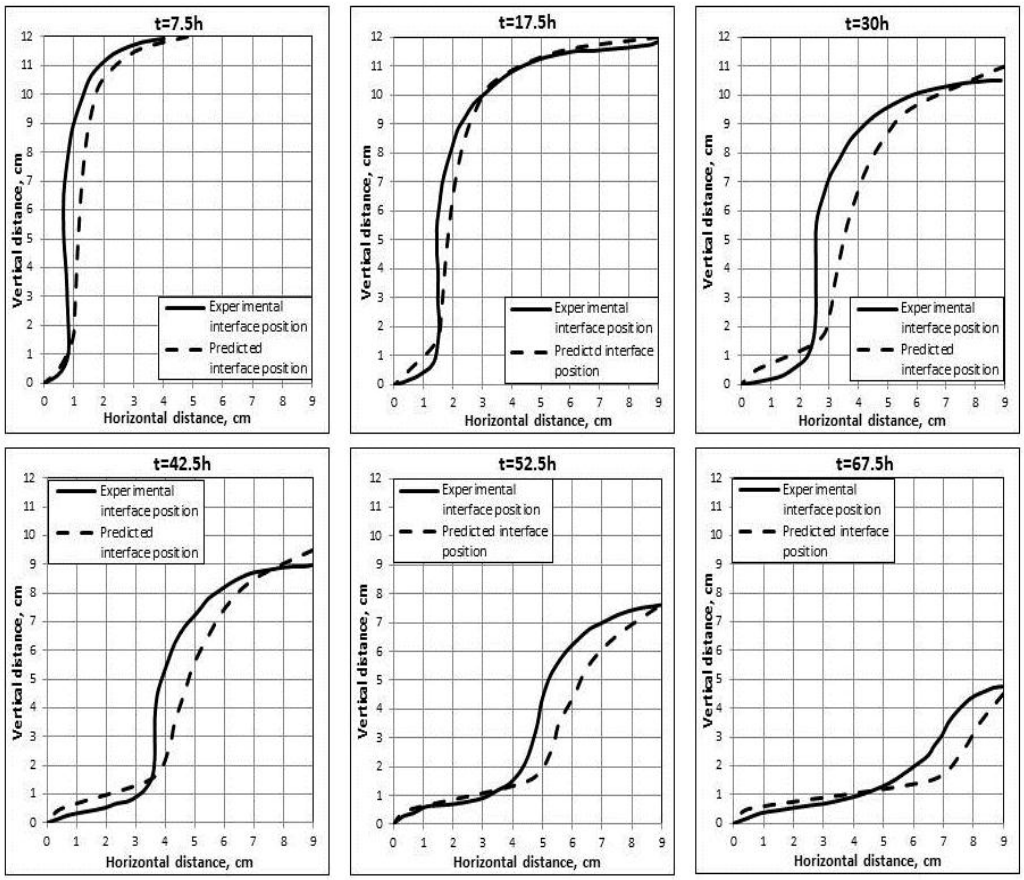

Figure 3-5. Comparison of solvent-bitumen interface position between Hele-Shaw experimental results (Butler and Mokrys 1989) and proxy model predictions for the Athabasca bitumen sample in case study 1.

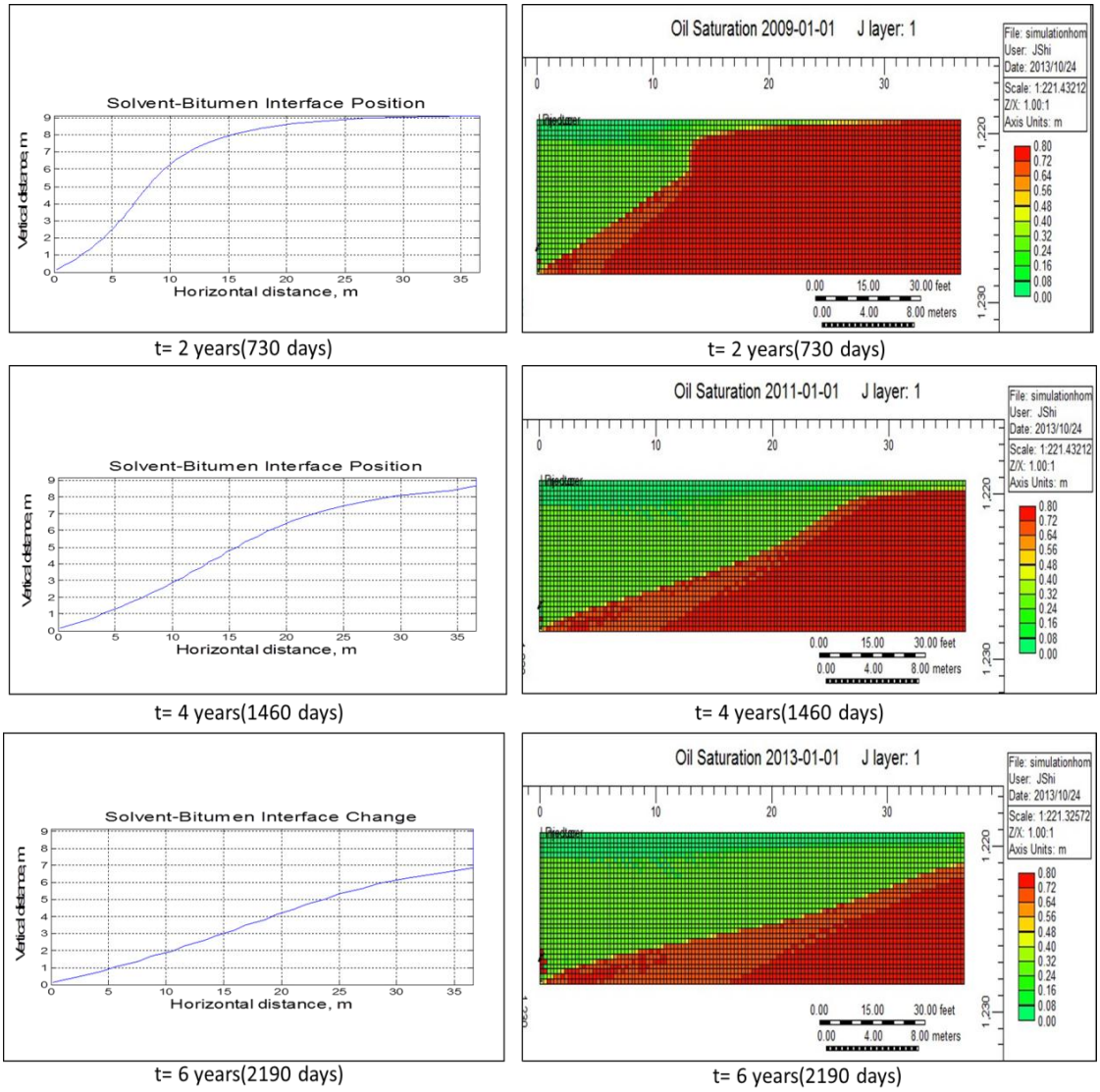

Figure 3-6. Comparison of solvent-bitumen interface position between detailed flow simulations and proxy model predictions for the homogeneous reservoir case study 2.

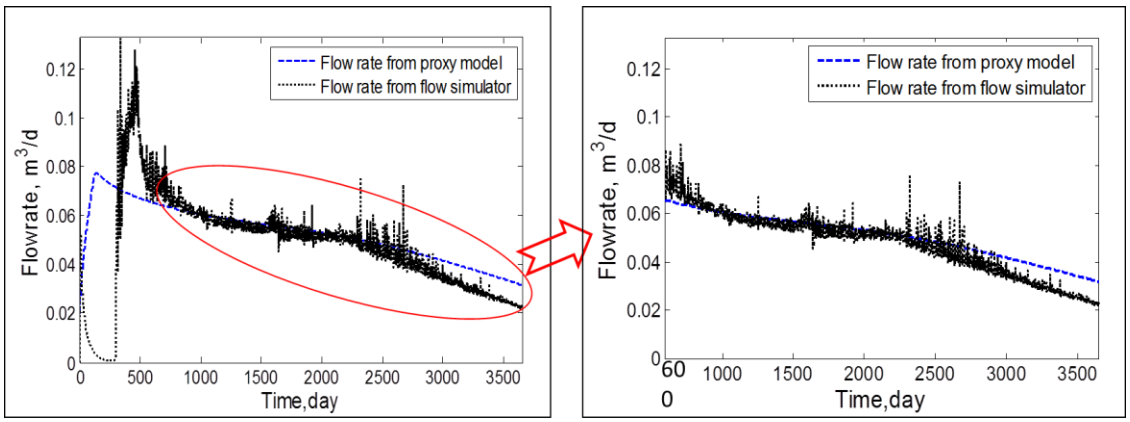

Figure 3-7. Comparison of oil production rate as a function with time between flow simulation results and proxy predictions (flow rate at the bottom interface node divided by the tuning parameter) for case study 2: (a) – Entire production period; (b) – Production after 600 days.

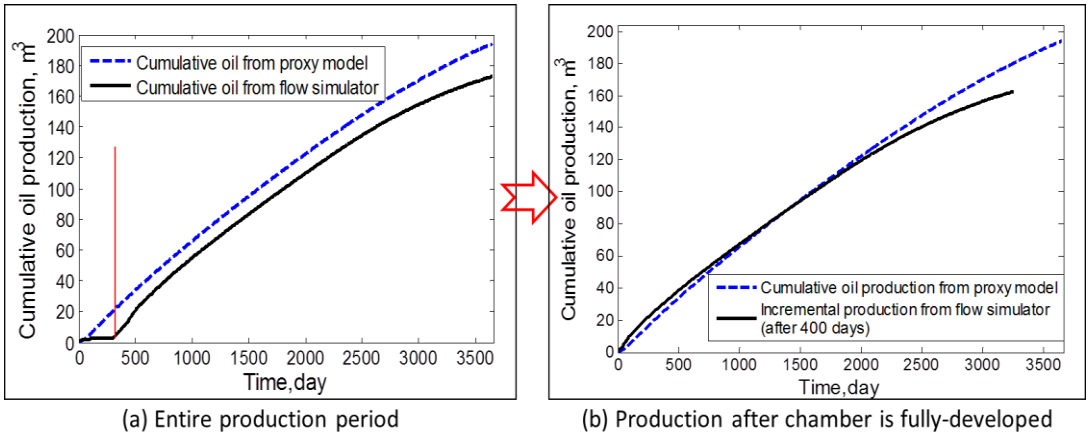

Figure 3-8. Comparison of cumulative oil production as a function with time between flow simulation results and proxy predictions (flow rate at the bottom interface node divided by the tuning parameter) for case study 2: (a) – Entire production period; (b) –Production after chamber is fully-developed.

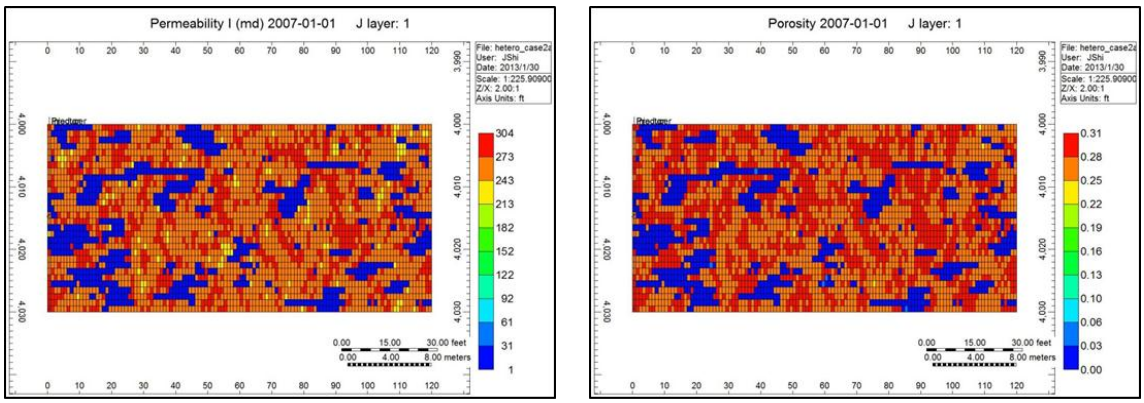

a. Absolute permeability field

b. Porosity field

Figure 3-9. Absolute permeability and porosity field in x-z cross-sectional view for heterogeneous case study 3.

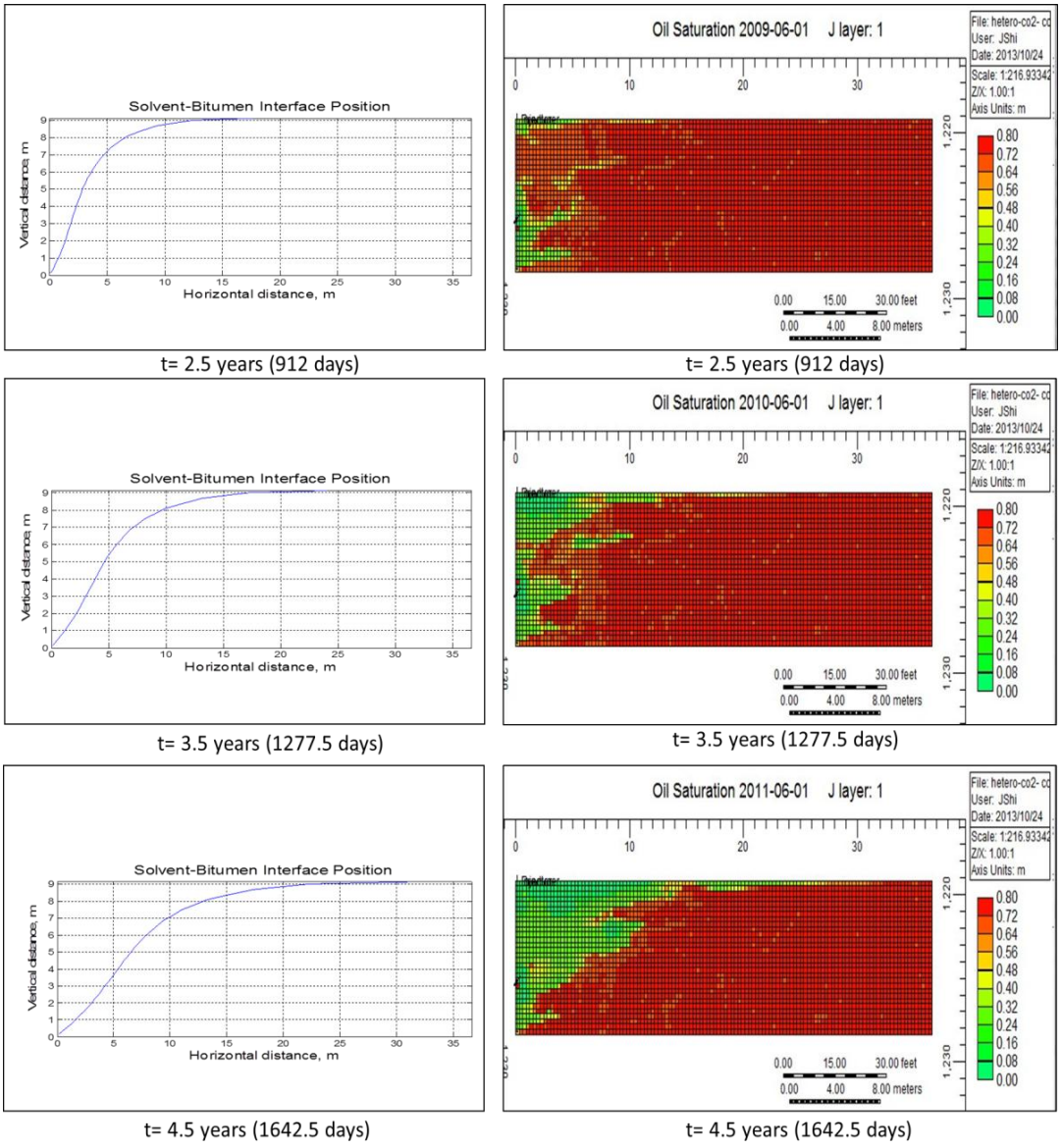

Figure 3-10. Comparison of solvent-bitumen interface position between detailed flow simulations and proxy model predictions for the heterogeneous case study 3.

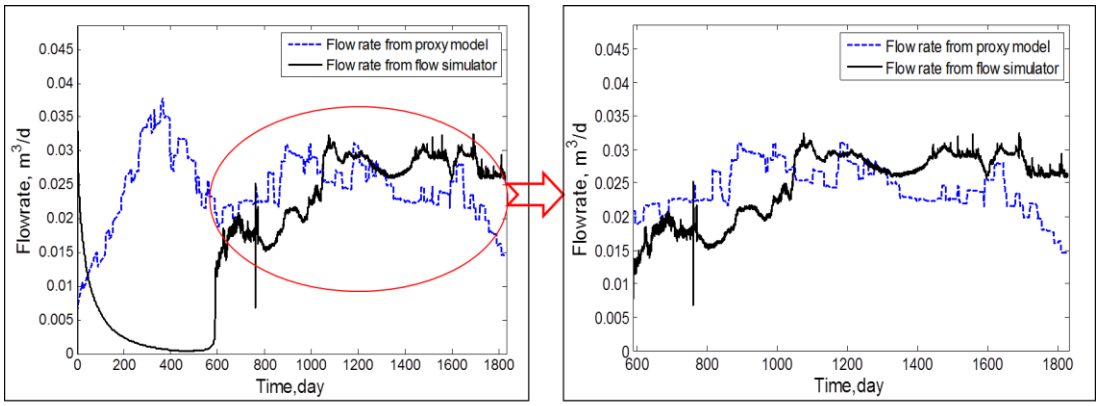

Figure 3-11. Comparison of oil production rate as a function with time between flow simulation results and proxy predictions (flow rate at the bottom interface node divided by the tuning parameter) for case study 3: (a) – Entire production period; (b) – Production after 600 days.

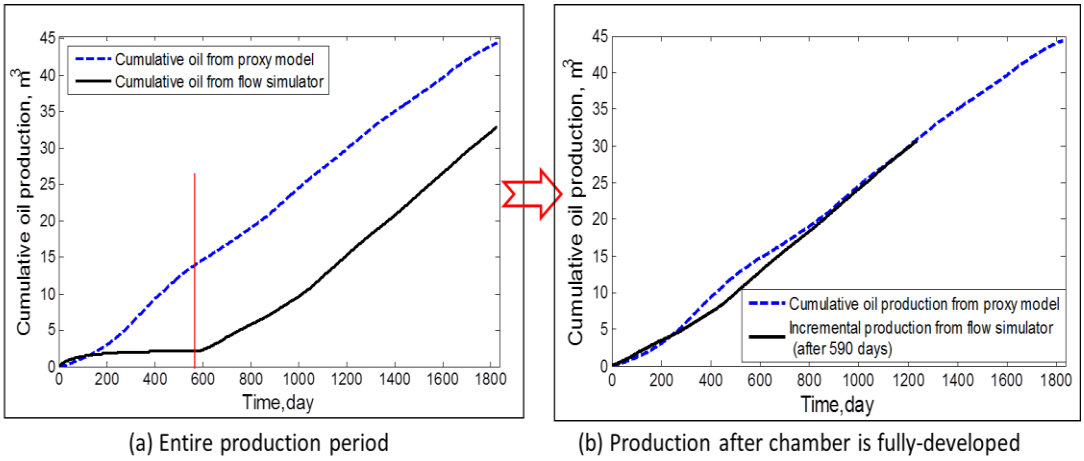

Figure 3-12. Comparison of cumulative oil production as a function with time between flow simulation results and proxy predictions (flow rate at the bottom interface node divided by the tuning parameter) for case study 3: (a) – Entire production period; (b) – Production after chamber is fully-developed.

Appendix

Section A. Derivation of mass penetration rate with time

We begin by performing a mass balance over the cell element in Figure 3-1. Mass of solvent is transported into the bitumen with a forward flux:

$$Mass(\ forward) = -\phi S_o D_s\big|_{C_s=C_{sc}} \rho_s \left(\frac{\partial C_s}{\partial \xi}\right)_{\xi=0} \quad \text{..... (A1)}$$

Mass of solvent being left behind in the reservoir because of the forward motion of the front:

$$Mass(left) = U\rho_s\left(C_{sc} - C_{sr}\right) \quad \text{..... (A2)}$$

Thus net result of these two fluxes is the rate of mass accumulated ahead of the front, as shown in Eq.A3:

$$\frac{1}{A}\frac{dm_r}{dt} = -\phi S_o D_s\big|_{C_s=C_{sc}} \rho_s \left(\frac{\partial C_s}{\partial \xi}\right)_{\xi=0} - U\rho_s\left(C_{sc} - C_{sr}\right) \quad \text{..... (A3)}$$

Eq.A3 can be written in terms of the mass penetration variable γ_m as in Eq.A4:

$$\frac{d(\frac{\partial m_r}{\partial A})}{dt} = \frac{d(\gamma_m \phi S_o \rho_s (C_{sc} - C_{sr}))}{dt} = -\phi S_o D_s\big|_{C_s=C_{sc}} \rho_s \left(\frac{\partial C_s}{\partial \xi}\right)_{\xi=0} - U\rho_s\left(C_{sc} - C_{sr}\right) \text{.... (A4)}$$

Assuming the term $\phi S_o \rho_s (C_{sc} - C_{sr})$ being constant with time and factoring it out of the derivative and rearranging Eq.A4, we express the mass penetration rate in Eq.A5:

$$\frac{d\gamma_m}{dt} = \frac{-D_s\big|_{C_s=C_{sc}} \left(\frac{\partial C_s}{\partial \xi}\right)_{\xi=0}}{\left(C_{sc} - C_{sr}\right)} - \frac{U}{\phi S_o} \quad \text{..... (A5)}$$

Define the dimensionless solvent concentration distribution C_s* as:

$$C_s^* = \frac{C_s - C_{sr}}{C_{sc} - C_{sr}} \quad \text{.....(A6)}$$

Then the solvent concentration gradient $\frac{\partial C_s^*}{\partial \xi}$ can be calculated as:

$$\frac{\partial C_s^*}{\partial \xi} = \frac{1}{C_{sc} - C_{sr}} \frac{\partial C_s}{\partial \xi} \quad \text{.....(A7)}$$

At solvent-bitumen interface where ξ= 0, Eq.A7 can be expressed as:

$$\left(\frac{\partial C_s^*}{\partial \xi}\right)_{\xi=0} = \frac{1}{C_{sc} - C_{sr}} \left(\frac{\partial C_s}{\partial \xi}\right)_{\xi=0} \quad \text{.....(A8)}$$

Substituting Eq.A8 in Eq.A5 gives:

$$\frac{d\gamma_m}{dt} = -D_s\big|_{C_s=C_{sc}} \left(\frac{\partial C_s^*}{\partial \xi}\right)_{\xi=0} - \frac{U}{\phi S_o} \quad \text{.....(A9)}$$

The above equation can be solved by following the approximation in Butler (1985) and assessing the solvent concentration gradient $\left(\frac{\partial C_s^*}{\partial \xi}\right)_{\xi=0}$ at the two extreme conditions:

1) Steady state case: U and ϕ are constants, and $\frac{d\gamma_m}{dt} = 0$; the solvent concentration gradient is given as:

$$\left(\frac{\partial C_s^*}{\partial \xi}\right)_{\xi=0} = -\frac{U}{\phi S_o D_s\big|_{C_s=C_{sc}}} \quad \text{.....(A10)}$$

Substituting Eq.24 into Eq.A10 to obtain Eq.A11:

$$\left(\frac{\partial C_s^*}{\partial \xi}\right)_{\xi=0} = -\frac{1}{\gamma_m} \quad \text{..... (A11)}$$

2) Stationary interface case: $C_s = C_{sc}$ at $\xi = 0$ and $C_s = C_{sr} = 0$ at $t = 0$. The solvent concentration is given by Eq.A11:

$$C_s^* = erfc\left(\frac{\xi}{2\sqrt{\phi S_o D_s t}}\right) \quad \text{..... (A12)}$$

The corresponding concentration gradient at the interface is then given by Eq.A13:

$$\left(\frac{\partial C_s^*}{\partial \xi}\right)_{\xi=0} = -\frac{2e^{-\left(\frac{\xi}{2\sqrt{\phi S_o D_s t}}\right)^2}}{\sqrt{\pi}}\left[\frac{1}{2\sqrt{\gamma_m{}^2}}\right] = -\frac{1}{\sqrt{\pi}\gamma_m} \quad \text{..... (A13)}$$

Assuming the concentration gradient varies linearly with velocity between two limiting cases, the solvent concentration gradient can be approximated by Eq.A13 as:

$$\left(\frac{\partial C_s^*}{\partial \xi}\right)_{\xi=0} = -\frac{1}{\sqrt{\pi}\gamma_m} - \left(1 - \frac{1}{\sqrt{\pi}}\right)\frac{U}{\phi S_o D_s} \quad \text{..... (A14)}$$

Eq.A14 is still valid for the two extreme cases. If $U = 0$, the limiting case 2) applies; if U is constant, the limiting case 1) applies. Finally, we substitute Eq.A14 into Eq.A9 and rearrange it, the mass penetration rate is given by Eq.A15:

$$\frac{d\gamma_m}{dt} = \frac{D_s\big|_{C_s=C_{sc}}}{\sqrt{\pi}\gamma_m} + \frac{U D_s\big|_{C_s=C_{sc}}}{\phi S_o D_s}\left(1 - \frac{1}{\sqrt{\pi}}\right) - \frac{U}{\phi S_o} \quad \text{..... (A15)}$$

Further rearranging of Eq.A15 gives:

$$\frac{d\gamma_m}{dt} = \frac{D_s}{\sqrt{\pi}\gamma_m} - \frac{1}{\sqrt{\pi}}\frac{U}{\phi S_o} = \frac{1}{\phi S_o\sqrt{\pi}}\left(\frac{\phi S_o D_s}{\gamma_m} - U\right) \quad \text{..... (25)}$$

If ϕ and S_o are set to unity as in the case for a Hele-Shaw cell, the above equation becomes:

$$\frac{d\gamma_m}{dt} = \frac{1}{\sqrt{\pi}}\left(\frac{D_s}{\gamma_m} - U\right) \quad \text{..... (13)}$$

Section B. Derivation of the total production rate for half-side drainage

The horizontal and vertical displacement of the interface at any point is given by Eq.27 and Eq.28, respectively:

$$\left(\frac{\partial q}{\partial y}\right)_t = -\phi\Delta S_o\left(\frac{\partial x}{\partial t}\right)_y \quad \text{..... (27)}$$

$$\left(\frac{\partial q}{\partial x}\right)_t = \phi\Delta S_o\left(\frac{\partial y}{\partial t}\right)_x \quad \text{..... (28)}$$

Since

$$U = -\cos\theta\left(\frac{\partial y}{\partial t}\right)_x \quad \text{..... (B1)}$$

Substitute Eq.B1 into Eq.28 gives:

$$\left(\frac{\partial q}{\partial x}\right)_t = \frac{\phi\Delta S_o U}{-\cos\theta} \quad \text{..... (B2)}$$

Eq.B2 can be rearranged to obtain the expression for *U* as:

$$U = -\frac{\cos\theta}{\phi\Delta S_o}\left(\frac{\partial q}{\partial x}\right)_t \quad \text{..... (B3)}$$

Substitute the above expression back into Eq.5 gives:

$$q = \frac{k_o g \sin\theta}{U} N_s = -\frac{k_o g \sin\theta}{\frac{\cos\theta}{\phi \Delta S_o}\left(\frac{\partial q}{\partial x}\right)_t} N_s \quad \text{..... (B4)}$$

Also, from the interface geometry,

$$\frac{\sin\theta}{\cos\theta} = \frac{\partial y}{\partial x} \quad \text{..... (B5)}$$

Eq.B4 can be written as:

$$q = -\frac{k_o g \phi \Delta S_o}{\left(\frac{\partial q}{\partial y}\right)_t} N_s \quad \text{..... (B6)}$$

Eq.B6 can be integrated by separation of variables, which provides the total production rate for half-side drainage as presented in Eq.29 previously:

$$Q = \sqrt{2 k_o g \phi \Delta S_o h N_s} \quad \text{..... (29)}$$

If ϕ and S_o are set to unity as in the case for a Hele-Shaw cell, the above equation becomes Eq.17 as shown previously:

$$Q = \sqrt{2 k_o g h N_s} \quad \text{..... (17)}$$

Chapter 4: Uncertainty Assessment of Vapex Performance in Heterogeneous Reservoirs Using a Semi-Analytical Proxy Model[3]

Introduction

Vapex (vapor extraction) is an in-situ non-thermal bitumen recovery process, which is analogous to the commonly adopted SAGD (Steam-Assisted Gravity Drainage) method (Butler and Mokrys 1989). Vaporized hydrocarbon solvent is injected into the reservoir via a horizontal injection well, and the diluted low-viscosity oil is drained to the bottom production well by gravity. The key recovery mechanism is molecular diffusion enhanced by various spreading mechanisms such as velocity variations known as dispersion (Das and Butler 1998, Boustani 2001, Das 2005). It has been widely established that dispersion is a strong function of heterogeneities occurring at various scales (Lake 1989) including those randomly distributed, discontinuous, thin shale lenses commonly found in oil sands deposits (Das 1998, Chen et al. 2008).

After the initial physical model of the Vapex process was developed by Butler and Mokrys (1989) in a series of Hele-Shaw cell experiments, subsequent improvement to this process has been proposed in many studies over the years (Das and Butler 1994, Yazdani and Maini 2005 & 2008). Most of these works focus on estimating recovery performance at the laboratory scale. This

[3]A version of this chapter will be submitted for review by a referred journal.

understanding, however, is not sufficient to describe the recovery mechanisms at the reservoir scale, where geology is sufficiently complex that there is significant uncertainty due to the heterogeneous reservoir properties. A number of published works over recent years have attempted to quantify the effects of heterogeneity and distribution of shale barriers on SAGD performance. For example, Yang and Butler (1992) constructed a 2-D experimental model to simulate SAGD performance in two different types of heterogeneous reservoir settings: one with thin shale layers and another one containing horizontal layers of varying permeability. They concluded that a horizontal barrier with limited areal extent does not have significant impact on the cumulative production; the chamber is distorted only slightly near these shale barriers.

Detailed compositional simulators have been employed widely for modeling Vapex performance (Nghiem 2001). However, complexities of its recovery mechanisms render numerical modeling of such process in heterogeneous reservoirs highly cumbersome and expensive. Efficient alternatives, like semi-analytical proxy models, can overcome such computational challenges by providing an approximate solution without solving all the detailed equations. A number of these proxy models have been proposed for assessment of SAGD and solvent-assisted processes in the past (Vanegas et al. 2008 & 2009, Azom and Srinivasan 2013, Gupta and Gittins 2011), but its application for modeling Vapex process is lacking.

Computational requirement is further intensified because heterogeneity informed by insufficient information leads to uncertainty in reservoir models.

Descriptions of heterogeneity are incomplete because data is typically noisy and sparse (Leung and Srinivasan 2012), rendering uncertainty an intrinsic characteristic of any reservoir geological modeling effort (Forster 2008, Leung 2012, Yang et al. 2011). Therefore, accounting for the uncertainty exists in heterogeneous reservoir in terms of rock properties (i.e., lithofacies, porosity and permeability) in the modeling or simulation workflow is critical for improved oil recovery and reservoir management (Deutsch and Srinivasan 1996).

Several optimization studies of SAGD projects were conducted in the past considering reservoir heterogeneities: Li et al. (2011) conducted a simulation study to investigate the impact of shale barriers on SAGD performance and proposed optimization injection strategies including solvent co-injection and/or placement of additional steam injectors above the shale barrier. They stated that solvent coinjection with mixtures of C_7 and C_{12} can reduce the flow resistance at the end of a shale barrier and deliver higher recovery factor as well as a lower cumulative energy/oil ratio; Kumar et al (2010) investigated the influence of heterogeneity (i.e., low permeability regions) on SAGD wellbore design by optimizing the length and positioning of tubular strings, as well as the allocation of injected steam among tubing strings; Al-Gosayir et al. (2012) proposed a hybrid genetic algorithm to optimize cumulative steam-oil ratio (cSOR) and recovery factor in two synthetic heterogeneous reservoir models exhibiting different shale distributions. In these studies, only a couple of realizations were randomly selected and utilized in the optimization procedure, which may ignore the uncertainty of reservoirs and deviate significantly from the actual solution. To

capture reservoir uncertainties, a large number of realizations honoring geological properties (i.e., porosity and permeability) are often needed. In an optimization procedure described by Yang et al. (2011), preliminary screening using detailed flow simulation was performed using a large number of realizations, and a reduced subset is selected for subsequent detailed optimization of well placement and operating strategy including bottom-hole pressure and steam injection rate. However, only a few works have alluded to the uncertainty assessment of Vapex performance due to variability in reservoir heterogeneities (Forster 2008, Leung 2012).

In most practical scenarios, a large number (hundreds) of equally probable realizations of reservoir properties (i.e., facies, porosity, and permeability) are constructed (Kelkar and Perez 2002); however, it is typically impractical to subject all the realizations to flow simulation. Some researchers have proposed various ranking schemes for selecting a subset of these realizations that would capture the response uncertainty exhibited by those multiple realizations prior to optimization. For example, realizations are ranked based on particular recovery indicators such as average oil production rate, cumulative oil production, and cumulative steam-oil ratio for characterizing SAGD performance (Fenik et al 2009, Vanegas et al. 2009, Pooladi-Darvish and Mattar 2002). Mclennan and Deutsch (2005) implemented a number of ranking schemes that are based on static measurements including volumetric measurement of original oil in place (OOIP) and global/local connectivity measures; these schemes are in contrast to those that are based on measures derived from dynamic information such as flow-

based connectivity between injectors and producers and travel time of a natural tracer along streamlines (Saad et al. 1996, Ates et al. 2005, McCarthy 1993). Deutsch and Srinivasan (1996) commented that dynamic ranking criteria derived from fast flow simulation (i.e., tracer and streamline simulation) or other flow-based proxy should be preferred. Recently, Vanegas et al. (2009) applied a semi-analytical SAGD proxy for ranking realizations for recovery modeling.

Our research objective is to apply the semi-analytical proxy model developed by Shi and Leung (2013 & in press) to assess the impacts on Vapex performance due to uncertainty in reservoir heterogeneities. In our previous works, a novel semi-analytical proxy was developed to model solvent transport in Vapex at isothermal conditions. Analytical formulations were derived and implemented in a calculation procedure to advance the solvent-oil interface and to estimate producing oil rate with time. A mass penetration parameter was formulated, and its change with time was tracked. This proxy has been applied to various reservoirs discretized with spatially-varying porosity and permeability values; oil drainage rate and solvent penetration were calculated along the solvent-oil interface over incremental time steps. Results obtained with the proxy were validated against experimental data available in the literature as well as detailed compositional simulation studies.

In this paper, the proxy model is employed to illustrate its application in uncertainty assessment. In a case study, it is used to facilitate ranking of geostatistical realizations; cumulative oil production estimated using the proxy becomes the basis for the ranking scheme. A smaller, more manageable subset of

models representing the low-side, expected, and high-side realizations (Deutsch and Srinivasan 1996) is identified, and they can be subjected to further detailed compositional simulation analysis. The ranking results demonstrate good agreement with those based on detailed compositional simulations but with significant savings in computational costs. In another case study, a suite of coarse-scale models capturing the uncertainty in the sub-modeling scale is subjected to the semi-analytical proxy to assess the response uncertainty. The workflow discussed in this paper presents an important potential for integrating proxy models with flow simulation such that recovery performance can be properly assessed by accounting for the overall reservoir uncertainties in an efficient manner.

The paper is organized as follows: first, key implementation details of proposed proxy model are presented; next, components and steps of the uncertainty assessment workflow are introduced; finally, two case studies are presented to illustrate the applicability of this workflow for the applications of heterogeneous realizations ranking and assessment of recovery performance uncertainty due to sub-modeling scale heterogeneity.

Methodology and Workflow

Proxy model description and implementation

Due to the similarity of chamber formation in SAGD and Vapex processes, Butler and other researchers have developed analytical solutions for oil drainage rate from a Hele-Shaw cell in a fashion analogous to those of SAGD: heat transfer by

conduction is replaced by mass transfer due to diffusion, where heated bitumen is replaced by diluted bitumen (Butler and Mokrys 1989, Das and Butler 1994). In our previous work, those analytical solutions together with the formulation of a new mass penetration parameter were implemented in an explicit calculation sequence to model the Vapex process in Hele-Shaw cell experiment, which allowed the prediction of total drainage rate with time and the position change of solvent chamber boundary during the spreading chamber period. The drainage rate in this model is defined as the stabilized rate for a fully-developed solvent chamber with an S-shape interface. A schematic illustrating the mass transfer and concentration variation that are occurring inside the mixing zone between the liquid solvent and bitumen interface is explained in **Figure 4-1**.

This Hele-Shaw model was based on simple conditions where porosity and oil saturation change were all set to unity; certain modifications were made to account for the influences of porosity, tortuosity, and oil saturation for a porous medium. Details of the analytical derivations and mathematical formulations for the Hele-Shaw model and porous media models can be found in Shi and Leung (2013 and in press). Only key features of the semi-analytical proxy are described next.

By performing a steady-state material balance over a thin segment inside the solvent-oil interface (Figure 4-1), the one-dimensional convection-diffusion equation gives:

$$U\left(C_s - C_{sr}\right) + \phi S_o D_s \frac{dC_s}{d\xi} = 0 \quad \text{..... (1)}$$

Where U represents a constant advancing velocity of interface, D_s is the intrinsic diffusion coefficient of solvent, C_s is the solvent concentration (volume fraction) at a distance ξ from the interface. C_{sr} denotes the solvent concentration in the reservoir at a distance far away from the interface ($\xi = \xi_{max}$), representing the minimum solvent concentration. Parameters ϕ and S_o denote porosity and oil saturation, respectively. Das and Butler (1998) has noted that in porous media, the value of D_s should be corrected using a cementation factor Ω, which is a measure of consolidation and tortuosity in a porous medium. For the sake of simplicity, it was assumed the tortuosity effect has already been incorporated into the definition of D_s in Eq.1 by adopting a value of 2 for Ω in this work.

The oil flow rate at a point along the interface can be expressed by Eq.2:

$$q = \frac{k_o g \sin\theta \gamma_m}{\phi S_o D_s} N_s \quad \text{..... (2)}$$

In which the dimensionless number N_s is given by Eq.3:

$$N_s = \int_{Csr}^{Csc} \frac{\Delta\rho \phi S_o D_s (1 - C_s) dC_s}{\mu_b (C_s - C_{sr})} \quad \text{..... (3)}$$

It should be noted in Eq.2 that the oil drainage rate is a function of effective oil permeability (k_o), gravitational constant (g), angle between the interface and horizontal axis (θ), mass penetration depth (γ_m), density difference between solvent and oil ($\Delta\rho$), bitumen viscosity (μ_b), and other previously-defined variables including D_s, ϕ and S_o, which are also incorporated in the dimensionless variable N_s. The new variable, mass penetration depth γ_m, is defined

as the depth to which mass of solvent would have penetrated if C_s has achieved a uniform value of C_{sc} in the solvent-oil mixing zone. It can also be interpreted as the penetration capacity of solvent into the bitumen. This variable is analogous to the heat penetration parameter in its SAGD analog (Butler 1985), and by performing a mass balance over a cell element in Figure 4-1, mass penetration rate can be expressed by Eq.4.

$$\frac{d\gamma_m}{dt} = \frac{1}{\phi S_o \sqrt{\pi}} \left(\frac{\phi S_o D_s}{\gamma_m} - U \right) \quad \text{..... (4)}$$

The expression of horizontal and vertical displacement velocity of the interface at any point are given by:

$$\left(\frac{\partial q}{\partial y} \right)_t = -\phi \Delta S_o \left(\frac{\partial x}{\partial t} \right)_y \quad \text{..... (5)}$$

$$\left(\frac{\partial q}{\partial x} \right)_t = \phi \Delta S_o \left(\frac{\partial y}{\partial t} \right)_x \quad \text{..... (6)}$$

The cumulative oil drainage along the cross section per unit well length at a particular location (x, y) over the time t is represented by the shaded area in **Figure 4-2**. Advancing velocity of interface can also be expressed by combining Eqs.5-6 with trigonometric relationship between U and θ (see **Figure 4-3**) in Eq.7:

$$U = -\frac{1}{\phi \Delta S_o} \frac{\partial q}{\partial L} \quad \text{..... (7)}$$

Besides, the total production rate per unit length for half-side drainage is given by Eq.8:

$$Q = \sqrt{2k_o g \phi \Delta S_o h N_s} \quad \text{..... (8)}$$

Where h is the total vertical height for drainage process.

As the diluted oil starts to drain by gravity, the flow is directed downward along the interface, and the drainage rate at each node calculated by Eq.2 will cumulate downward to the bottom node. Theoretically, the flow rate q determined using Eq.2 at the bottom interface node can be treated as the total drainage rate as calculated by Eq.8. This is validated by comparing the average bottom-node flow rate, predicted total flow rate, and experimental observation for the Hele-Shaw cell experiments. However, when applying the semi-analytical model to porous media, the total drainage rate calculated using Eq.8 matches well with compositional flow simulation results, but the bottom-node flow rate calculated with Eq.2 is approximately 4 times bigger than the other two values. In the Hele-Shaw model, a sharp solvent-oil interface is typically assumed (Figure 4-1), where the oil saturation changes from its residual value (i.e., zero in a Hele-Shaw cell) to its initial value (i.e., unity in a Hele-Shaw cell) across the interface. While in the porous media, the mass transfer process takes place in a contact zone or the diffusion boundary layer as described by Das (2005). We postulate that the averaged approximations of S_o, k_o, and D_s in the diffusion boundary layer are responsible for the deviations. Another possible explanation is that analytical formulation assumes that the bottom of the chamber remains stationary at the producer, while in reality, the chamber grows slowly away from the well pair; hence the direct comparison of flow rate value obtained at the bottom interface node using the proxy model to actual producing rate from flow simulation might

reveal some discrepancy. We treated this factor of 4 as the tuning parameter. Details of the calibration procedure and validation of this tuning parameter are presented in Shi and Leung (2013).

The above analytical formulations can be applied to describe the growth of spreading period of a fully-developed solvent chamber and to calculate stabilized oil drainage rate. The above equations are discretized numerically and solved in an explicit calculation sequence. The developed semi-analytical proxy consists of the following steps:

1) Assign a number of evenly distributed nodes along the interface as shown in Figure 4-3. These nodes would advance laterally along the reservoir width (or plate width for Hele-Shaw cell) as the solvent chamber grows.

2) Initialize values of mass penetration γ_m at each node defined in step 1. The criterion for assigning the initial values seems arbitrary when referring to Butler (1985) as he described the initialization of the analogous heat penetration parameter for SAGD. In his work, it is stated that the value of heat penetration should decrease from bottom to top (i.e., largest near the well pair and smallest near the chamber top). We concluded from a sensitivity analysis that impacts on ensuing recovery performance are insignificant (Shi and Leung in press).

3) Calculate the oil flow rate q for each node using Eqs.2-3. It is convenient to assume an interface angle θ of $90\,^\circ$ at the beginning of the spreading period. The oil rate right below the overburden is set to zero by assuming the mass penetration value at the first grid node next to the upper boundary to be zero. To calculate N_s, it is necessary to determine the correlation of $\Delta\rho$ and μ_b as functions of solvent

concentration C_s. This can be achieved using an equation of state such as the Peng-Robinson (PR-EOS) model (Sandler 2006). For a heterogeneous medium, arithmetic averages of permeability and porosity, which are calculated using k_o and ϕ values at grid blocks along the interface, at time level n are used in Eqs.2-3.

4) Calculate the interface change in x or y direction at next time step using Eq.5 or Eq.6. If the interface is nearly vertical (θ>45°), the horizontal movement of interface can be determined by Eq.5, whereas if it is generally horizontal (θ<45°), vertical advance of the interface can be calculated by Eq.6. Consider a small time step Δt, using central difference approximation in space and forward difference approximation in time, Eq.5 and Eq.6 can be discretized as follows:

$$\frac{q_{i+1}^n - q_{i-1}^n}{y_{i+1}^n - y_{i-1}^n} = -\phi \Delta S_o \frac{x_i^{n+1} - x_i^n}{t^{n+1} - t^n} \quad \text{..... (9)}$$

$$\frac{q_{i+1}^n - q_{i-1}^n}{x_{i+1}^n - x_{i-1}^n} = \phi \Delta S_o \frac{y_i^{n+1} - y_i^n}{t^{n+1} - t^n} \quad \text{..... (10)}$$

The superscripts n and n+1 refer to quantities evaluated at the present and next time levels. The subscripts i indicate the i^{th} interface node and its neighboring interface nodes are denoted by the subscripts i-1 and i+1, as shown in Figure 4-3. By using Eq.9 and Eq.10, the horizontal and vertical locations for each node can be advanced explicitly with time.

5) Calculate the length between two neighboring nodes around i as approximated by L_i in Figure 4-3:

$$L_i = \sqrt{(x_{i-1} - x_{i+1})^2 + (y_{i-1} - y_{i+1})^2} \quad \text{..... (11)}$$

Similarly, the interface angle θ for grid node i can be evaluated using the trigonometric relation in Eq.12:

$$\theta_i = \arcsin\left(\frac{y_{i-1} - y_{i+1}}{L_i}\right) \quad \text{..... (12)}$$

6) Calculate the advancing velocity of interface using discretized form of Eq.7:

$$U_i^n = -\frac{1}{\phi \Delta S_o} \frac{q_{i+1}^n - q_{i-1}^n}{L_i^n} \quad \text{..... (13)}$$

7) Calculate a new value of mass penetration at the next time level using discretized form of Eq.4:

$$\frac{\gamma_{m,i}^{n+1} - \gamma_{m,i}^n}{\Delta t} = \frac{1}{\sqrt{\pi}(\phi S_o)_i^n}\left(\frac{\phi S_o D_s}{\gamma_{m,i}^n} - U_i^n\right) \quad \text{..... (14)}$$

8) Repeat steps 2 to 7 until the final time is reached.

It should be emphasized that our proxy model assumes that an interface can be defined and exists at $\xi = 0$, and its movement with time along with the size of the diffusion boundary layer (i.e., γ_m), where C_s decreases along $\xi > 0$, are tracked. The spatial concentration profile across the diffusion zone, however, is not explicitly calculated; hence, detailed discretization across the diffusion boundary layer is not necessary. Results obtained from the proxy have been validated against experimental data available in the literature as well as detailed compositional simulation studies for both homogeneous and heterogeneous media. Computational efficiency of the proxy in comparison to numerical simulations was also highlighted in our previous work (Shi and Leung 2013).

Uncertainty assessment workflow

Factors such as oil sand thickness, facies changes, shale barriers, faults, fractures, and thief zones have an overarching impact on the shape of solvent chamber and resultant recovery performance (Venuto 1989). Recovery performance for a heterogeneous reservoir with spatially-varying porosity and permeability (**Figure 4-4**) is compared with that of a homogeneous reservoir given all other conditions remain identical. As shown in **Figure 4-5**, the low permeability zones (or shale contents) act as barriers to the development of solvent chamber, whose position is delineated by the jagged irregular interface. Heterogeneity also reduces the recovery efficiency, as evidenced by the decreasing oil production rate as shown in **Figure 4-6**.

In this work, the semi-analytical proxy discussed in the previous section is applied to assess the impacts of heterogeneity in terms of spatially-varying permeability and porosity on Vapex recovery. Oil production rate and solvent-bitumen interface position are estimated as functions of time for the entire suite of realizations. The variability exhibited by these realizations reflects the response uncertainty. Realizations representative of the low-side, expected, and high-side can also be reliably selected based on ranking criteria including cumulative oil production and stabilized oil rate. A representative subset of realizations can be identified for further detailed (more expensive) compositional flow simulation analysis.

The workflow for uncertainty assessment of Vapex performance using a semi-analytical proxy model is shown in **Figure 4-7.** The first step of this workflow is

to generate multiple equi-probable geological realizations with different heterogeneity distributions, which includes the spatial distributions of the geological variables such as permeability and porosity. In the examples presented in this paper, cumulative oil production is used as a ranking parameter to select a representative subset of realizations, as in Application 1 in Figure 4-7, which is then subjected to detailed flow simulations. Whenever possible, simulation results should be compared with proxy results for verification purposes.

Application

Case study 1 - Ranking of heterogeneous reservoir models

A synthetic 2-D cross-sectional reservoir is modeled. A grid of $50 \times 15 \times 1$ blocks is prepared to simulate the Vapex process, where vaporized CO_2 is injected as solvent. The grid blocks are of uniform size (i.e. $\Delta x = \Delta z = \Delta y = 1$ ft). The injection well is placed 5 ft above the production well, which is located at the bottom of the reservoir. Both production well and injection well are of unit length oriented along *j* direction. Other reservoir parameters are adopted from those presented in Forster (2008). Initial reservoir conditions and other operating constrains are summarized in **Table 4-1**. Only half of the solvent vapor chamber is modeled.

Fluid properties of a heavy oil sample provided by Sharma (1994) for the Schrader Bluff oil pool is used. A detailed description of the fluid model and all the PVT properties are given in Forster (2008). The oil sample has a viscosity of 41 cp at reservoir conditions, with an API gravity of 18 and bubble-point pressure of 1300 psia.

To represent the uncertainty in the underlying heterogeneity, a set of 40 unconditional realizations of the facies distribution are generated using SGeMS (Remy et al. 2009). A total of 4 facies model (histogram and covariance), as summarized in **Table 4-2**, have been used; and 10 realizations are generated for each facies model via sequential indicator simulation (Deutsch and Journel 1998). Within each facies, porosity values are populated using sequential Gaussian simulation (Deutsch and Journel 1998) according to the histograms adopted from Leung (2012) as shown in **Figure 4-8** and an isotropic variogram $\gamma(h)$ described by a spherical model with range of 3 ft, nugget value of 0.5 and 0 ° dip angle. The absolute permeability is correlated to porosity according to Eqs.15 and 16:

Sand: $k = 1230 \times \phi^{1.2}$ .....(15)

Shale: $k = 547 \times \phi^{1.2}$ .....(16)

All 40 realizations are subjected to flow modeling using compositional flow simulator GEM® (Computer Modeling Group 2011) and proxy model for a total production of 3 years. The average computational time of executing each simulation run is about 2300 seconds (approximately 38 min) using a 3.4 GHz, 16 GB of RAM, Intel® Core™ i7-2600 CPU; while the run time for the proxy model is about 1 second using the University of Alberta's Numerical and Statistical Server with two 3 GHz quad core Xeon processors and 64 GB RAM. It indicates a huge improvement in terms of calculation efficiency by using proxy.

Recovery responses of all 40 realizations obtained from both proxy analysis and detailed compositional flow simulations are assembled and ranked. Ranking results based on final cumulative oil derived from proxy analysis and detailed

compositional flow simulation are compared in **Figure 4-9**. Higher ranking represents higher cumulative oil production. The comparison suggests a good agreement between the two approaches. In addition, a subset of realizations representing the low-side (i.e., realization 35, 3), expected (i.e., realization 38, 31) and high-side (i.e., realization 28, 26) scenarios can be readily identified from Figure 4-9. This observation encourages the application of the proxy model for realization screening and ranking.

Based on the ranking results shown in Figure 4-9, distributions of porosity (and its histogram) and absolute permeability are shown in **Figure 4-10** for three randomly-selected realizations. As an example, a representative low-side realization (i.e., #35) that is generated using facies model 4 with the highest shale proportions as illustrated in Table 4-2, is shown. Areal distribution of the shale facies is substantial in terms of both quantity and lateral extent. The high-side sample (i.e. #28), on the other hand, is generated using facies model 3 consisting of the lowest shale proportions; only a small number of shale facies are present with limited areal extent, representative of a reservoir with high flow conductivity. The quantity and continuity of shale facies in the expected sample (i.e., #38 generated using facies model 4) are observed to be in between those of the low-side and high-side samples according to Figure 4-10.

Figure 4-11 shows the comparison of predicted oil rate as a function of time obtained from proxy analysis and flow simulation for the three randomly-selected realizations. A substantial variability in oil rate can be observed between the representative low-side and high-side realizations. Oil production decreases as

reservoir heterogeneities (proportion and continuity of shale) increase. Shale layers exist as barriers to solvent chamber growth. It slows down the solvent transfer process and drainage rate of diluted bitumen.

For both the expected and high-side realizations (i.e., realizations #38 and 28), stabilized oil rates predicated from proxy analysis demonstrate good agreement with those obtained from flow simulation, indicating the impacts of heterogeneity on the recovery performance are less severe in reservoirs with good qualities (i.e., few shaly facies). For low-side realization #35, the average oil rate calculated from the proxy is approximately two times than that obtained from flow simulation. However, considering the results are exhibiting orders of magnitude differences among these realizations, the proxy predictions appear to be reasonable. It should be noted that the averaging scheme applied in the proxy is only an approximation and tends to smooth out the interface. As shown in **Figure 4-12**, after two years production, a smooth solvent-oil interface is obtained from proxy modeling, which deviates from the jagged interface predicted from detailed flow simulations. The shale distributions around the well pair have the most significant impact in slowing down and obstructing the growth of solvent chamber. Nevertheless, the proxy model still provides reasonable approximation of the interface position in an average sense.

Case study 2 – Uncertainty assessment of sub-modeling scale heterogeneities

The proxy model is applied to assess the uncertainty in recovery response due to sub-modeling scale heterogeneities. Consider a synthetic 2D reservoir that is 120

ft x 30 ft. An injection well is placed 5 ft above the production well, which is located at the bottom of the reservoir. Both production and injection wells are of unit length oriented along *j* direction. In practice, the true reservoir model is always unknown; however, values of rock properties at wells can be inferred quantitatively from petrophysical measurements. In this example, porosity values at a resolution of 0.2 ft are available at the injector and producer location. Porosity is assumed to follow a histogram as shown in **Figure 4-13 (a)** and a spherical variogram model as shown in **Figure 4-14 (a).** Absolute permeability is correlated with porosity as $24500\phi^2$. The ratio of vertical to horizontal permeability is assumed to be 1.0 (i.e., $k_v = k_h$). Fluid properties and all other reservoir conditions are the same as described in case study 1.

Instead of generating a suite of equi-probable realizations of porosity and permeability models at a fine-scale of 0.2 ft (same as measurement scale) and subjecting each to detailed flow modeling, which would have been practically impossible because of the overwhelming computational costs, the proxy will be used to assess the recovery performance due to reservoir heterogeneity and its uncertainty with a suite of coarse-scale models with uniform grid size ($\Delta x = \Delta z = \Delta y = 1$ ft). Therefore, the objectives of this study are to: (1) construct a suite of equi-probable realizations of porosity and permeability models that takes into account (a) uncertainty in reservoir heterogeneity at the modeling scale and (b) variability introduced by scale-up of reservoir attributes from fine-(measurement) scale to coarse-(modeling) scale; and (2) perform proxy simulation using the entire suite of coarse-scale models to capture the response uncertainty.

Procedures for scale-up of reservoir attributes are described in detail in Leung and Srinivasan (2011). First, volume variance at the coarse scale is computed corresponding to the fine-scale spatial correlation (or variogram) model (Journel and Huijbregts 1978). Next, numerous sets of "conditioning data" are then sampled from probability distributions whose mean is the block average of the actual measure values and the variance is the volume variance. Then, averaged variogram appropriate at the coarse scale is computed via arithmetic averaging of the fine-scale variogram model. Finally, sequential simulations are carried out to generate multiple realizations at the coarse scale using the numerous conditioning data sets and the averaged variogram. The main idea is that variability introduced by averaging or scale-up at well locations leads to additional uncertainty in the conditioning data.

Following the aforementioned procedure, 10 sets of conditioning data are sampled at the well locations (injector and producer). A total of 100 realizations of the coarse-scale porosity models are generated by sequential Gaussian simulation, as implemented in GSLIB (Deutsch and Journel 1998). Each model contains 120×30 gridblocks with uniform grid size of 1 ft. Histogram of the coarse-scale porosity model is shown in **Figure 4-13 (b),** and the corresponding averaged (scaled-up) variogram is also plotted in **Figure 4-14 (b)**. Conditional sequential Gaussian simulations are performed with scaled-up histogram and averaged variogram for each set of conditioning data. As an example, a randomly-selected realization of the coarse-scale porosity model is shown in **Figure 4-15**.

All 100 realizations are then simulated with the proxy model for a total production time of 3 years and time step of 0.5 day. The execution time is about 3 minutes using the same server described in case study 1. Cumulative probability distributions (CDF) of the stabilized oil flow rate calculated using Eq.2-3 at the bottom node and cumulative oil calculated at the end of production obtained by aggregating results derived with all 100 realizations are illustrated in **Figure 4-16**. A summary of the response uncertainty in predicted oil rate and cumulative oil in terms of low-side (P10), expected (P50) and high-side estimate (P90) is shown in **Table 4-3**.

Figure 4-17 (a) illustrates the uncertainty in oil rate as a function of time across all 100 realizations. All profiles show a similar trend where production rate peaks at a maximum value after some time and then declines slowly to a stabilized constant value. **Figure 4-17 (b)** also shows the uncertainty in cumulative oil as a function of time. This uncertainty appears to increase with time because cumulative production volume also increases with time. Superimposed on these two figures are the average oil rate and average cumulative oil, which are simply arithmetic averages of the 100 profiles. They are denoted by the black solid lines and represent the expected profiles of oil rate and cumulative oil production.

Our results demonstrate that response uncertainty due to sub-modeling scale heterogeneity can be captured and quantified using the proxy model with little computational time. Uncertainty distributions in recovery obtained by accounting for variability owing to scale-up of conditioning data leads to an increase in overall uncertainty. This observation implies that ignoring sub-scale uncertainties

would underestimate the ensuing uncertainty in recovery performance. This example also reinforces the notion that "hard" data does not exist in reservoir modeling (Leung and Srinivasan 2011).

Conclusions

1. The semi-analytical proxy model provides an efficient and reliable alternative to predict solvent-oil interface position, producing oil rate, and cumulative oil production in heterogeneous reservoirs. Predicted solvent-oil interface position and oil production rate obtained from the proposed proxy show good agreement with flow simulation results.

2. An uncertainty assessment workflow is presented that applies the proxy model to assess Vapex performance in the presence of geologic uncertainty. The workflow can be used to rank and screen many geostatistical realizations representing heterogeneity at various scales and to quickly identify a smaller, more manageable subset of models for further detailed flow simulations.

3. The proxy simulation requires a significantly reduced computational cost. It allows robust assessment of heterogeneity effects on recovery performance and presents an important potential in efficient production optimization for decision-making processes.

4. Future work should focus on improvements in proxy model to consider oil saturation variance in solvent-oil mixing zone and to better capture the irregular advancement solvent-oil interface around shale barriers.

Acknowledgements

This research was supported by the Sustainable Technologies for Energy Production Systems (STEPS) program managed by the Petroleum Technology Research Centre (PTRC). The authors would also like to thank the Computer Modeling Group (CMG) for providing the academic licenses for GEM and the University of Alberta for granting access to the Numerical and Statistical Server.

Nomenclature

g = gravitational constant, ft/d^2

h = vertical drainage height, ft

k = absolute permeability of reservoir, mD

k_o = effective oil permeability, mD

k_v = vertical permeability, mD

k_h = horizontal permeability, mD

q = cell flow rate for a certain grid block, bbl/d

t = time, days

C_s = solvent concentration (volume fraction) at a distance ξ from interface

C_{sc} = solvent concentration in the edge of solvent chamber

C_{sr} = the solvent concentration in the reservoir

D_s = intrinsic diffusion coefficient of solvent, ft^2/d

L_i = length along interface between two neighboring nodes around node i, ft

N_s = dimensionless integral

Q = total oil drainage rate per unit length of well ft^3/d ft

S_o = oil saturation, %

S_{wi}= irreducible water saturation, %

ΔS_o = oil saturation difference between initial and residual, %

U = frontal advancing velocity of interface, ft/d

V = average drainage velocity due to gravity, ft/d

Greek symbols:

ξ = distance from interface, ft

μ_b= dynamic viscosity of bitumen in solution, cp

θ= the angle of interface from horizontal, °

ϕ = porosity, %

γ_m = mass penetration, ft

$\gamma(h)$ = variogram at a lag distance of h

$\Delta\rho$ = density difference between solvent and oil, kg/ft^3

Subscripts

i = grid block index

max = maximum

Superscripts

n = time level

References

Al-Gosayir, M., Leung, J.Y., and Babadagli, T. 2012. Design of Solvent-Assisted SAGD Processes in Heterogeneous Reservoirs Using Hybrid Optimization Techniques. *Journal of Canadian Petroleum Technology* **51**(6): 437-448. Doi:10.2118/149010-PA

Ates, H., Bahar, A., El-Abd, S., Charfeddine, M., Kelkar, M., and Datta-Gupta, A. 2005. Ranking and Upscaling of Geostatistical Reservoir Models Using Streamline Simulation: A Field Case Study. *SPE Reservoir Evaluation & Engineering* **8**(1): 22-32. Doi: 10.2118/81497-PA

Azom, P.N. and Srinivasan, S. 2013. Modeling Coupled Heat Transfer and Multiphase Flow during the Expanding Solvent Steam-Assisted Gravity Drainage (ES-SAGD) Process. SPE Annual Technical Conference and Exhibition, New Orleans, Louisiana, USA, 30 September- 2 October. Doi: 10.2118/166357-MS

Boustani.A. 2001. Investigation of Interfacial Mass Transfer in Vapor Extraction Process. Msc thesis. University of Calgary, AB, Canada.

Butler, R.M. 1985. A New Approach to the Modeling of Steam-Assisted Gravity Drainage. *Journal of Canadian Petroleum Technology* **24**(3): 42-51. Doi: 10.2118/85-03-01

Butler, R.M. and Mokrys, I.J. 1989. Solvent Analog Model of Steam Assisted Gravity Drainage. *AOSTRA Journal of Research* **5**(1):17-32.

Chen, Q., Gerritsen, M.G. and Kovscek, A.R. 2008. Effects of Reservoir Heterogeneities on the Steam-Assisted Gravity Drainage Process. *SPE*

Reservoir Evaluation & Engineering **11**(5): 921-932. Doi: 10.2118/109873-PA

Computer Modeling Group. 2011. *GEM: Advanced Compositional Reservoir Simulator User's Guide (Version 2011)*. Computer Modeling Group Limited, Calgary, Alberta, Canada.

Das, S.K. 1998. Vapex: An Efficient Process for the Recovery of Heavy Oil and Bitumen. *SPE Journal* **3**(3): 232-237. Doi: 10.2118/50941-PA.

Das, S.K. 2005. Diffusion and Dispersion in the Simulation of Vapex Process. SPE/PS-CIM/CHOA International Thermal Operations and Heavy Oil Symposium, Calgary, Alberta, Canada, 1-3 November. Doi: 10.2118/97924-MS

Das, S.K. and Butler, R.M. 1994. Investigation of 'VAPEX' Process in a Packed Cell Using Butane As a Solvent, Canadian SPE/CIM/CANMET International Conference on Recent Advances in Horizontal Well Applications, Calgary, 20-24 March. Doi: 10.2118/HWC-94-47

Das, S.K. and Butler, R.M. 1998. Mechanism of the Vapor Extraction Process for Heavy Oil and Bitumen. *Journal of Petroleum Science and Engineering* **21**(1-2): 43-59. Doi: 10.1016/S0920-4105(98)00002-3

Deutsch, C.V. and Srinivasan, S. 1996. Improved Reservoir Management Through Ranking Stochasitc Reservoir Models. SPE/DOE Improved Oil Recovery Symposium, Tulsa, Oklahoma, USA, 21-24 April. Doi: 10.2118/35411-MS

Deutsch, C.V. and Journel, A.G. 1998. *GSLIB: Geostatistical Software Library and User's Guide, 2nd edn*. Oxford University Press, New York.

Fenik, D.R., Nouri, A., and Deutsch, C.V. 2009. Criteria for Ranking Realizations in the Investigation of SAGD Reservoir Performance. Canadian International Petroleum Conference, Calgary, Alberta, Canada, 16 -18 June. Doi: 10.2118/2009-191

Forster, L.J. 2008. Numerical Modeling of the VAPEX Process in Heterogeneous Media. MSc thesis dissertation. University of Texas at Austin, Austin, Texas.

Gupta, S. and Gittins, S. 2011. A Semi-analytical Approach for Estimating Optimal Solvent Use in a Solvent Aided SAGD Process. SPE Annual Technical Conference and Exhibition, Denver, Colorado, USA, 30 October-2 November, Doi: 10.2118/146671-MS

Journel, A.G. and Huijbregts, C.J. 1978. *Mining Geostatistics*. London: Academic Press Limited.

Kelkar, M. and Perez, G. 2002. *Applied Geostatistics for Reservoir Chracterization*. Society of Petroleum Engineers Inc, Richardson, Texas.

Kumar, A., Oballa, V., and Card, C. 2010. Fully-Coupled Wellbore Design and Optimization for Thermal Operations. Canadian Unconventional Resources and International Petroleum Conference, Calgary, Alberta, Canada, 19-21 October. Doi: 10.2118/137427-MS

Lake, L.W. 1989. *Enhanced Oil Recovery*. Englewood Cliffs, New Jersey: Prentice Hall.

Leung, J.Y. 2012. Scale-up of Effective Mass Transfer in Vapor Extraction Process for Heterogeneous Reservoirs. SPE Improved Oil Recovery Symposium, Tulsa, Oklahoma, USA, 14-18 April. Doi: 10.2118/153862-MS

Leung, J.Y. and Srinivasan, S. 2011. Analysis of Uncertainty Introduced by Scaleup of Reservoir Attributes and Flow Response in Heterogeneous Reservoirs. *SPE Journal* **16**(3):713-724. Doi: 10.2118/145678-PA

Leung, J.Y. and Srinivasan, S. 2012. Scale-Up of Mass Transfer and Recovery Performance in Heterogeneous Reservoirs. *Journal of Petroleum Science and Engineering* **86**–**87**: 71-86. Doi: 10.1016/j.petrol.2012.03.010.

Li, W., Mamora, D.D., Li, Y., and Qiu, F. 2011. Numerical Investigation of Potential Injection Strategies To Reduce Shale Barrier Impacts on SAGD Process. *Journal of Canadian Petroleum Technology* **50**(3): 57-64. Doi: 10.2118/133298-PA

McCarthy, J. F. 1993. Reservoir Characterization: Efficient Random-Walk Methods for Upscaling and Image Selection. SPE Asia Pacific Oil and Gas Conference, Singapore, 8-10 February. Doi: 10.2118/25334-MS

McLennan, J.A. and Deutsch, C.V. 2005. Selecting Geostatistical Realizations by Measures of Discounted Connected Bitumen. SPE/PS-CIM/CHOA International Thermal Operations and Heavy Oil Symposium, Calgary, Alberta, Canada, 1-3 November. Doi: 10.2118/98168-MS

Nghiem, L.X., Kohse, B.F. and Sammon, P.H. 2001. Compositional Simulation of the Vapex Process. *Journal of Canadian Petroleum Technology* **40**(8):54-61. Doi: 10.2118/01-08-05

Pooladi-Darvish, M. and Mattar, L. 2002. SAGD Operations in the Presence of Overlying Gas Cap and Water Layer-Effect of Shale Layers. *Journal of Canadian Petroleum Technology* **41**(6): 40-51. Doi: 10.2118/02-06-04

Remy, N., Boucher, A., and Wu, J. 2009. *Applied Geostatistics with SGeMS: A User's Guide*. Cambridge University Press, Cambridge, UK.

Saad, N., Maroonge, V., and Kalkomey, C.T. 1996. Ranking Geostatistical Models Using Tracer Production Data. European 3-D Reservoir Modelling Conference, Stavanger, Norway, 16-17 April. Doi: 10.2118/35494-MS

Sandler, S.I. 2006. *Chemical, Biochemical and Engineering Thermodynamics, 4th edn*. Hoboken, NJ: John Wiley & Sons Inc, New York.

Sharma, G.D. 1994. Study of hydrocarbon miscible solvent slug injection process for improved recovery of heavy oil from Schrader Bluff Pool, Milne Point Unit, Alaska. U.S. Department of Energy, Annual Report, January 1, 1994-December 31, 1994.

Shi, J. and Leung, J.Y. 2013. Physics-Based Proxy for Vapex Process Modelling in Heterogeneous Reservoirs. SPE Heavy Oil Conference, Calgary, Alberta, Canada, 11-13 June. Doi: 10.2118/165558-MS

Shi, J. and Leung, J.Y (in press). Physics-Based Proxy Modeling of Solvent Transport in VAPEX Process. *Canadian Journal of Chemical Engineering*.

Vanegas, J.W.P., Deutsch, C.V. and Cunha, L.B. 2008. Uncertainty Assessment of SAGD Performance Using a Proxy Model Based on Butler's Theory. SPE Annual Technical Conference and Exhibition, Denver, Colorado, USA, 21-24 September. Doi: 10.2118/115662-MS

Vanegas, J.W., Deutsch, C.V., and Cunha, L.B. 2009. Transference of Reservoir Uncertainty in Multi SAGD Well Pairs. SPE Annual Technical Conference and Exhibition, New Orleans, Louisiana, USA, 4-7 October. Doi: 10.2118/124153-MS

Venuto, P.B. 1989. Tailoring EOR Processes to Geologic Environments. *World Oil* **209**: 5

Yang, G. and Butler, R.M. 1992. Effects of Reservoir Heterogeneities on Heavy Oil Recovery by Steam-Assisted Gravity Drainage. *Journal of Canadian Petroleum Technology* **31**(8): 37-43. Doi: 10.2118/92-08-03

Yang, C., Card, C., Nghiem, L., and Fedutenko, E. 2011. Robust Optimization of SAGD Operations under Geological Uncertainties. SPE Reservoir Simulation Symposium, The Woodlands, Texas, USA, 21-23 February. Doi: 10.2118/141676-MS

Yazdani, A. and Maini, B.B. 2005. Effect of Drainage Height and Grain Size on Production Rates in the Vapex Process: Experimental Study. *SPE Reservoir Evaluating & Engineering* **8**(3):205-213. Doi: 10.2118/89409-PA

Yazdani, A. and Maini, B.B. 2008. Modeling of the VAPEX Process in a Very Large Physical Model. *Energy & Fuels* **22**(1): 535-544. Doi: 10.1021/ef700429h

Tables

Table 4-1. Initial reservoir and operating conditions for case study 1

Initial reservoir conditions			
Temperature (F °)	Pressure (psi)	Irreducible water saturation S_{wi} (%)	Diffusion coefficient D_s (ft^2/d)
82	1300	20	4.65×10^{-3}
Operating conditions			
Solvent injected	Producing pressure (psi)	Injection pressure (psi)	Flow rate constrains
CO2	967.5	968	None

Table 4-2. Summary of facies models for 40 realizations for case study 1

Realization group name	Realization number	Marginal Probabilities (Proportions)		Variogram Model				
				Range			Angles	
		Shale	Sand	Max	Med	Min	Azimuth	Dip
1 – base case	1-10	0.2	0.8	8	2	2	90	0
2 – increased correlation range	11-20	0.2	0.8	10	2	2	90	0
3 – decreased shale proportions	21-30	0.1	0.9	8	2	2	90	0
4 – increased shale proportions	31-40	0.3	0.7	8	2	2	90	0

Table 4-3. Uncertainty in Vapex recovery performance for 100 realizations in case study 2

Vapex performance parameter	Low-side (P10)	Expected (P50)	High-Side (P90)
Oil rate (based on bottom node) (bbl/day)	0.552	0.564	0.576
Cumulative oil (bbl)	1210	1235	1263

Figures

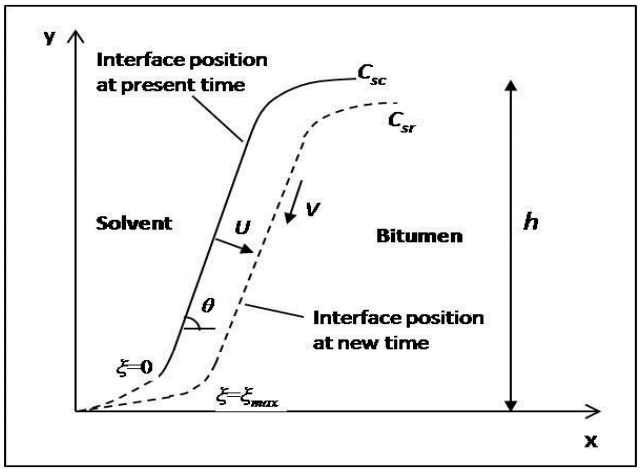

Figure 4-1. Schematic of the solvent-oil interface in Vapex (adapted from Butler and Mokrys 1989).

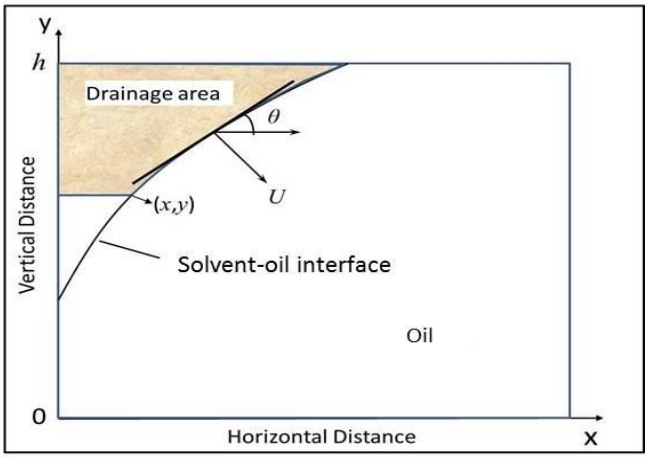

Figure 4-2. Illustration of the observed drainage area in a Hele-Shaw cell Vapex experiment (adapted from Butler and Mokrys 1989).

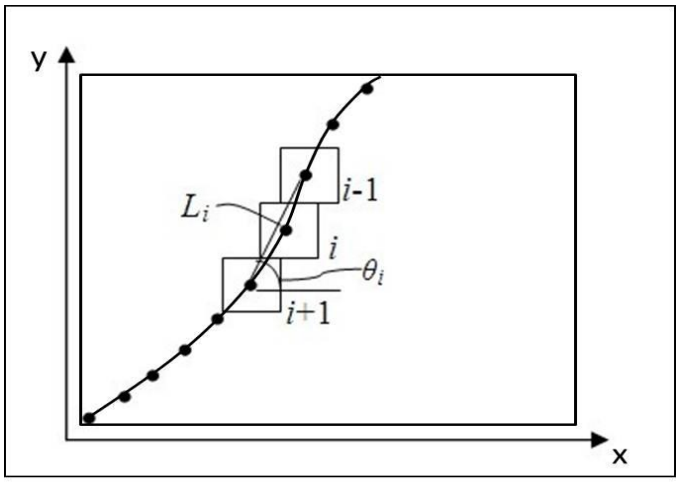

Figure 4-3. Discretization of the solvent-oil interface: dots denote centers of grid blocks where the interface nodes are located (from Shi and Leung 2013).

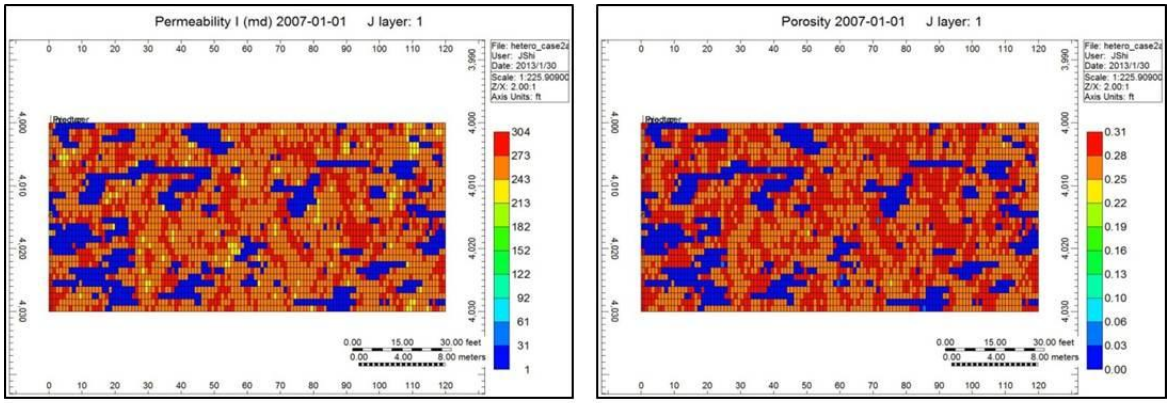

a. Absolute permeability field b. Porosity field

Figure 4-4. Absolute permeability and porosity distribution in x-z cross-sectional view for a heterogeneous reservoir: a. absolute permeability (in mD); b. porosity (adopted from Shi and Leung 2013).

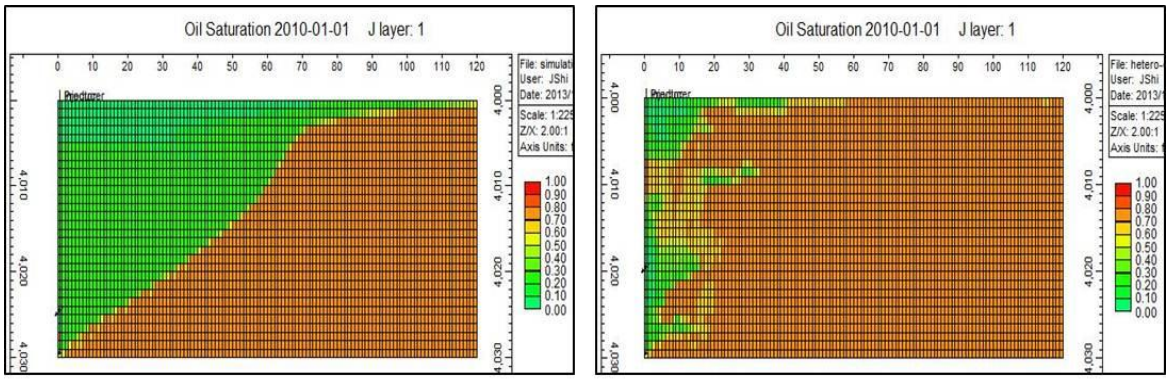

a. Homogeneous case b. Heterogeneous case

Figure 4-5. Comparison of solvent-oil interface between homogeneous and heterogeneous case predicted by flow simulation at the same production time: a. homogeneous case; b. heterogeneous case (adopted from Shi and Leung 2013).

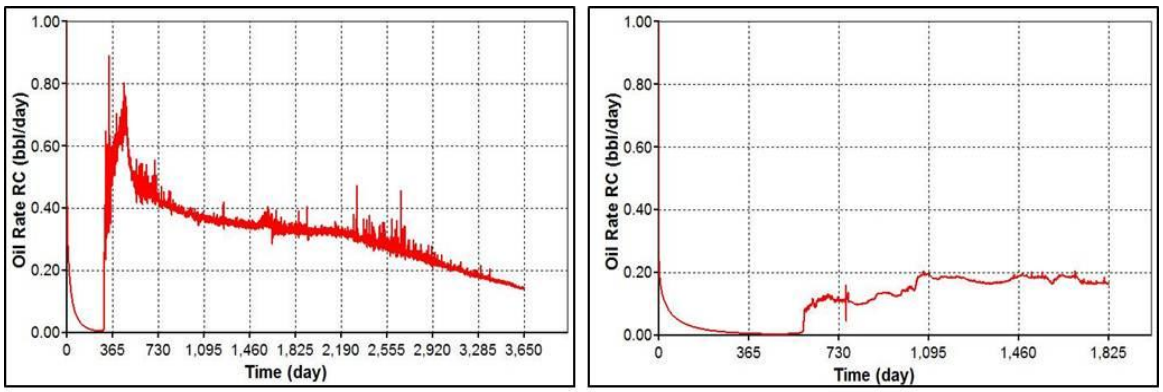

a. Homogeneous case b. Heterogeneous case

Figure 4-6. Comparison of oil rate change between homogeneous and heterogeneous case predicted by flow simulation: a. homogeneous case; b. heterogeneous case (adopted from Shi and Leung 2013).

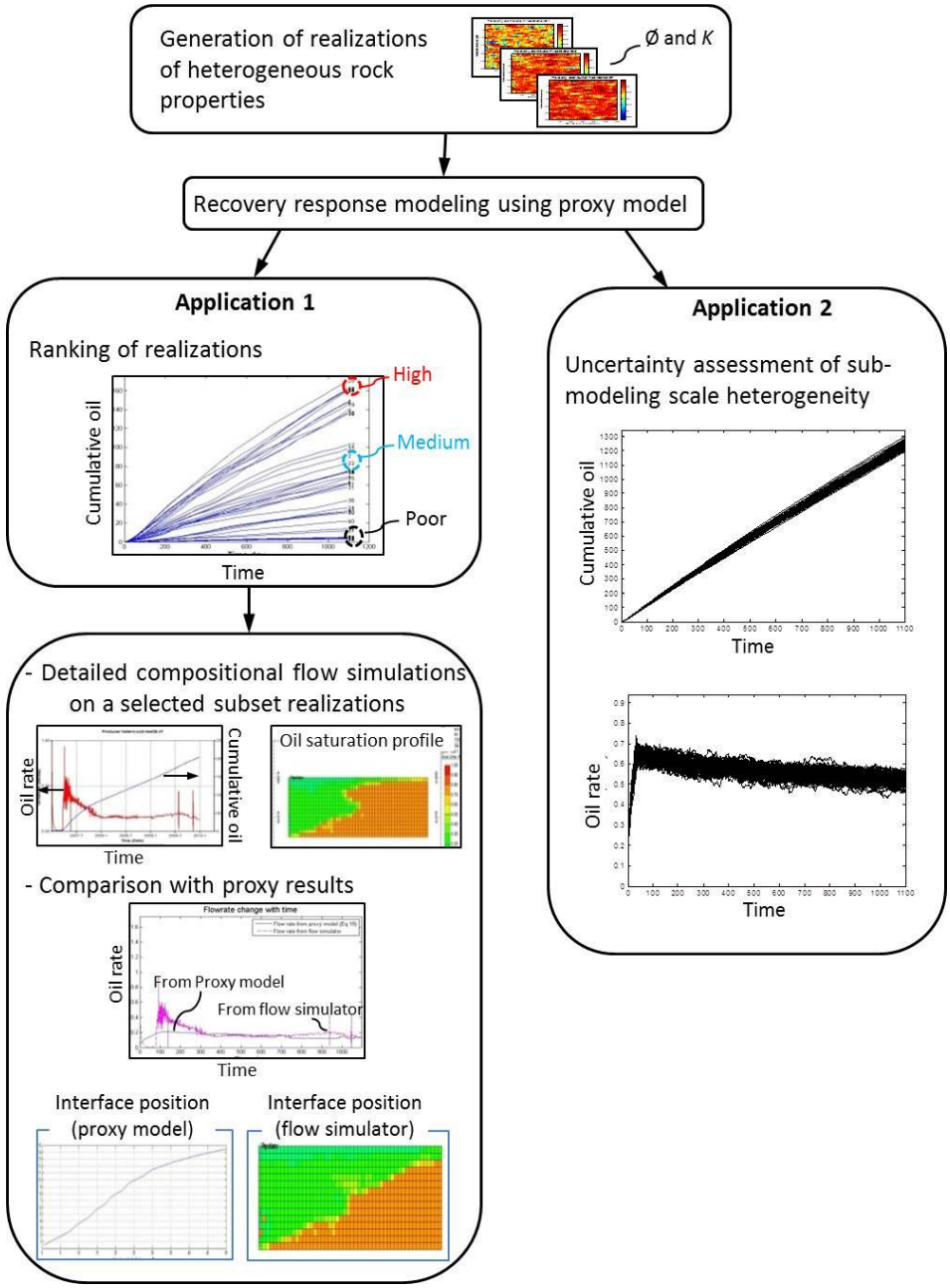

Figure 4-7. Workflow for uncertainty assessment of Vapex performance using semi-analytical proxy model

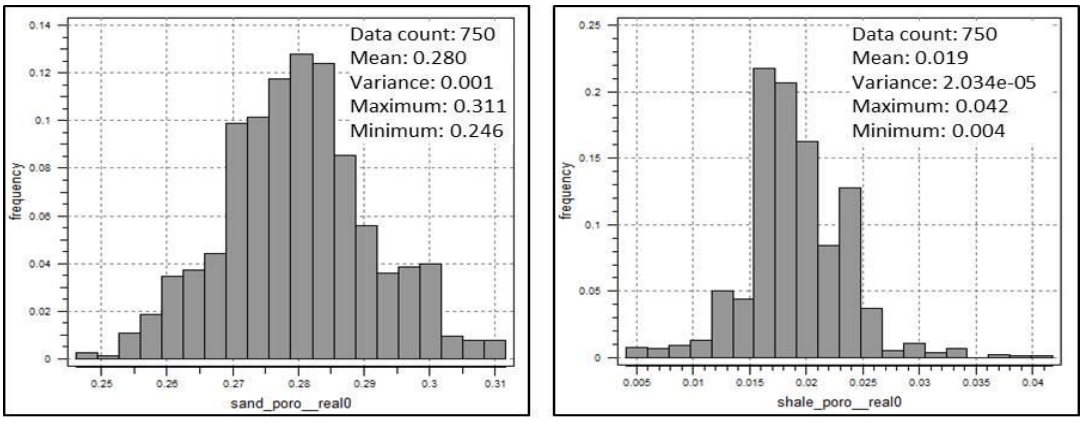

Figure 4-8. Histograms of porosity distribution in sand and shale facies for case study 1 (adopted from Leung 2012).

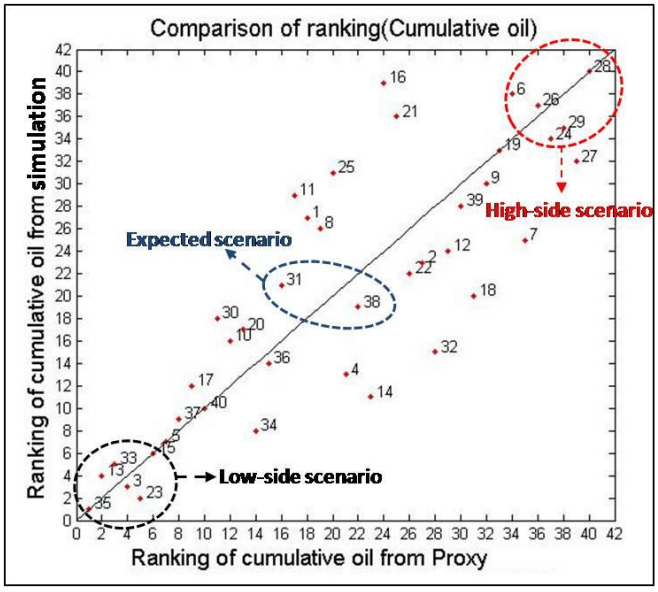

Figure 4-9. Comparison of ranking results (based on final cumulative oil production) derived from compositional simulations (CMG) and proxy predictions for case study 1. All 40 realizations are numbered. 45 degree line indicates perfect correlation. Cases representing the high-side, expected, and low-side scenarios are circled.

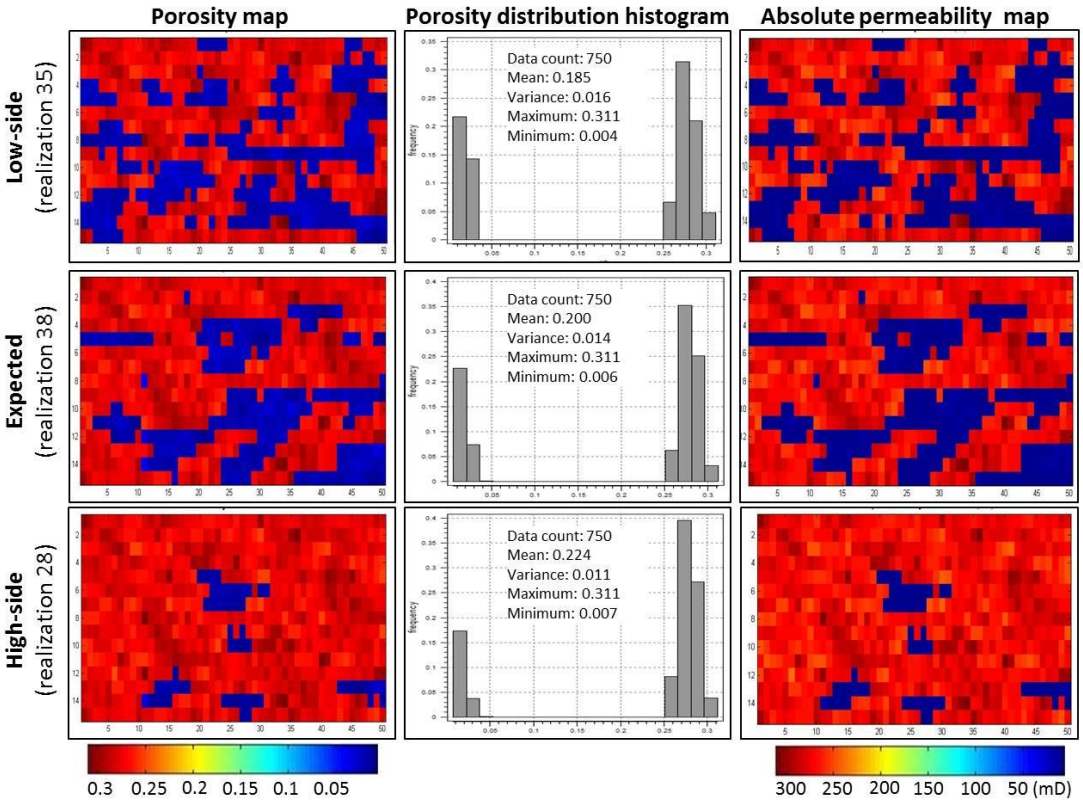

Figure 4-10. Porosity map, porosity distribution, and absolute permeability map for three randomly-selected realizations representative of the low-side, expected, and high scenarios in case study 1. The absolute permeability is correlated to porosity as described by Eq.15 and 16.

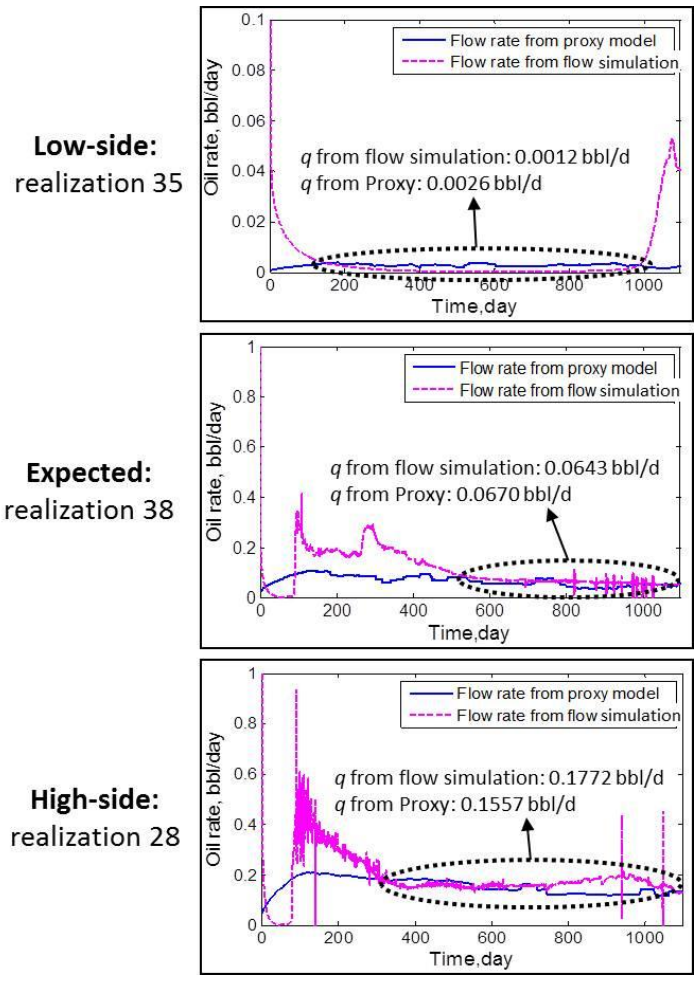

Figure 4-11. Comparison of stabilized average oil flow rate (q) change with time predicted from proxy analysis and compositional flow simulation for the three randomly-selected realizations (shown in Figure 4-10) in case study 1.

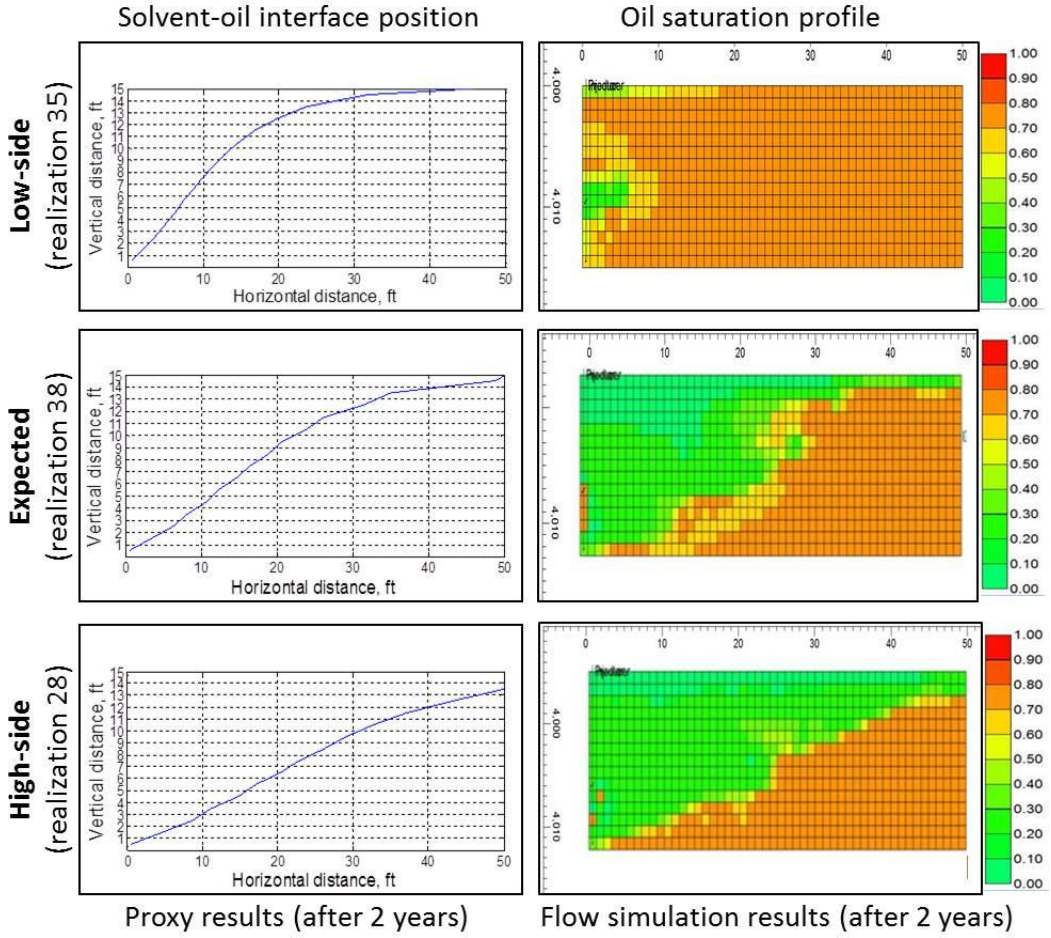

Figure 4-12. Comparison of solvent-oil interface position between proxy and simulation predictions for the three randomly-selected realizations (shown in Figure 4-10) in case study 1. Oil saturation profile obtained from flow simulation is used to visualize the solvent-oil interface.

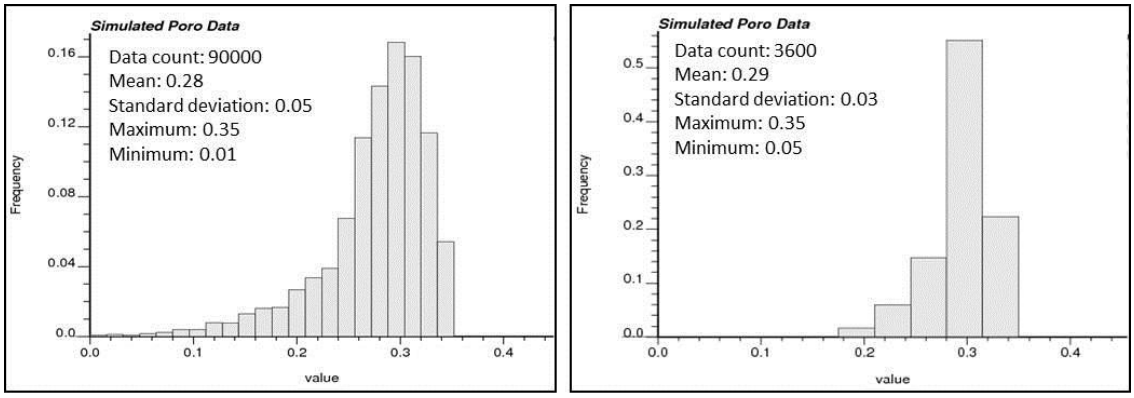

(a) Fine-scale porosity histogram **(b) Coarse-scale porosity histogram**

Figure 4-13. Histograms of fine-scale and coarse-scale porosity models in case study 2.

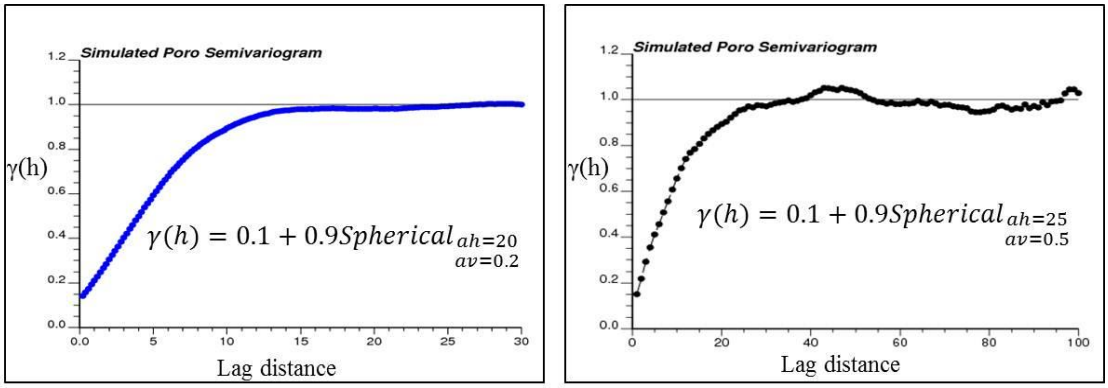

(a) Variogram for fine-scale porosity **(b) Variogram for coarse-scale porosity**

Figure 4-14. Variograms for the fine-scale and coarse-scale porosity distributions. Notation *ah* indicates the isotropic horizontal correlation range, *av* indicates the vertical correlation range.

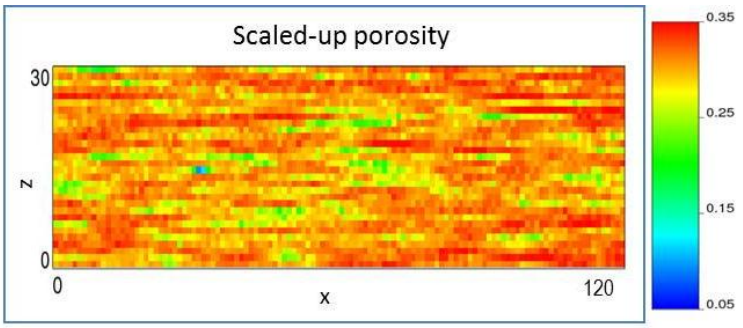

Figure 4-15. A random-selected realization of the coarse-scale porosity model for case study 2.

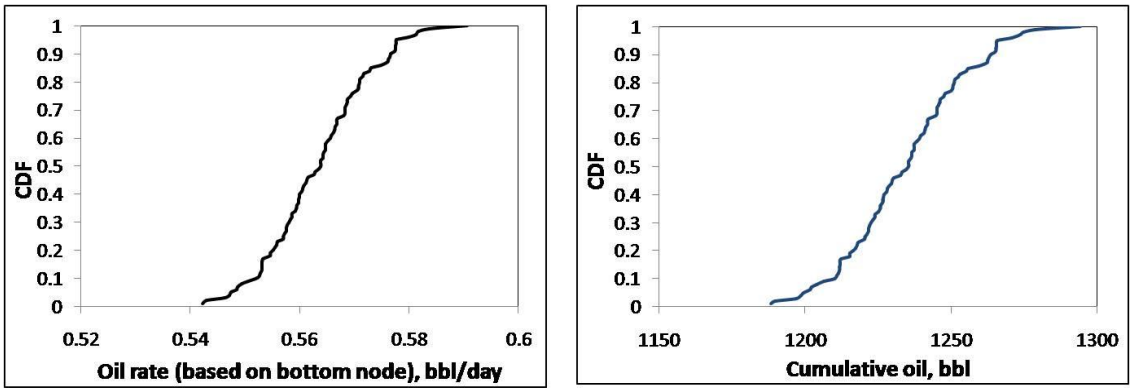

Figure 4-16. Cumulative probability distribution (CDF) of stabilized oil rate and cumulative oil obtained from proxy simulation for 100 realizations in case study 2.

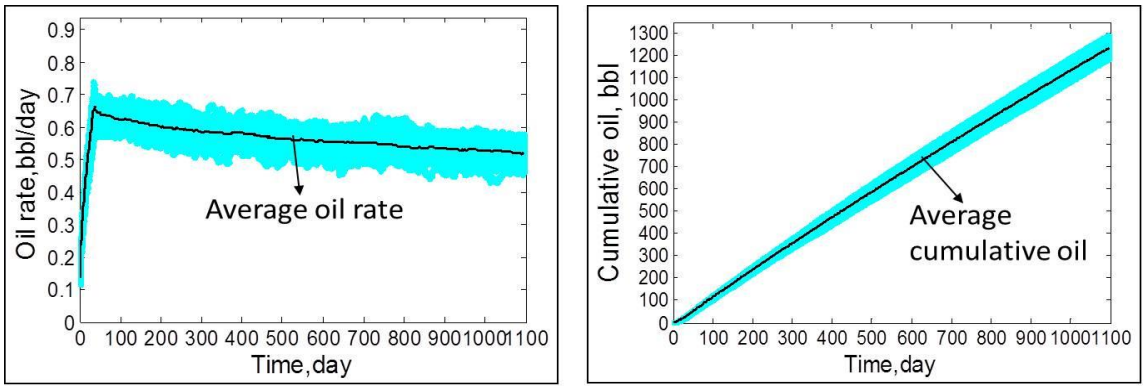

(a) Oil rate vs. time for all realizations (b) Cumulative oil vs. time for all realizations

Figure 4-17. Performance response uncertainty obtained from proxy simulation for 100 realizations in case study 2. Solid black lines indicate average value for oil rate and cumulative oil.

Chapter 5: Conclusions and Recommendations

Contributions and Conclusions

The major contributions and conclusions of this research work are listed as follows:

1. In this work, a new semi-analytical proxy model has been proposed to model solvent transport and oil recovery for the Vapex process at isothermal conditions. The model is based on Butler's analytical solution that was developed for the conditions applicable for typical Hele-Shaw cell experiments.

2. An explicit calculation sequence of the analytical equations in this proxy model is presented to predict the solvent-oil interface position and producing oil rate as a function of time. The original formulations have been extended to account for porous medium properties. In addition, a new parameter of mass penetration is introduced. The derivations of the proxy formulations follow closely of those developed for its SAGD analog.

3. Modifications of the proxy model via a set of averaging schemes are implemented for heterogeneous reservoirs, which provide an efficient and reliable alternative to predict solvent-oil interface position, producing oil rate, and cumulative oil production in Vapex process. One empirical tuning parameter is introduced to obtain a more reliable estimate of producing oil rate from the proxy model.

4. The results obtained from the proposed proxy show good agreement with published experimental observations and results from flow simulation in terms of

solvent-bitumen interface position and oil production rate, implying promising future application to field cases.

5. The proxy simulation requires a significantly reduced computational cost. It allows robust assessment of heterogeneity effects on recovery performance and presents an important potential in efficient production optimization for decision-making processes.

6. An uncertainty assessment workflow is presented that applies the proxy model to assess Vapex performance in the presence of geologic uncertainty. The workflow can be used to rank and screen many geostatistical realizations representing heterogeneity at various scales and to quickly identify a smaller, more manageable subset of models for further detailed flow simulations.

7. Given that heterogeneity modeling informed by incomplete data leads to uncertainty about rock properties, most practical approaches require generation of large number of equi-probable realizations of rock properties at reservoir scales. Computational constraints preclude detailed numerical solution of the flow and transport differential equations using the entire suite of plausible realizations. The proposed proxy can be used to mimic the transport physics without solving all the detailed equations, allowing us to assess the recovery performance of many geologic realizations efficiently.

8. An important contribution from this work is that process physics are built directly into this proxy, giving it an advantage over other data-driven modeling approaches (i.e., regression). It can be used as an efficient alternative to expensive detailed flow simulations. This type of proxy models can also be easily integrated

in existing workflows to optimize production scenarios. It presents an important potential for assessing the uncertainty in reservoir properties on effective mass transfer and the ensuing recovery performance, as well as assisting decisions-making for future pilot and field development planning.

Recommendations and Future Interest

1. Due to the complexity of fluid PTV properties, the proxy model doesn't include detailed Equation Of State (EOS) model, since we assume constant pressure and temperature at reservoir conditions. This may not be true in practice. A dynamic change in oil and solvent properties as a function of pressure and temperature may need further investigation to make this proxy more precise and reliable.

2. The present model cannot handle the situation of mobile water since it is developed based on the assumption of irreducible water saturation. Both Hele-Shaw model and simulation case studies do not take into consideration of the presence of moveable water. Although the presence of mobile water doesn't change the key recovery mechanism in the Vapex process, certain modifications might need to add the accuracy of the predictions.

3. To capture the solvent-oil interface advancement with time, an average constant value of oil saturation is used in the proxy, so that the exact solvent-oil mixing zone is not explicitly described in this work. Future interest may focus on improvements in proxy model to consider oil saturation variance in solvent-oil mixing zone.

4. The actual jagged solvent-oil interface cannot be captured by proxy due to many assumptions introduced (i.e., constant diffusion coefficient, constant density difference between oil and solvent, and constant oil saturation in diffusion zone.), as well as the averaging scheme used to calculate permeability and porosity at each time step. A more comprehensive study should focus on better capturing the irregular advancement of solvent-oil interface around shale barriers.

5. Extension of the current work can be focused on some sensitivity studies. For example, the sensitivity studies of using different solvent, different location of the well pairs, different injection rate, or different heterogeneity. The sensitivity study of these parameters can improve the practical significance of this research.

Appendixes

Appendix 1: Code for Hele-Shaw Cell Experiment

```
clear
%***************calculate interface change************
h=12;%cm
l=9;%cm
h_cell=1; %cm
l_cell=h_cell;
num_cell=h/h_cell; %
time_length=243000;%s
delta_t=60;%s
num_t=time_length/delta_t;
Gama=zeros(num_cell+1,num_t);%
Theta=zeros(num_cell+1,num_t);%
Sin_Theta=zeros(num_cell+1,num_t);%
Q_cell=zeros(num_cell+1,num_t);%
U=zeros(num_cell+1,num_t);%
X_co=zeros(num_cell+1,num_t);%
Y_co=zeros(num_cell+1,num_t);%
L=zeros(num_cell+1,num_t);%
%***************initial condition**********************
Ns=9.44e-7;
Delta_So=1;
So=1;
phi=1;
Gama(2:end,1)=[0.038;0.06;0.08;0.098;0.114;0.128;0.14;0.15;0.158;0
.164;0.168;0.17];%initial gama
Ko=1.09E-5;%cm2
g=980;%cm2/s
Ds_avg=4.268e-6;%cm2/s
Theta(:,1)=90;
Sin_Theta=sind(Theta);
Q_cell=Ko*g*Ns*Sin_Theta.*Gama./Ds_avg;
for i=1:num_cell+1
if i==1
        Y_co(i,1)=h;
else
        Y_co(i,1)=h-(i-1.5)*h_cell;
end
    X_co(i,1)=l_cell/2;
end
%*************** main calculation ************************%
X_boundary=l;
for j=1:num_t
for i=1:num_cell+1
if i==1
if X_co(i,j)<X_boundary
                X_co(i,j+1)=(-
(delta_t/phi/Delta_So))*(Q_cell(i+1,j)-0)/(Y_co(i+1,j)-
Y_co(i,j))+X_co(i,j);
                Y_co(i,j+1)=h;
Theta(i,j+1)=0;
U(i,j)=inf;
```

```
Gama(i,j+1)=0;
                    Q_cell(i,j+1)=0;
else
                    X_co(i,j+1)=X_boundary;
                    Y_co(i,j+1)=Y_co(i,j);
U(i,j)=0;
Gama(i,j+1)=0;
Theta(i,j+1)=90;
                    Q_cell(i,j+1)=0;
end
elseif i>=2&&i<=num_cell-1
if X_co(i,j)<X_boundary
                    X_co(i,j+1)=(-
(delta_t/phi/Delta_So))*(Q_cell(i+1,j)-Q_cell(i-
1,j))/(Y_co(i+1,j)-Y_co(i-1,j))+X_co(i,j);
                    Y_co(i,j+1)=Y_co(i,j);
                    X_co(i+1,j+1)=(-
(delta_t/phi/Delta_So))*(Q_cell(i+2,j)-Q_cell(i,j))/(Y_co(i+2,j)-
Y_co(i,j))+X_co(i+1,j);
                    Y_co(i+1,j+1)=Y_co(i+1,j);
                    L(i,j)=sqrt((X_co(i-1,j)-X_co(i+1,j))^2+(Y_co(i-
1,j)-Y_co(i+1,j))^2);
                    L(i,j+1)=sqrt((X_co(i-1,j+1)-
X_co(i+1,j+1))^2+(Y_co(i-1,j+1)-Y_co(i+1,j+1))^2);
                    Sin_Theta(i,j+1)=(Y_co(i-1,j+1)-
Y_co(i+1,j+1))/L(i,j+1);
Theta(i,j+1)=asind(Sin_Theta(i,j+1));
                    U(i,j)=(Q_cell(i+1,j)-Q_cell(i-1,j))/L(i,j);

Gama(i,j+1)=delta_t/(pi^0.5*phi*So)*(Ds_avg/Gama(i,j)-
U(i,j))+Gama(i,j);

Q_cell(i,j+1)=Ko*g*Ns*Sin_Theta(i,j+1)*Gama(i,j+1)/Ds_avg;
else
                    X_co(i,j+1)=X_boundary;
                    Y_co(i,j+1)=Y_co(i,j);
U(i,j)=0;
Gama(i,j+1)=0;
Theta(i,j+1)=90;
                    Q_cell(i,j+1)=0;
end
elseif i==num_cell+1
                    X_co(i,j+1)=X_co(end,1);
                    Y_co(i,j+1)=Y_co(end,1);
                    L(i,j)=sqrt((X_co(i-1,j)-X_co(i,j))^2+(Y_co(i-
1,j)-Y_co(i,j))^2);
                    L(i,j+1)=sqrt((X_co(i-1,j+1)-
X_co(i,j+1))^2+(Y_co(i-1,j+1)-Y_co(i,j+1))^2);
                    Sin_Theta(i,j+1)=(Y_co(i-1,j+1)-
Y_co(i,j+1))/L(i,j+1);
Theta(i,j+1)=asind(Sin_Theta(i,j+1));
                    U(i,j)=(Q_cell(i,j)-Q_cell(i-1,j))/L(i,j);

Gama(i,j+1)=delta_t/(pi^0.5*phi*So)*(Ds_avg/Gama(i,j)-
U(i,j))+Gama(i,j);

Q_cell(i,j+1)=Ko*g*Ns*Sin_Theta(i,j+1)*Gama(i,j+1)/Ds_avg;
```

```
else
                L(i,j)=sqrt((X_co(i-1,j)-X_co(i+1,j))^2+(Y_co(i-
1,j)-Y_co(i+1,j))^2);
                L(i,j+1)=sqrt((X_co(i-1,j+1)-
X_co(i+1,j+1))^2+(Y_co(i-1,j+1)-Y_co(i+1,j+1))^2);
                Sin_Theta(i,j+1)=(Y_co(i-1,j+1)-
Y_co(i+1,j+1))/L(i,j+1);
Theta(i,j+1)=asind(Sin_Theta(i,j+1));
                U(i,j)=(Q_cell(i+1,j)-Q_cell(i-1,j))/L(i,j);

Gama(i,j+1)=delta_t/(pi^0.5*phi*So)*(Ds_avg/Gama(i,j)-
U(i,j))+Gama(i,j);

Q_cell(i,j+1)=Ko*g*Ns*Sin_Theta(i,j+1)*Gama(i,j+1)/Ds_avg;
end

end
end
%************plot interface change with time*******************
X_CO=X_co(:,1:100:end);
Y_CO=Y_co(:,1:100:end);
figure;
plot(X_CO,Y_CO)
axis([0,l,0,h])
xlabel('Horizontal distance, cm','fontsize',12)
ylabel('Vertical distance, cm','fontsize',12)
title('Solvent-Bitumen Interface Change','fontsize',13)
gridon
holdon
%******************flowarte of each cell in colormap***********%
Q_Cell=Q_cell(2:num_cell+1,:);

figure;
imagesc(Q_Cell);
colormap(gray)
colorbar
xlabel('Time,minute','fontsize',12)
ylabel('Interface nodes','fontsize',12)
title('Change of element flowrate along interface','fontsize',13)
holdon

%******************flowrate change with time*****************%
Q_last=Q_cell(end,:);
Q_avg=mean(Q_last)
Q_total=sqrt(2*Ko*g*Delta_So*phi*h*Ns)
Max=max(Q_last);

figure;
plot(Q_last);
axis([0,num_t+5,0,Max+0.0002])
xlabel('Time,minute','fontsize',12)
ylabel('Flowrate, cm^2/s','fontsize',12)
title('Flowrate change with time','fontsize',13)
holdon
```

Appendix 2: Code for Homogeneous Case

```
clear;clc
%***calculate integral***********
Soi=0.8;
So_avg=0.51;%***********
%So=Soi;%%%%*****use Soi
So=So_avg;%%%******use So_avg
Delta_So=0.7;%***********
phi=0.28;%***********
x=0.1:0.001:0.92;
y=(1-x).*(-10.28*x.^2-0.816*x+47.554)./((3546.2*exp(-
(5.718*x)).*(215*x-0.1*(-189.813*x+234.59))));
Int=trapz(x,y)*215^2/44.01;
Ds_avg=4.65E-03;%ft2/d
Ns=phi^2*Ds_avg*So*Int;
%***************calculate interface change***********
num_cell=30; %1ft
time_length=3650;%d
delta_t=1;%d
h=30;%ft
l=120;%ft
h_cell=h/num_cell;
l_cell=h_cell;
dz=1;%ft,length of horizontal well
K_absolute=267;%md
Ko=K_absolute*0.001*0.000000000009869233*3.281^2;%convert m2 to
ft2,effective perm of field
g=2.400E+11;% ft/d2
num_t=time_length/delta_t;
Gama=zeros(num_cell+1,num_t);%
Theta=zeros(num_cell+1,num_t);%
Q_cell=zeros(num_cell+1,num_t);%
U=zeros(num_cell+1,num_t);%
X_co=zeros(num_cell+1,num_t);%
Y_co=zeros(num_cell+1,num_t);%
L=zeros(num_cell+1,num_t);%
%*************Total flow rate************************
Q_total=sqrt(2*Ko*g*Delta_So*phi*h*Ns);%ft2/d
Cs_avg=0.976;%
Q=Q_total*dz/(1-Cs_avg);%ft3/d
Gama_last=Q_total*phi*So*Ds_avg/Ns/Ko/g; %ft
Q=Q*0.0283 %convert ft3/d to m3/d
%***************initial gama**********************
Gama(2:end,1)=xlsread('CO2.xlsx','gama','b2:b31');%Straightline
Theta(:,1)=90;
Sin_Theta=sind(Theta);
Q_cell=Ko*g*Ns*Sin_Theta.*Gama./(Ds_avg*phi*So);

for i=1:num_cell+1
if i==1
        Y_co(i,1)=h;
else
        Y_co(i,1)=h-(i-1.5)*h_cell;
end
    X_co(i,1)=l_cell/2;
```

```
end
%*************** main calculation ************************%
X_boundary=l;
for j=1:num_t
for i=1:num_cell+1
if X_co(i,j)<=X_co(end,1);
              X_co(i,j)=X_co(end,1);
end
if i==1
if X_co(i,j)<X_boundary
                  X_co(i,j+1)=(-
(delta_t/phi/Delta_So))*(Q_cell(i+1,j)-0)/(Y_co(i+1,j)-
Y_co(i,j))+X_co(i,j);
                  Y_co(i,j+1)=h;
Theta(i,j+1)=0;
U(i,j)=inf;
Gama(i,j+1)=0;
                  Q_cell(i,j+1)=0;
else
                  X_co(i,j+1)=X_boundary;
                  Y_co(i,j+1)=Y_co(i,j);
U(i,j)=0;
Gama(i,j+1)=0;
Theta(i,j+1)=90;
                  Q_cell(i,j+1)=0;
end
elseif i>=2&&i<=num_cell-1
if X_co(i,j)<X_boundary
                  X_co(i,j+1)=(-
(delta_t/phi/Delta_So))*(Q_cell(i+1,j)-Q_cell(i-
1,j))/(Y_co(i+1,j)-Y_co(i-1,j))+X_co(i,j);
                  Y_co(i,j+1)=Y_co(i,j);
                  X_co(i+1,j+1)=(-
(delta_t/phi/Delta_So))*(Q_cell(i+2,j)-Q_cell(i,j))/(Y_co(i+2,j)-
Y_co(i,j))+X_co(i+1,j);
                  Y_co(i+1,j+1)=Y_co(i+1,j);
                  L(i,j)=sqrt((X_co(i-1,j)-X_co(i+1,j))^2+(Y_co(i-
1,j)-Y_co(i+1,j))^2);
                  L(i,j+1)=sqrt((X_co(i-1,j+1)-
X_co(i+1,j+1))^2+(Y_co(i-1,j+1)-Y_co(i+1,j+1))^2);
                  Sin_Theta(i,j+1)=(Y_co(i-1,j+1)-
Y_co(i+1,j+1))/L(i,j+1);
Theta(i,j+1)=asind(Sin_Theta(i,j+1));
                  U(i,j)=(Q_cell(i+1,j)-Q_cell(i-
1,j))*phi*Delta_So/(L(i,j));

Gama(i,j+1)=delta_t/(pi^0.5*phi*So)*(Ds_avg*phi*Soi/Gama(i,j)-
U(i,j))+Gama(i,j);

Q_cell(i,j+1)=Ko*g*Ns*Sin_Theta(i,j+1)*Gama(i,j+1)/(Ds_avg*So*phi);

else
                  X_co(i,j+1)=X_boundary;
                  Y_co(i,j+1)=Y_co(i,j);
U(i,j)=0;
Gama(i,j+1)=0;
Theta(i,j+1)=90;
```

```
                Q_cell(i,j+1)=0;
end
elseif i==num_cell+1
                X_co(i,j+1)=X_co(end,1);
                Y_co(i,j+1)=Y_co(end,1);
                L(i,j)=sqrt((X_co(i-1,j)-X_co(i,j))^2+(Y_co(i-
1,j)-Y_co(i,j))^2);
                L(i,j+1)=sqrt((X_co(i-1,j+1)-
X_co(i,j+1))^2+(Y_co(i-1,j+1)-Y_co(i,j+1))^2);
                Sin_Theta(i,j+1)=(Y_co(i-1,j+1)-
Y_co(i,j+1))/L(i,j+1);
Theta(i,j+1)=asind(Sin_Theta(i,j+1));
                U(i,j)=(Q_cell(i,j)-Q_cell(i-
1,j))*phi*Delta_So/(L(i,j));

Gama(i,j+1)=delta_t/(pi^0.5*phi*So)*(Ds_avg*phi*Soi/Gama(i,j)-
U(i,j))+Gama(i,j);

Q_cell(i,j+1)=Ko*g*Ns*Sin_Theta(i,j+1)*Gama(i,j+1)/(Ds_avg*So*phi);

else
                L(i,j)=sqrt((X_co(i-1,j)-X_co(i+1,j))^2+(Y_co(i-
1,j)-Y_co(i+1,j))^2);
                L(i,j+1)=sqrt((X_co(i-1,j+1)-
X_co(i+1,j+1))^2+(Y_co(i-1,j+1)-Y_co(i+1,j+1))^2);
                Sin_Theta(i,j+1)=(Y_co(i-1,j+1)-
Y_co(i+1,j+1))/L(i,j+1);
Theta(i,j+1)=asind(Sin_Theta(i,j+1));
                U(i,j)=(Q_cell(i+1,j)-Q_cell(i-
1,j))*phi*Delta_So/(L(i,j));%*****w

Gama(i,j+1)=delta_t/(pi^0.5*phi*So)*(Ds_avg*phi*Soi/Gama(i,j)-
U(i,j))+Gama(i,j);

Q_cell(i,j+1)=Ko*g*Ns*Sin_Theta(i,j+1)*Gama(i,j+1)/(Ds_avg*So*phi);



end
end
end

%************PLOT INTERFACE CHANGE************
%*****UNIT CONVERSION***********
X_co=X_co.*0.3048;%convert foot to metre
Y_co=Y_co.*0.3048;%convert foot to metre
l=l*0.3048;%convert foot to metre
h=h*0.3048;%convert foot to metre

figure;
X_CO=X_co(:,1:50:end);
Y_CO=Y_co(:,1:50:end);
figure;
plot(X_CO,Y_CO);
xlabel('Horizontal distance, m','fontsize',19)
ylabel('Vertical distance, m','fontsize',19)
title('Solvent-Bitumen Interface Change','fontsize',20)
```

```
gridon
axis([0,l,0,h])
set(gca,'fontsize',12)
holdon
%***********flow rate change with time****
Q_last=Q_cell(end,:).*dz/(1-Cs_avg);%ft3/d
Q_last=Q_last*0.0283;%convert ft3/d to m3/d
%*********introduce tuning parameter
tuning=4;
Q_last_tuning=Q_last/tuning;%including tuning parameter
Q_avg=mean(Q_last_tuning)
%*********plot flow rate vs. time
figure;
plot(Q_last_tuning,'--b','LineWidth',2)
xlabel('Time,day','fontsize',15)
ylabel('Flowrate, m^3/d','fontsize',15)
title('Flowrate change with time','fontsize',17)
holdon
%***********plot cumulative oil vs. time**************
Q_lt_cum=cumsum(Q_last_tuning);

figure;
Q_lt_cum=cumsum(Q_last_tuning);
y1max=max(Q_lt_cum);
x11=linspace(0,num_t+1,num_t+1);
y11=Q_lt_cum;
plot(x11,y11)
axis([0,num_t+5,0,y1max+5]);
set(gca,'fontsize',12);
xlabel('Time,day','fontsize',15)
ylabel('Cumulative oil, m^3','fontsize',15)
title('Cumulative oil vs. time ','fontsize',17)
hold on
```

Appendix 3: Code for Heterogeneous Case

```
%%This file include all the functions for the heterogeneous case
showed in Chapter 3

%% function readinput.m to read the input value of permeability
and porosity

function [K_absolute,PHI]=readinput()
K_read=xlsread('CO2-Heterogenous.xlsx','permeability','A1:A3600');
K_read=reshape(K_read,120,30);
K_absolute=transpose(K_read);%
PHI_read=xlsread('CO2-Heterogenous.xlsx','porosity','A1:A3600');
PHI_read=reshape(PHI_read,120,30);
PHI=transpose(PHI_read);
End

%% function Int_cal.m to calculate integral Ns

function Int=Int_cal()
x=0.1:0.001:0.92;
y=(1-x).*(-10.28*x.^2-0.816*x+47.554)./((3546.2*exp(-
(5.718*x)).*(215*x-0.1*(-189.813*x+234.59))));
Int=trapz(x,y)*215^2/44.01;
End

%% function Inputpar.m to read other input parameter

function
[num_cell,time_length,delta_t,h,l,h_cell,l_cell,dz,Ds_avg,Delta_So
,Soi,So_avg,So,K_relative,g,num_t]=Inputpar()
num_cell=30; %
time_length=1825;%d(5year)
delta_t=1;%d
h=30;%ft
l=120;%ft
h_cell=h/num_cell;
l_cell=h_cell;
dz=1;%ft length of well
Ds_avg=4.65E-03;%ft2/d
Delta_So=0.7;
Soi=0.8;
So_avg=0.5;
So=So_avg;
K_relative=0.5;
g=2.400E+11;% ft/d2
num_t=time_length/delta_t;
end

%% function perm_cal3 to calculate permeability at each time step

function K_actual=perm_cal3(j)
t=j;
l=120;
K_store=evalin('base','K');
```

```
K_reshape=[zeros(1,l);K_store];
X_store=evalin('base','X_co');
delta_x=evalin('base','l_cell');
K_1=evalin('base','K_ini');
Ncell=evalin('base','num_cell');
J_ind=zeros(1,Ncell+1);
I_ind=linspace(1,31,31);
K_new=zeros(1,Ncell+1);
if t==1
    K_actual=K_1;
else
for i=1:Ncell+1
        J_ind(i)=round(X_store(i,t-1)/delta_x);
if J_ind(i)==0;
            J_ind(i)=1;
end
end
for n=1:Ncell+1
        K_new(n)=K_reshape(I_ind(n),J_ind(n));
end
K_actual=mean(K_new(1,2:end));
end
end

%% function poro_cal3 to calculate porosity at each time step

function PHI_actual=poro_cal3(j)
t=j;
l=120;
PHI_store=evalin('base','PHI');
PHI_reshape=[zeros(1,l);PHI_store];
X_store=evalin('base','X_co');
delta_x=evalin('base','l_cell');
PHI_1=evalin('base','PHI_ini');
Ncell=evalin('base','num_cell');
J_ind=zeros(1,Ncell+1);
I_ind=linspace(1,31,31);
PHI_new=zeros(1,Ncell+1);
if t==1
    PHI_actual=PHI_1;
else
for i=1:Ncell+1
        J_ind(i)=round(X_store(i,t-1)/delta_x);
if J_ind(i)==0;
            J_ind(i)=1;
end
end
for n=1:Ncell+1
        PHI_new(n)=PHI_reshape(I_ind(n),J_ind(n));
end
PHI_actual=mean(PHI_new(1,2:end));
end
end


%% function main.m to do the main calculation
```

```
clear,clc
global num_cell time_length delta_t h l h_cell l_cell dz Ds_avg
Delta_So Soi So_avg So K_relative g num_t

% ***Calculate integral************
Int=Int_cal();
% **************read input parameter*********
[num_cell,time_length,delta_t,h,l,h_cell,l_cell,dz,Ds_avg,Delta_So
,Soi,So_avg,So,K_relative,g,num_t]=Inputpar();
%******initialization**********************
Theta=zeros(num_cell+1,num_t);%
Q_cell=zeros(num_cell+1,num_t);%
U=zeros(num_cell+1,num_t);%
X_co=zeros(num_cell+1,num_t);%
Y_co=zeros(num_cell+1,num_t);%
L=zeros(num_cell+1,num_t);%
K_actual=zeros(num_cell+1,num_t);
PHI_actual=ones(num_cell+1,num_t);
Ns_actual=zeros(num_cell+1,num_t);
Gama=zeros(num_cell+1,num_t);%
% *************READ PERM&POROSITY FIELD***********************
[K_absolute,PHI]=readinput();
%***************Calculate total flow rate***********
K_abmean=mean2(K_absolute);
K=K_absolute.*K_relative*0.001*0.0000000000009869233*3.281^2;
K_mean=mean2(K);
PHI_mean=mean2(PHI);
Ns_mean=PHI_mean^2*Ds_avg*So*Int;
Q_total=sqrt(2*K_mean*g*Delta_So*PHI_mean*h*Ns_mean);%ft2/d
Cs_avg=0.976;
Q=Q_total*dz/(1-Cs_avg);%ft3/d
Gama_last=Q_total*PHI_mean*So*Ds_avg/Ns_mean/K_mean/g %ft
Q=Q*0.0283 %convert ft3/d to m3/d

%******Calculate interface change********
%***************initial condition**********************
Gama(2:end,1)=xlsread('CO2-
Heterogenous.xlsx','gama','g2:g31');%Straightline
Theta(:,1)=90;
Sin_Theta=sind(Theta);
K_ini=mean(K(:,1));
PHI_ini=mean(PHI(:,1));
K_actual(2:end,1)=K_ini;
PHI_actual(2:end,1)=PHI_ini;
Ns_actual(:,1)=PHI_actual(:,1).^2*Ds_avg*So*Int;

for i=1:num_cell+1

Q_cell(i,1)=K_actual(i,1)*Ns_actual(i,1)*Sin_Theta(i,1)*Gama(i,1)*
g/(Ds_avg*PHI_actual(i,1)*So);
end

for i=1:num_cell+1
if i==1
        Y_co(i,1)=h;
else
```

```
        Y_co(i,1)=h-(i-1.5)*h_cell;
end
    X_co(i,1)=l_cell/2;
end
% *************** main calculation ************************
X_boundary=l;
for j=1:num_t
    K_actual(:,j)=perm_cal3(j);
    PHI_actual(:,j)=poro_cal3(j);
    Ns_actual(:,j)=PHI_actual(:,j).^2*Ds_avg*So*Int;
for i=1:num_cell+1
if X_co(i,j)<=X_co(end,1);
                    X_co(i,j)=X_co(end,1);
end
if i==1
if X_co(i,j)<X_boundary
                  X_co(i,j+1)=(-
(delta_t/PHI_actual(i,j)/Delta_So))*(Q_cell(i+1,j)-
0)/(Y_co(i+1,j)-Y_co(i,j))+X_co(i,j);
                  Y_co(i,j+1)=h;
Theta(i,j+1)=0;
U(i,j)=inf;
Gama(i,j+1)=0;
                  Q_cell(i,j+1)=0;
else
                  X_co(i,j+1)=X_boundary;
                  Y_co(i,j+1)=Y_co(i,j);
U(i,j)=0;
Gama(i,j+1)=0;
Theta(i,j+1)=90;
                  Q_cell(i,j+1)=0;
end
elseif i>=2&&i<=num_cell-1
if X_co(i,j)<X_boundary
                  X_co(i,j+1)=(-
(delta_t/PHI_actual(i,j)/Delta_So))*(Q_cell(i+1,j)-Q_cell(i-
1,j))/(Y_co(i+1,j)-Y_co(i-1,j))+X_co(i,j);
                  Y_co(i,j+1)=Y_co(i,j);
                  X_co(i+1,j+1)=(-
(delta_t/PHI_actual(i,j)/Delta_So))*(Q_cell(i+2,j)-
Q_cell(i,j))/(Y_co(i+2,j)-Y_co(i,j))+X_co(i+1,j);
                  Y_co(i+1,j+1)=Y_co(i+1,j);
                  L(i,j)=sqrt((X_co(i-1,j)-X_co(i+1,j))^2+(Y_co(i-
1,j)-Y_co(i+1,j))^2);
                  L(i,j+1)=sqrt((X_co(i-1,j+1)-
X_co(i+1,j+1))^2+(Y_co(i-1,j+1)-Y_co(i+1,j+1))^2);
                  Sin_Theta(i,j+1)=(Y_co(i-1,j+1)-
Y_co(i+1,j+1))/L(i,j+1);
Theta(i,j+1)=asind(Sin_Theta(i,j+1));
                  U(i,j)=(Q_cell(i+1,j)-Q_cell(i-
1,j))*PHI_actual(i,j)*Delta_So/(L(i,j));

Gama(i,j+1)=delta_t/(pi^0.5*PHI_actual(i,j)*So)*(Ds_avg*PHI_actual
(i,j)*So/Gama(i,j)-U(i,j))+Gama(i,j);

Q_cell(i,j+1)=K_actual(i,j)*g*Ns_actual(i,j)*Sin_Theta(i,j+1)*Gama
(i,j+1)/(Ds_avg*So*PHI_actual(i,j));
```

```
else
                X_co(i,j+1)=X_boundary;
                Y_co(i,j+1)=Y_co(i,j);
U(i,j)=0;
Gama(i,j+1)=0;
Theta(i,j+1)=90;
                Q_cell(i,j+1)=0;
end
elseif i==num_cell+1
                X_co(i,j+1)=X_co(end,1);
                Y_co(i,j+1)=Y_co(end,1);
                L(i,j)=sqrt((X_co(i-1,j)-X_co(i,j))^2+(Y_co(i-
1,j)-Y_co(i,j))^2);
                L(i,j+1)=sqrt((X_co(i-1,j+1)-
X_co(i,j+1))^2+(Y_co(i-1,j+1)-Y_co(i,j+1))^2);
                Sin_Theta(i,j+1)=(Y_co(i-1,j+1)-
Y_co(i,j+1))/L(i,j+1);
Theta(i,j+1)=asind(Sin_Theta(i,j+1));
                U(i,j)=(Q_cell(i,j)-Q_cell(i-
1,j))*PHI_actual(i,j)*Delta_So/(L(i,j));

Gama(i,j+1)=delta_t/(pi^0.5*PHI_actual(i,j)*So)*(Ds_avg*PHI_actual
(i,j)*So/Gama(i,j)-U(i,j))+Gama(i,j);

Q_cell(i,j+1)=K_actual(i,j)*g*Ns_actual(i,j)*Sin_Theta(i,j+1)*Gama
(i,j+1)/(Ds_avg*So*PHI_actual(i,j));
else
                L(i,j)=sqrt((X_co(i-1,j)-X_co(i+1,j))^2+(Y_co(i-
1,j)-Y_co(i+1,j))^2);
                L(i,j+1)=sqrt((X_co(i-1,j+1)-
X_co(i+1,j+1))^2+(Y_co(i-1,j+1)-Y_co(i+1,j+1))^2);
                Sin_Theta(i,j+1)=(Y_co(i-1,j+1)-
Y_co(i+1,j+1))/L(i,j+1);
Theta(i,j+1)=asind(Sin_Theta(i,j+1));
                U(i,j)=(Q_cell(i+1,j)-Q_cell(i-
1,j))*PHI_actual(i,j)*Delta_So/(L(i,j));

Gama(i,j+1)=delta_t/(pi^0.5*PHI_actual(i,j)*So)*(Ds_avg*PHI_actual
(i,j)*So/Gama(i,j)-U(i,j))+Gama(i,j);

Q_cell(i,j+1)=K_actual(i,j)*g*Ns_actual(i,j)*Sin_Theta(i,j+1)*Gama
(i,j+1)/(Ds_avg*So*PHI_actual(i,j));

end
end
end
%*****UNIT CONVERSION************
X_co=X_co.*0.3048;%convert foot to metre
Y_co=Y_co.*0.3048;%convert foot to metre
l=l*0.3048;%convert foot to metre
h=h*0.3048;%convert foot to metre
%*****PLOT RESULTS****************
figure;
X_CO=X_co(:,1:50:end);
Y_CO=Y_co(:,1:50:end);
figure;
plot(X_CO,Y_CO);
```

```
xlabel('Horizontal distance, m','fontsize',19)
ylabel('Vertical distance, m','fontsize',19)
title('Solvent-Bitumen Interface Change','fontsize',20)
gridon
axis([0,l,0,h])
set(gca,'fontsize',12)
holdon
%***********flow rate change with time****
Q_last=Q_cell(end,:).*dz/(1-Cs_avg);%ft3/d
Q_last=Q_last*0.0283;%convert ft3/d to m3/d
%*********introduce tuning parameter
tuning=4;
Q_last_tuning=Q_last/tuning;%including tuning parameter
Q_avg=mean(Q_last_tuning)
%*********plot flow rate vs. time
figure;
plot(Q_last_tuning)
axis([0,num_t+5,0,Q_avg*2])
set(gca,'fontsize',12)
xlabel('Time,day','fontsize',15)
ylabel('Flowrate, m^3/d','fontsize',15)
title('Flowrate change with time','fontsize',17)
holdon
%***********plot cumulative oil vs. time**************
Q_lt_cum=cumsum(Q_last_tuning);

figure;
Q_lt_cum=cumsum(Q_last_tuning);
y1max=max(Q_lt_cum);
x11=linspace(0,num_t+1,num_t+1);
y11=Q_lt_cum;
plot(x11,y11)
axis([0,num_t+5,0,y1max+5]);
set(gca,'fontsize',12);
xlabel('Time,day','fontsize',15)
ylabel('Cumulative oil, m^3','fontsize',15)
title('Cumulative oil vs. time ','fontsize',17)
holdon
```